N d'ordre: 00000 ANNEE 2010

THESE

présentée devant
L'ECOLE CENTRALE DE LYON

pour obtenir
Le titre de DOCTEUR
SPECIALITE ACOUSTIQUE

par

Ying HU

DEVELOPPEMENT DE PANNEAUX HYBRIDES PASSIFS/ACTIFS POUR L'ACOUSTIQUE

à soutenir le 17 Décembre 2010 devant la commission d'examen

Mme.	Marie-Annick	GALLAND	(Directeur de thèse)
M.	Kean	CHEN	(Codirecteur)
M.	Philippe	HERZOG	(Rapporteur)
M.	Jincai	SUN	(Rapporteur)
M.	Shuyu	LIN	(invité)
M.	Boxiao	CHEN	(invité)
M.	Hong	HOU	

Laboratoire de Mécanique des Fluides et d'Acoustique, UMR CNRS 5509
Ecole Centrale de Lyon

Abstract

Active acoustic structure is an effective structure for reducing the unwanted noise, and it has been widely studied for engineering application. In this thesis, a hybrid active acoustic structure having good acoustical absorption and insulation is developed, combining the porous materials and active control technique. The secondary source is realized by an active plate consisting of two piezoelectric patches bonded to an elastic thin plate in order to improve acoustic insulation at low and resonances frequencies. The numerical results and measurement data show that this structure has good absorption coefficient and transmission loss after active control. The following works have been completed:

(1) The acoustic characteristic of the double-wall passive acoustic structure is analyzed by the transfer matrix method. The definition of four acoustic matrices: the transfer matrix, the scattering matrix, the impedance matrix, and the admittance matrix are given in the acoustic structure, and the relationship between them is also expressed. Based on the sound propagation principle, the transfer matrix of the elastic plate, the air gap, the porous material and the interface between each layer are expressed and then the total transfer matrix of the double-wall structure is deduced. Lastly, the absorption coefficient and transmission loss of the double-wall acoustic structure are calculated and analyzed with some numerical examples.

(2) A hybrid active acoustic structure allowing good acoustic insulation and absorption for a wide frequency range has been developed based on the scattering matrix method. The scattering matrix of the active plate with the piezoelectric ceramics is expressed, and the acoustic performance of the hybrid active structures has been calculated with and without active control. According to the analysis results, the hybrid active acoustic structure is designed for obtaining good acoustic insulation and absorption performance. The influence factors which affect the acoustic properties of the developed hybrid active acoustic structure have also been investigated.

(3) The acoustic performance of the hybrid active structure having poroelastic material is analyzed by the finite element method. The finite model of the poroelastic material is established based on the (u, p) formulation, considering the elasticity of the skeleton and the

strong coupling between the solid and fluid phases. The boundary conditions on the coupling surface of the elastic, poroelastic and air layers were formulated in Comsol modes. The surface impedance of the poroelastic material was validated by Biot's theory for different boundary conditions. The absorption coefficient and transmission loss of some hybrid active acoustic structures have been studied under plane wave excitation in Comsol environment and the results are validated by the scattering matrix method for s limited frequency range.

(4) Experiments for determining the acoustic properties of the hybrid active structure are carried out by the two source-location method. The reflection and transmission coefficients of each layer in the hybrid active structure are tested, and the acoustic performance of some hybrid active acoustic structure is measured, using FxLMS algorithm for finding the optimal secondary source command in active control. The results in measurement are in good agreement with that in the finite element method, and the transmission loss of these hybrid structures can be improved obviously with active control for resonance frequency.

(5) A multi-cell hybrid active acoustic structure concept is proposed by juxtaposing several single hybrid cells for reducing the noise in a large-area domain. The primary and secondary pathway matrices have been obtained based on the multi-cell hybrid structure consisting of an $m \times n$ ($m, n = 1, 2, 3, \cdots$) array of single hybrid cells. Some two-cell hybrid structures are developed, for example, and their acoustic properties have been studied with a rigid or elastic interface between each hybrid cell.

Key words: hybrid acoustic structure, porous material, transfer matrix, scattering matrix, active control

Résumé

Les panneaux passifs, en particulier les doubles-cloisons, permettent d'obtenir de bonnes performances en isolation acoustique pour éliminer les bruits indésirables en moyennes et hautes fréquences. Ils ont été largement utilisés dans les domaines du bâtiment ou encore de l'industrie du transport. Un panneau hybride actif/passif est ici étudié, afin d'obtenir de bonnes performances en absorption et en isolation sur une gamme incluant des basses fréquences. La source secondaire est réalisée par une plaque active composée de deux céramiques piézo-électriques collées sur une plaque en acier. Le cœur du double panneau peut inclure un matériau poreux pour améliorer les performances de l'ensemble. Les résultats numériques et les données de mesure montrent que ces panneaux présentent sur une large bandes de fréquences de bonnes performances avec contrôle actif. Les études suivantes ont été réalisées:

(1) Les caractéristiques acoustiques du panneau passif sont analysées par la méthode des matrices de transfert, qui est basée sur les expressions des ondes planes propagées dans chaque élément de la structure : la plaque élastique, l'air et le matériau poreux, considéré comme un fluide équivalent. Les conditions aux interfaces entre chaque couche sont exprimées, puis la matrice totale de transfert du panneau est déduite. Enfin, la perte par transmission et le coefficient d'absorption sont calculés et analysés. Des exemples d'applications sont donnés à titre indicatif.

(2) La méthode des matrices de diffusion a été ensuite introduite afin de modéliser la partie active du panneau hybride. La matrice de diffusion est ainsi exprimée pour une plaque active comportant des céramiques piézo-électriques, et les performances acoustiques des panneaux hybrides ont été calculées avec et sans contrôle actif. Une étude paramétrique a permis de faire un bilan sur les possibilités effets par des panneaux hybrides en absorption et/ou en isolation.

(3) Une méthode d'éléments finis est ensuite développée afin de prendre en compte le comportement élastique du matériau poreux. En effet dans les applications vibro-acoustiques

comme celles étudiées ici, il n'est pas possible de considérer que le matériau se comporte comme un fluide équivalent sur toute la gamme de fréquences. Le modèle éléments finis du matériau poroélastique développé sous Comsol, est établi sur la base de la formulation en déplacement- pression, compte-tenu de l'élasticité du squelette et du couplage fort entre les phases solide et fluide de matériau poreau. Les conditions aux limites sur l'interface entre ce matériau et les plaques ou l'air, ont été formulées et introduites dans la discrétisation du problème. L'impédance de surface d'un matériau poroélastique a été ainsi calculée et la méthode a été validée. La perte par transmission et le coefficient d'absorption des panneaux hybrides actif/passif ont été déterminés pour différentes configurations et comparées aux résultats obtenus par la matrice de diffusion. Les résultats sont en très bon accord sur une large gamme de fréquences. Les différences s'expliquent par la prise en compte du caractère élastique du matériau poreux et par les modes de flexion d'ordres supérieurs rencontrés dans la méthode numérique.

(4) Une mise en œuvre expérimentale des panneaux hybrides a été réalisée au LMFA, en conduit pour des ondes planes en incidence normale. La méthode des deux sources a été utilisée pour déterminer les coefficients de réflexion et de transmission des structures monocouche ou multicouches. Le contrôle actif a été réalisé au moyen de l'algorithme FXLMS. Les résultats expérimentaux concordent avec les résultats obtenus par la méthode des éléments finis. Notamment, la perte par transmission de ces panneaux hybrides peut être améliorée par contrôle actif au voisinage de la fréquence de résonance.

(5) Un panneau hybride multi-cellules est constitué par la juxtaposition de plusieurs cellules individuelles : l'objectif est de réaliser un traitement acoustique de surface étendue. Le fonctionnement en contrôle actif est formalisé par l'introduction des transferts primaires et secondaires. Un modèle éléments finis est proposé à titre d'exemple, avec deux cellules séparées par une plaque rigide ou élastique. Les résultats montrent une dégradation des performances lorsque le couplage inter-cellule est fort.

Mots clés: panneau hybride, matériau poreux, matrice de transfert, matrice de diffusion, contrôle actif

Acknowledgement

There are many people without whom this work would not have been possible. I would first like to thank my supervisor, Marie-Annick Galland, for taking me on as her student and allowing me to pursue my research interests, and for her support and friendship during the course of this thesis. She is, without question, a great master with genuine knowledge on acoustics. Besides, she gave me a lot of helps not only in the daily life but also in the work when I lived in France.

I would also like to thank my co-supervisor Kean Chen, who has quite good ideas for helping me improve my work. Besides I wish to thank him for teaching me a lot on the attitude of research. When I felt lonely in France or I was worried about my works, he encouraged me greatly, and gave me many valuable suggestions to promote the advance of the work, and he also patiently and critically proofread the manuscript.

I would like to give special thanks to my colleagues in France: Azzedine Sitel, Benjamin Betgen and Cederic Batifol, who helped me very much in both the work and the language. I'm really quite grateful for their kindness.

Also I would like to thank Prof. Jincai Sun, Prof. Meiping Sheng, Prof. Hong Hou and Prof. Xiangyang Zeng. They helped me on both the work and the life when I was in Northwestern Polytechnical University of China, and they are also concerned with my thesis. I am also grateful to Prof. Sun and Prof. Hou for accepting to be members of the jury.

I would like to thank my colleagues in China: Dr. Han HU and Ms. Bing Li. They helped me fill out the documents for preparing the oral defense when I was in France and could not go back to China.

Thanks also to the friends from Lyon, with a special mentioning of Hang Yu, Dabing Luo and Chuantao Yin. They are the closest friends of mine, and they made the life in Lyon more than pleasant.

The most special thanks are to my husband, Wenxin Qu, for his support in these years. And of course to my parents, I dedicate this thesis to them.

Contents

Chapter 1

Introduction

Noise and vibration control is a very important issue in the military and civilian applications. In social life and industrial production, the noise and vibration problem has become more and more acute. With the social and economic development, people's concern on the environment is becoming more important and noise pollution as a critical environmental issue is attracting widespread attention. General speaking, excessive noise and vibration will disturb people's normal life and work, whereas long-term exposure to high noise environment can have serious damages on human hearing and physical health. Meanwhile, the strong noise will result in sound fatigue of some industrial machinery and equipment, which could shorten their working lives and even lead to accidents. In the military field, noise will affect the operational performance of certain technical weapons. Especially for the naval ships and underwater weapons, self-radiation noise will not only expose them, but also reduce the working accuracy.

The reduction of noise and vibration is a major requirement for performance, sound quality and customer satisfaction. From the view point of control strategy, it can be carried on three sides: sound source, transmission path and receiver [1]. Noise control methods can be divided into two categories: passive control and active control. The passive control technology includes sound absorption, sound insulation, use of silencers, vibration isolation, damping, and so on. The mechanism of passive control is dissipating the sound energy by the interaction between the sound waves and acoustic materials or structures. However, the passive control strategy is efficient enough at medium and high frequencies but exhibit the drawbacks at low frequencies. For example, the porous material is widely used to eliminate noise in engineering applications because of its good sound absorption performance in high

frequency. However, it has very poor absorption effect in low-frequency. In addition, for a single material, the sound absorption ability and sound insulation effect are not balanced. Such as a steel plate, it can be used as a good insulation material, but it has very poor sound absorption effect; whereas, the glass wool can nearly absorb 99% of sound, but its transmission loss has only 20dB. Therefore, we need to combine the passive method and active control technique for remedying this problem.

Active control technique can be divided into two categories [1]: active noise control and active force control. Active noise control [2] refers to utilize the sound source (such as speakers) as the secondary source to produce the secondary sound field offsetting the unwanted noise, it is in some documents also known as the "Attenuator"; active force control [3] is exciting the acoustic structure (named the primary structure) to radiate the secondary sound field. In recent years, in order to promote the active noise control technology in engineering, a new active noise control is proposed, called active acoustic structure [4], which establishes the secondary sound field by the distributed acoustic actuator, and offsets the primary sound field via adjusting the strength of the secondary source. Active acoustic structure concentrates the advantages of the active noise control and active force control method, which represents a new development stage of active control technology.

Many active acoustic structures are already available and will be introduced as a background in the next section, including active absorber structure and active insulation structure. In Sec. 1.1.1 we review the development of the active noise control, and indicate that the disadvantage of active noise control is the numbers and positions of the secondary source and error sensor strongly depend on the external environment. In Sec. 1.1.2 the proposition and characteristic of active acoustic structure have been described. In addition, it has several advantages: less number of secondary sources, less dependent on the external and expanding the band of the control frequency. Besides, the development of the active acoustic structure is reviewed in Sec. 1.1.3. In Sec. 1.1.4 we review several hybrid active acoustic structures for enhancing sound absorption and/or insulation, which combine both methods of the passive control and active control.

The mathematical methods for calculating the acoustic performance of the hybrid active acoustic structure will be introduced in Sec. 1.2. The transfer matrix method and the scattering matrix method are efficient tools for modeling or optimizing these hybrid systems because of simplicity. Indeed, they are very easy to be incorporated in the computation program for the hybrid systems which cannot be modeled by analytical methods (ex: complex boundary conditions, geometries…). However, when the porous material in the hybrid systems is elastic or coupled with an elastic plate, the elasticity of the skeleton should be considered, and the strong coupling between the solid and fluid phases cannot be ignored due

to the biphasic nature of the porous material. In this case, we review the finite element method based on (*u, p*) formulation which is efficient for modeling the poroelastic medium. We describe the objective and structure of this thesis respectively in Sec. 1.3 and 1.4.

1.1 Background

1.1.1 Active noise control

The original form of active noise control presented by Paul Leug [5, 6] consisted of sound pressure reduction by the superposition of a secondary acoustic signal 180 degrees out of phase with the unwanted sound. This idea applies the principle of sound cancellation interference to eliminate the noise, the basic schematic diagram shown in Fig.1-1.

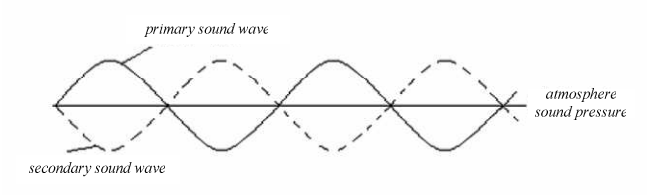

Fig.1-1 The schematic of sound cancellation interference

About 20 years later, Olson and May [7] carried out the first significant active control experiments and they also suggested a somewhat different active noise control method based on interference and proposed an electronic sound absorber to drive the acoustic pressure to zero near an error microphone placed close to a secondary loudspeaker. The electronic sound absorber consists of a microphone for receiving the error signal, a sound speaker used as secondary source, and a cavity filled with absorbent materials, shown in Fig.1-2. It has been validated that active noise control techniques are more efficient at low frequencies compared to passive method.

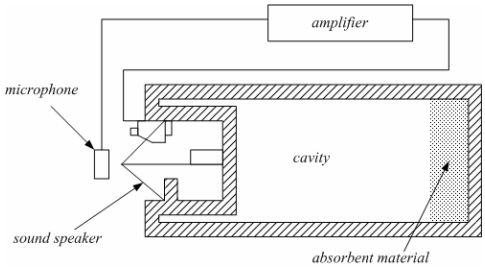

Fig.1-2 The electronic sound absorber

For several decades, active noise control has achieved great progress with the efforts of scientists in the world, and has established its own theoretical system and research methodology [8, 9], its application in engineering is also gradually becoming more mature [1,10]. In certain areas, active noise control has been applied into practical engineering, such as active control of duct noise [11, 12], active noise earmuffs, and active muffler [13~16] and so on. In three-dimensional space, the people have shown tremendous enthusiasm in active noise control. For example, 22 research institutes of European countries had finished a research on active noise control of the aircraft cabins [17]. The experimental results [18~23] proved that active noise control is feasible in large-scale complex three-dimensional sound field, however, it uses a large number of error sensors and speakers as secondary sources, which made the whole control system bulky, heavy, and very complex, thereby the stability was very poor. Besides, Deffaye and Nelson et al. [24] also proved that it is very limited to use point source offsetting the radiating noise of the structure.

Fuller and his colleagues developed the technique of active force control [25~36] for the noise vibration of the structure. They directly applied a secondary source into the vibrational structure (called primary structure), and changed the structural response to offset the radiating power. Over the past decade, although many great progresses have been obtained in active control technique, this technology has a few applications in practice. The reason is that the controlled structures in engineering application are very complex, and their vibration responses are very complicated, so that it is difficult to achieve satisfactory effect with active control [33~37]. In addition, if active force control is applied to light structures, the role of the secondary source is easy to induce the structural fatigue and to result in potential accidents, which is forbidden strictly in aviation, aerospace and other fields [36]; whereas for the massive and rigid structures (such as ships, aircraft shell, etc.), the secondary source would cost a lot of energy, inefficient and it is difficult to implement [38].

Overall, the fatal disadvantage of active noise control and active force control is the numbers and positions of the secondary sources and error sensors strongly depend on the external environment (noise source distribution, acoustic space type, etc.). For each new acoustic environment, we need to find the proper secondary sources and error sensors, which make it little progress in engineering applications [10]. In addition, it requires the error sensors in the far-field detecting acoustic radiating pressure as the error signal, which is not allowed in many cases, because the error sensor is often located at the space of people's activity.

1.1.2 The proposition and characteristic of active acoustic structure

In 1992, Fuller and his colleagues [39] proposed the concept of active acoustic structure and gave some research results. Then, Chen et al. [40] envisaged a large-area secondary source or the combination of some secondary sources based on the distributed acoustic actuator, and installed them in the surface of the primary structure. These results [39~45] show that the secondary source vibration signal and the acoustic signal in the internal cavity, which is formed by the secondary source and the primary structure, are related to the far-field acoustic parameters. Hence, these signals can be collected through the proper transformation to obtain the far-field radiated sound power, which can be called the near-field error sensing strategy [46~48]. Active acoustic structure integrates the secondary source, the reference sensor, and error sensor integrated with the adaptive controller to produce the secondary sound field for eliminating the unwanted noise. The objective of active control can be set to minimize the total radiated sound power or the reflected sound power, in which the former is called the active noise insulation structure, and the latter is named the active acoustic absorption structure.

Compared to previous active noise control system, active acoustic structure has many advantages: (1) Much less number of secondary sources are needed, which makes the controller structure and adaptive algorithm simple; (2) The sound insulation performance of the structure is less dependent on the external acoustic environment (the shape of the primary structure, spatial characteristics and the type of noise, etc.), because of the near-field error sensing strategy. It can be made as a module, which brings on the convenience to the actual installation, debugging and maintenance; (3) It combines the traditional acoustic structures and acoustic materials, which can greatly expand the band of the control frequency.

The key problems which should be solved in active acoustic structure are that: (1) the near-field error sensing strategy. The control objective of previous adaptive active noise control system is essentially based on far-field acoustic parameters (such as sound pressure, particle velocity, etc.). The disadvantage of these parameters is forming a distributed system, and even in some practical applications, these objectives can not be obtained. (2) Development of appropriate acoustic and vibration sensors and actuators to meet the system integration and reliability. Furthermore, the structures and algorithms of the active control are also very important in the design of active acoustic structure.

1.1.3 The development of active acoustic structure

Since the concept of the active acoustic structure is proposed by Fuller, more researches have attempted to develop the active acoustic structure in the aspect of smart materials. In recent years, the distributed acoustic components have made significant progress [49~52],

which excite the researches pay more attention to develop the active acoustic structure. Theses distributed acoustic components can be used as the secondary source and error sensor in active acoustic structure. For example, the elecotromechanical film (EMFi) is one of the distributed acoustic components. Its surface area can be made large enough, and its shape can be curved arbitrarily. The EMFi has been applied to reduce the cabin noise of a car and train, with the area of 1.5m×1.8m and the thickness less than 1mm [53, 54].

In 1996, the European committee of science and technology would spend 7 million euros on launching two projects for developing the distributed sound sources and the sensors in active acoustic structure. The two projects are: DAFNOR [55] (Distributed Active Foils for Noise Reduction) and the FACTS [56] (Film Actuators and Active Control of Sound for Comfort in Transportation System), the experimental results proved that the distributed acoustic actuator and sensor would be feasible in active noise control. The findings in the two projects encouraged them to carry out a further study: SOSMRT [57] (Smart Acoustics House).

Professor Chen from 2000 to 2001 in the Pennsylvania State University participated the study of the project DAFNOR [40, 58, 59]. During this period, he studied the theory of the distribution source in active insulation system and finished the experimental research. The results attracted his attention and encouraged him to study the active acoustic structure [4, 60~66], which was the first research on active acoustic structure in China. After then, he accomplished two researches of national science foundation on the active acoustic structure: “large area of active absorption layer theory” [60~62] and “Adaptive noise structure” [63~66].

The two prominent characteristics of the active acoustic structure are the distributed secondary source and the near-field error sensing strategy. In Ref. [58] and [63], a theoretical model of active acoustic structure was established and the disposition of the secondary source was proposed, but in this theoretical model the interaction between the sound field and the primary structure was neglected. Ref. [67] described the theoretical and experimental studies on the characteristics of the distributed sources, and it demonstrated the applicability of the distributed plane source in active acoustic structure. Whereas, the near-field acoustic pressure error sensing strategy is proposed in Ref. [65]. Based on the works of Ref. [65], the control effect of the distance from the pressure measuring surface to the sound source is researched in Ref. [66]. Besides, the optimization of the near-field acoustic pressure error sensor and the multi-channel algorithm of the controller have been represented respectively in Ref. [68] and [69].

In a word, many oversea and domestic researches have been made in the active acoustic structure, and great progress has been obtained in different occasions, however it is still a long

course to be developed in engineering application. Meanwhile, rapid development of high-speed microprocessors and piezoelectric ceramic materials activates active acoustic structure applied to vibration reduction and noise attenuation [70-76]. Because the efficient frequency of the active acoustic structure focuses on the low range, thereby it can be integrated with the passive absorbent materials to extend the work frequencies, which is also called the hybrid active acoustic structure. Therefore, the complementary strengths and weaknesses of passive and active noise control methods have motivated many researches to develop the hybrid active acoustic structure that combines both methods for improving the noise absorption and/or acoustical insulation.

1.1.4 The development of hybrid active acoustic structure

Active acoustic structure integrates the secondary source, the error sensing device and the controller by adjusting the signal of the secondary source so that the whole structure reaches the best acoustic performance. Its work frequency is mainly in low frequency band. For extending its work frequency to high band, numbers of experts try to apply the traditional passive materials into the active acoustic structure to form the hybrid active acoustic structure. Certain progress has been achieved in the development of the hybrid active acoustic structure, and indeed some of them also obtained a patent [77]. Researches on the hybrid active acoustic structure can be divided into two categories: the hybrid active absorption structure and the hybrid active insulation structure.

One of the first published works on the hybrid active absorption structure including both active and passive control methods is that of Guicking and Lorenz [78], and it referred to an active equivalent of the $\lambda/4$ resonance absorber, which is the conventional passive method for improving the acoustic absorption of porous layers. The passive component consisted of a porous plate located in an impedance tube of a small distance from the open end of the tube which was terminated by a control speaker. The signal from a microphone in front of the porous plate was sent to the control speaker after it was passed through a suitable amplification scheme. A second microphone controlled the complex amplification factor such that the sound pressure at that location was minimized so as to produce a pressure-release condition just behind the plate. Almost total absorption of the acoustic energy was reported over the frequency range 100-600Hz. Thereafter, Thenail [79] investigated an active system that included a fiberglass absorbing layer backed by an air cavity terminated with an active surface (shown in Fig.1-3).

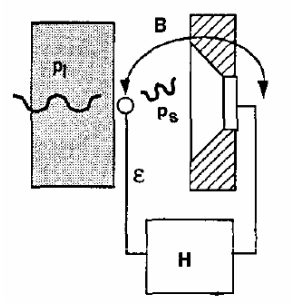

Fig.1-3 Active absorbent using a pressure-release condition

Their work was intended to show that a pressure-release condition on the back surface of the fiberglass leads to improvement in absorption. They investigated two different control approaches. In the first control approach, an error microphone was located on the back surface of the fiberglass layer, and the pressure at that location was minimized. The result of this study showed an improvement of absorption that declines with an increase in the frequency range of 200-800Hz. The second control approach investigated was identical to Guicking and Lorenz's work, where the porous plate was replaced with the fiberglass layer. Their results show almost total absorption for the frequency range of 500-1400Hz. In both control approaches, the authors used an optimum fiberglass layer thickness of 2cm.

Beyene et al. [80] proposed a hybrid passive/active system for sound absorption which is again based on the concept of mounting a layer of sound-absorbing material at a distance from a wall (shown in Fig.1-4). The motion of the wall is used to modify the layer's back impedance so as to match the characteristic impedance of air. This condition is referred as impedance matching to differentiate it from the pressure-release (zero impedance) condition. In practice, the impedance-matching condition is simply achieved by minimizing the reflected wave in the airspace behind the absorbing layer. The numerical results show high absorption (0.8-1.0) over a wide frequency range of 100-2000Hz.

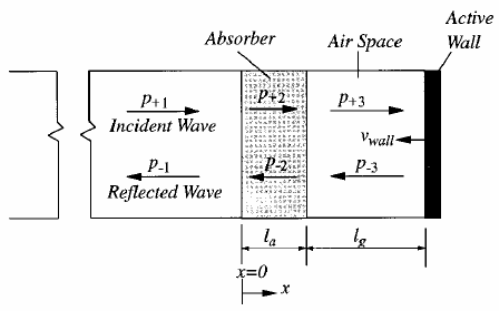

Fig.1-4 Passive/active sound absorption system

Furstoss and his colleagues [81] investigated and tested two different active systems for controlling surface normal impedance in an anechoic chamber (shown in Fig.1-5). In the first, direct impedance control simultaneously processes the acoustic pressure and velocity near a loudspeaker membrane which was driven by the controller in order to assign a prescribed impedance value for both normal and oblique plane waves. The result showed reflected waves can be cancelled over the 150-500Hz frequency wave. In the second impedance control procedure active control of the impedance at the rear face of a porous material panel was used so that the front face impedance took on a desired value. Results show that pressure release at the back face of an appropriately chosen porous panel produced high absorption over wide ranges of frequency and incidence angle.

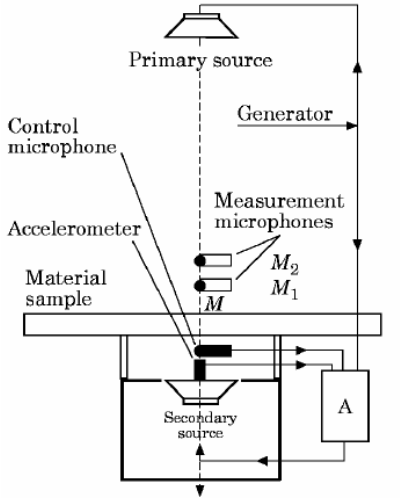

Fig.1-5 Experimental schema of active absorber in normal incident

The LMFA, Centre Acoustique, at Ecole Centrale de Lyon has developed over the last ten years a design of hybrid broadband absorbing liner which combines the passive properties of absorbent materials and active control [82-87], shown in Fig.1-6. In each cell, the passive part is considered with the determination of a suitable porous material and the cut-off frequency separating the active low frequency regime from the passive high frequency one. The active part is realized by a piezoelectric actuator as secondary source. Several single cells can be juxtaposed to form a larger active surface. The numerical results show that the combined passive/active operation can achieve significant noise reductions, between 8dB and about 20dB in flow duct, for velocities up to 50 m/s with a treated area of 0.22 m by 0.055m.

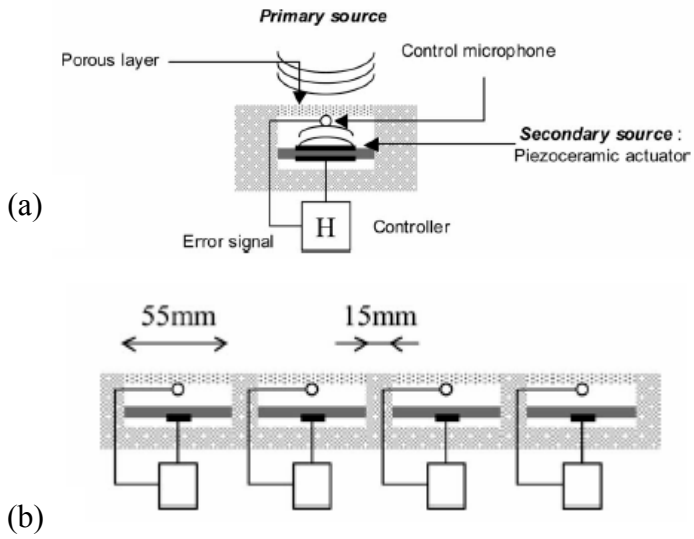

Fig.1-6 The hybrid broadband absorbing liner a) One-cell hybrid absorber; b) Extension of the liner surface.

Herzog and his colleagues [88] investigated a prototype hybrid active/passive structure consisting of a small loudspeaker in the rear of porous material. The numerical and experimental results showed that this structure has a good absorption performance at large frequency range. Leroy [89] proposed a hybrid passive/active absorber (smart foam) made up from the combination of a passive absorbent (melamine foam) and a curved PVDF film to enhance low frequency performance. The results showed that for a white noise perturbation, it is possible to achieve an absorption coefficient higher than 0.95 starting from 300 Hz for 100 dB incident pressure.

Another hybrid active insulation structures aim to improve the acoustic attenuation and transmission loss of sound waves. Many progresses have been achieved in these systems. Guigou [90] introduced a smart skin consisting of cylindrically curved PVDF piezoelectric film embedded in partially reticulated polyurethane acoustic foam for reducing the aircraft interior noise. The PVDF film is curved into a half-cylinder and embedded in two foam halves with spray glue, which leads an active cell encased in a frame. The smart skin element is composed of three active cells and is then mounted on a fuselage crown panel. The results show that as much as 13dB global passive/active attenuation was achieved at the pilot's ear level for band-limited excitation (200 Hz bandwidth).

Johnson [91] developed a piezoelectric double-amplifier active-skin with structural acoustic sensing for reducing broadband acoustic radiation from a clamped, aluminum plate. The active-skin is a continuous covering of the vibrating portions of the plate with active,

independently controllable piezoelectric, double-amplifier elements. The results indicate that total radiated power attenuation in excess of 10dB may be achieved between 250 and 750Hz.

One of the hybrid active insulation structures with superior sound insulation is the double-wall active acoustic structure, in which active control techniques have been explored to increase the noise transmission loss in the low-frequency [92-109]. The traditional double-wall structure is mainly composed of two elastic plates with the "a core" composition. The core can be an air layer or porous materials, but if only the air layer is used in this structure, less noise reduction would be obtained; thereby we often apply porous materials into the core, which can greatly improve the noise reduction of the structure, especially the sound absorption effect in high-frequency. Indeed, we can also use the combination of the air layer and porous material as the core according to the actual environmental situation, then the effective absorption frequency band would be broadened. The elastic plate can be a normal elastic plate or a micro-perforated plate, which greatly improves the absorption coefficient and sound insulation. However, such structures are efficient enough at medium and high frequencies but exhibit a lack of performance at low frequencies, where resonance inherent to the layer distribution occurs. Therefore, the active control technology can be applied into the double-wall structure with the piezoelectric ceramic as a secondary force source or the loudspeaker as a secondary sound source to improve the sound insulation in low frequency, called double-wall active acoustic structure.

Pan et al. [92] presented a theoretical model for active control of sound transmission through double-panels, in which three different control arrangements were investigated. Using control loudspeakers inside the air gap, Fonseca et al. [93] experimentally demonstrated that an active sound transmission reduction could be achieved by reducing energy transmission through the gap. After a few years, Carneal [105] developed a robust analytical model of a simply supported plate-air-plate system (shown in Fig.1-7), finding an optimal position for piezoelectric patches. The noise transmission performance from the exterior of an aircraft fuselage to the interior noise field was increased by this double-wall system consisting of a stiffer radiating panel due to its lower modal density and also as a result of better impedance matching between the piezoelectric actuator and the radiating plate.

Lee and his colleagues [106] demonstrated some experimental results obtained with a hybrid concept involving a double-plate panel with a porous material and active control (shown in Fig.1-8). A remarkable noise reduction of 5 dB at the resonance frequency was observed in addition to the 8dB reduction obtained from passive sound absorbing material in the mid frequency region.

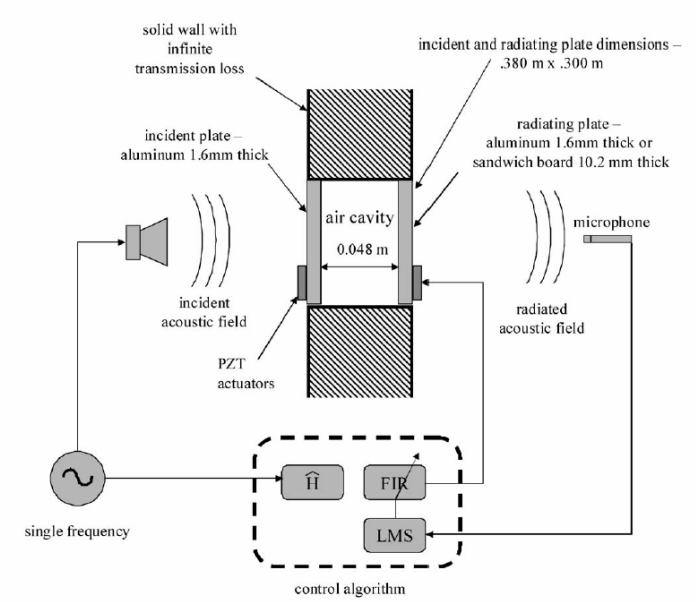

Fig.1-7 Schematic of active structural acoustic control of double panel systems

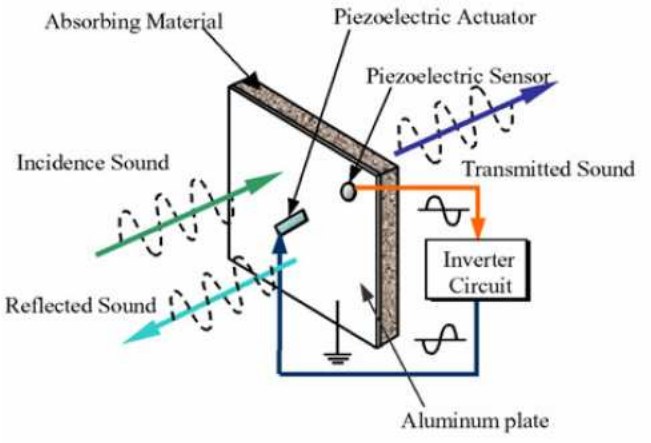

Fig.1-8 Schematic diagram of active hybrid panels

As reviewed in the above, many investigations of the hybrid active acoustic structures have been accomplished by researchers, however, the widespread design of such hybrid systems with perfect noise absorber and insulation is still an open topic, because the appropriate air gaps or porous materials, their parameters, and the optimal signal of the secondary sound sources affect strongly the noise reduction. Thus proper design and optimization of the acoustical properties of these double-wall hybrid systems has become an attractive subject.

1.2 Research method

1.2.1 Mathematical methods for modeling hybrid active acoustic structure

In real applications, in order to know the acoustical properties of a certain multilayer system easily and rapidly, prediction is often needed instead of direct measurement. Many theories have been developed for multilayer systems [110-124]. In most cases, feasible prediction via a so-called transfer matrix method [114-124] is often used. This method is based on a theory, which says that the relation between the pressure and bulk flow of two ends of a sound propagating route can be expressed by a matrix. The transfer matrix can be looked up on as an inherent property of a material because of its invariance. If the transfer matrix of a material is known, most of the acoustical properties of the material can be obtained. Because of the continuity of sound pressure and velocity, the matrices of all the component layers can be combined together into a total matrix which can be used to predict the acoustical properties of multilayer systems. The type of transfer matrix is determined by such factors as physical properties of the material, boundary conditions, selected state variables and so on.

When multilayer active acoustic structures are passive, analytical absorption coefficient and acoustic insulation can be deduced from the transfer matrix method. This matrix is easily deduced from elementary transfer matrices associated with each element or interface of the passive sandwich under consideration. Kwon and his colleague [120, 125] estimated the absorption coefficient of the perforated panel systems from the overall transfer matrix obtained by multiplying unit transfer matrices. The proposed transfer matrix method is confirmed by comparing the estimated absorption coefficient with the measured value. Lee [123] developed a modified transfer matrix method for evaluating normal incidence sound transmission loss of multilayer solid materials by taking advantage of thin plate theory and the mass law effect. The predicted results were comparable to the direct measurements via a standing wave tube method.

However, when active acoustic structures are hybrid (including active control), the transfer matrix method is not suitable to model the problem since calculations become complicate. On the other hand, it has been shown by Aböm [126-128] that the scattering matrix theory is a very suitable formulation for predicting acoustical proprieties of both passive and active discontinuities in duct systems. This scattering matrix is used to predict acoustic performances of passive two-port discontinuities in ducts such as silencers, mufflers [126] and also of two-port sources [127] for example: pump, fans having one inlet and one outlet opening. Yet, the scattering-matrix method gives the best basic description of wave interaction problem (anechoic transmission and reflection on both sides of the discontinuity,

symmetry...). It can be used even for modeling complex networks including several kinds of discontinuities [128].

Nevertheless, the scattering matrix method is not a perfect method when the hybrid active acoustic structure having the porous material which is elastic or coupled with an elastic plate. Due to the biphasic nature of porous material, the characterization of its acoustical behavior is crucial to predict the acoustic performance of the hybrid systems. For high-frequency excitation of porous materials attached to a rigid wall structure, the porous material is often considered as an equivalent fluid with effective density and bulk modulus [129]. This type of modeling applies to porous materials having a rigid skeleton, i.e., motionless or a very limp skeleton. In this case, only one compression wave propagates in the air-saturated medium, and five important parameters are needed to define the equivalent density and the equivalent impedance: porosity, resistivity, tortuosity, viscous length, and thermal length [130].

For low-frequency excitation, or porous materials attached to an elastic plate, the porous material is subject to three basic waves propagating simultaneously in the solid and fluid phase: one shearing and two compression waves. In this case, the elasticity of the skeleton should be considered, and the strong coupling between the solid and fluid phases cannot be ignored [131-135]. The mechanical behavior of poroelastic materials has been established by Biot's theory describing the propagation of elastic waves. For several decades, many works were made specifically to adapt Biot's theory to acoustic problems in porous materials [136-142]. Following these works, the equations of dynamic equilibrium of the porous medium were solved in terms of the solid and fluid displacements: u describing the displacement of the solid phase, and U describing the displacement of the fluid phase. The first model [138, 139], motivated by biomedical and geomechanical problems, are based on classical plate theory with Kirchhoff's assumptions and the (u,U) formulation of Biot's relations. More recently, Leclaire et al. [140] used the (u,U) formulation of Biot's equations to derive two equations of equilibrium for the porous plate. The main advantages of this model are the simplicity of the equations, and their capability to be solved under boundary conditions other than simply-supported edges. This model has been validated by experiments on high density clamped porous plates [141]. For simple one- or two-dimensional structures, their vibroacoustic responses can be accurately calculated by the finite element method with the (u,U) formulation, however, for complex three-dimensional structures, six degrees of freedom per node are required at least in order to calculate the vibration response, which leads to cumbersome calculations for large finite element models and spectral analysis.

To alleviate these difficulties, a mixed formulation using the displacement of the solid phase and the interstitial fluid pressure as variables was proposed by Atalla [143], called the

(u, p) formulation, which seems more suitable for large size finite element models and requires only four degrees of freedom per node. Lately, the strain couplings between the fluid and solid phases of porous materials have been derived according to the continuity of the solid phase displacement vector and the interstitial fluid pressure [144]. However, because of the biphasic nature of porous materials, in the case of broadband source excitation, excessive computing problems still exist in finite element models, hence, the (u, p) formulation needs to be simplified according to the characteristics of solid and fluid media. Dazel [145] proposed a simplified (u, p) formulation based on the dominant vibration modes of porous materials; Bermudez [146] gave a simplified finite element model for porous materials with the non-viscous and pore-interlinked fluid medium; Batifol [147, 148] deduced the partial differential equations of porous materials in the Comsol environment based on the (u, p) formulation. Etchessahar et al. used the (u, p) formulation of Biot's equations in association with the classical theory of plates to derive two coupled equations of equilibrium of a homogeneous and isotropic poroelastic plate [149, 150]. This theory is valid in the case of porous materials as long as the wavelength of the bending waves is much greater than the size of the pores. Because of these simplified finite element models, the (u, p) formulation has been widely used to the sound propagation in porous materials.

1.2.2 Measurement method of hybrid active acoustic structure

When the active acoustic structures or the boundary conditions are very complex and their acoustical properties can not be calculated by mathematical methods, direct measurement is an effective approach to predict the transmission loss and absorption. Generally speaking, the reverberation room method [151] and the standing wave tube method [152] are the two useful methods which have been widely applied to measure the acoustical properties of a certain material. In fact, the reverberation room method provides authoritative test results, but it is not easy to use. This method not only takes time, but also requires some types of equipment such as reverberation room, high quality microphone etc. Besides, the dimension of the tested structure should be large enough.

For remedying the drawback of the reverberation room method, the standing wave tube method which can measure the acoustic property of the small-dimension structures has also been used widely and adopted as an ISO standard [152]. Apfel et al. [153] developed a new laboratory method to evaluate the acoustical properties of expandable and other automotive sealants in the standing wave tube. In the method, ASTM E 1050 [154] absorption measurement equipment is used along with a new sample holder, a downstream microphone holder (providing two additional microphone locations) and an anechoic termination. Bolton et al. [155] described a two-microphone standing wave tube method for evaluating the

acoustical properties of homogeneous and isotropic porous materials based on the transfer matrix method. Zhu Beili et.al [156-158] proposed a four-microphone method to measure sound transmission loss in the standing wave tube. This method can separate the transmission wave from the reflected wave in the absorbent ending and raise the precision of the measurement in the low frequency range.

Nevertheless, the major drawback of the standing wave tube method is that an anechoic termination is required. In practice, an anechoic termination could be constructed using a long exhaust tube, high absorbing materials, horn shapes pipes or an active sound anechoic termination [159]. However, a fully anechoic termination is difficult to be built, particularly one that is effective at low frequencies. Thus, two alternative measurement approaches are considered, which do not require an anechoic termination: the two-load method [160] and the two source-location method [161]. Both methods are realized by measuring acoustic pressures at four fixed locations, two upstream and two downstream of the tested structure, with a different load or a random source on both sides of the test tube respectively. Then the four-pole parameters of the tested structure are calculated by means of a dual-channel FFT analyzer and use of the time-domain ensemble averaging. Due to the two-load method suffers from an additional disadvantage in that the two loads may not be sufficiently different at all frequencies of interest, the two source-location method is much more stable and entirely independent of the loading terminations.

1.3 Objectives of the thesis

The objective of the thesis is to design a new type of hybrid active acoustic structure combining the passive absorption properties and the principle of active noise control. It aims at not only providing perfect acoustical absorption, but also a good insulation in wide frequency band. This hybrid active acoustic structure consists of an elastic plate, an active plate and several layers such as air gaps or porous material. The piezoelectric ceramics are glued to the active plate and the positive/negative voltage is imposed on the piezoelectric ceramics to make the active plate vibrating as a secondary source. In order to analyze the acoustic properties (absorption coefficient and transmission loss) of the hybrid active acoustic structure, the structure model is first established, and the response equations of each layer in the hybrid active acoustic structure have been set up. Then the boundary conditions between the layers would be modeled according to the continuity nature of the sound pressure and the normal velocity. In addition, because of the biphasic of the porous material, the viscous and thermal effects cannot be neglected when the incident sound wave transmits through the entrance and exit of the pore in the porous material.

The designed hybrid active acoustic structure is applied to eliminate the unwanted noise. An experimental device, mainly in the assessment of performance of acoustic treatment, has been established at the **LMFA** at the **Ecole Centrale de Lyon**. Optimization of the hybrid active acoustic structure is thus directly carried out in the test section in order to achieve high levels of noise reduction. Besides, the multi-cell hybrid active acoustic structure is realized by juxtaposing several single hybrid cells for eliminating the noise in a large-area domain. In the multi-cell hybrid structures, the interface between each hybrid cell is rigid or elastic, and each cell has an error sensor for active control with the objective function of a minimum sound pressure.

1.4 Structure of the thesis

The structure of this thesis is described as follows.

In chapter 2, the transfer matrix method is applied to analyze the acoustic characteristic of the double-wall passive acoustic structure. The definition of the transfer matrix and scattering matrix are given in the acoustic structure, and the relationship between them is also expressed. Based on the sound propagation principle, the transfer matrix of the elastic plate, the air gap, the porous material and the interface between each layer are modeled and then deduced to establish the total transfer matrix of the double-wall structure. Lastly, the absorption coefficient and transmission loss of the double-wall passive acoustic structure are calculated and analyzed with some numerical examples.

In chapter 3, the work aims to develop a hybrid active acoustic structure allowing good acoustic insulation and absorption for a wide frequency range. These hybrid active acoustic structures combine passive and active means by using passive layers and active plate. The secondary source is realized by an active plate consisting of two piezoelectric patches bonded to an elastic thin plate in order to improve acoustic insulation at low and resonances frequencies. Using the scattering matrix method, the active plate has been completely described in form of a scattering matrix and a source strength vector which represents respectively the passive and active proprieties of this plate. In active control, the source strength vector of the active plate is calculated in order to minimize the sound pressure or power at the location of the error sensor. The acoustic performances of the hybrid system, the absorption coefficient and transmission loss, are then deduced from the secondary source vector and the scattering matrix coefficients of all layers or elements composing this system. Lastly, the influence factors which affect the acoustic performance of the hybrid system have been investigated by simulation on different parameters of each layer.

In chapter 4, a finite element model of hybrid active acoustic structure is developed with the (u, p) formulation in the Comsol environment. This model has considered the elasticity of

the skeleton of the poroelastic material and the strong coupling between the solid and fluid phases. Besides, the boundary conditions on the coupling surface of the elastic, poroelastic and air layers were formulated in Comsol modes. The dynamic responses of some hybrid active acoustic structures have been studied under plane wave excitation, in which piezoelectric patches are added onto the excited plate behaving as a secondary vibrational source. The resonance frequencies of these hybrid structures have been calculated by the scattering matrix method and Comsol environment. The numerical results show that sound insulation of the hybrid active acoustic structure can be improved at resonance frequencies with active control.

In chapter 5, the work aims at applying the two source-location method based on the scattering matrix for measuring the acoustic performance of the hybrid active acoustic structure, using a dSPACE-DS1103 controller implemented with Simulink for finding the optimal signal of the secondary sound source in active control. The measurement was carried out in a rectangular tube, and no anechoic termination is required. The reflection and transmission coefficients of each layer in the hybrid active acoustic structure are determined. Besides, the acoustic performance of some hybrid active acoustic structure are measured and compared to the numerical data. Their transmission losses are improved by active control, which agrees well with the numerical results in the scattering matrix method and the finite element method with Comsol software.

In chapter 6, the multi-cell hybrid active acoustic structure concept is proposed by compositing single hybrid cells for controlling the noise in a large-area domain. In the multi-cell hybrid active acoustic structure, the interface between each hybrid cell can be rigid or elastic. Each cell has an error sensor for active control and a minimum sound power can be used as the objective function. The acoustic absorption and transmission performance of these multi-cell hybrid systems have been calculated with the mixed (u, p) formulation and finite element method in Comsol environment.

In chapter 7, we give the conclusions and perspectives.

Chapter 2

Acoustic performance analysis of double-wall passive acoustic structure by transfer matrix method

The transfer matrix method is a simple method for static, dynamic and stability analysis of structures, and it means that the relationship between input and output of the linear system can be expressed in the form of a matrix. An acoustic unit, for example, as shown in Fig.2-1, considering the acoustic parameters (sound pressure and particle velocity) in the front of the unit as the input, and that in the back of the unit as the output, the transfer function of this unit based on the transfer matrix can be established, T_{11} , T_{12} , T_{21} , T_{22} are the elements of the transfer matrix.

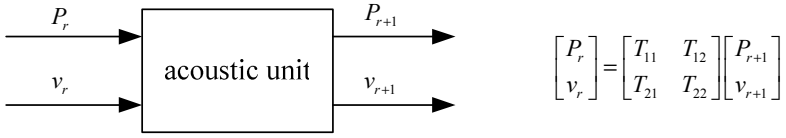

Fig.2-1 The transfer matrix of an acoustic unit

If the system's transfer matrix is known, the acoustic properties of the system (such as absorption coefficient and transmission loss) can be calculated by these four elements of the transfer matrix. For the multilayer structures, such as double-wall structures containing the elastic plate, the air gap or/and the porous material, the total transfer matrix of the structure

can be obtained by multiplying the transfer matrix of each layer, because of the continuity of sound pressure and velocity. Worthy of note is that the transfer matrix is derived based on the physical characteristics of the structure, and hence it depends on only the physical properties of the structure and boundary conditions, and is independent of external environment. In addition to the transfer matrix, the acoustic characteristics of the structure can also analyzed by the scattering matrix, the impedance matrix, and the admittance matrix.

This chapter aims to analyze the acoustic characteristic of the double-wall passive acoustic structure by the transfer matrix method. Firstly, the definition of the transfer matrix and scattering matrix are given in the acoustic structure, and the relationship between them is also expressed. Based on the sound propagation principle, the transfer matrix of the elastic plate, the air gap, the porous material and the interface between each layer are modeled and then deduced to establish the total transfer matrix of the double-wall structure. Lastly, the absorption coefficient and transmission loss of the double-wall passive acoustic structure are calculated and analyzed with some numerical examples.

2.1 The acoustic parameters of double-wall passive structures

The acoustic properties of the double-wall passive structure excited by sound waves can be described by four matrices: the transfer matrix, the scattering matrix, the impedance matrix and the admittance matrix. These four matrices depend on the characteristic of the structures, and are independent of the sound source location and intensity. Besides, the linear relationship exists between each other. In this section, the sound pressure and the normal particle velocity are firstly expressed on both sides of double-wall passive structure. Then, the definitions of the transfer matrix, the scattering matrix, the impedance matrix and the admittance matrix and the relationship between each matrix are described. Lastly, the transmission loss and the absorption coefficient of the structure derived from the transfer matrix.

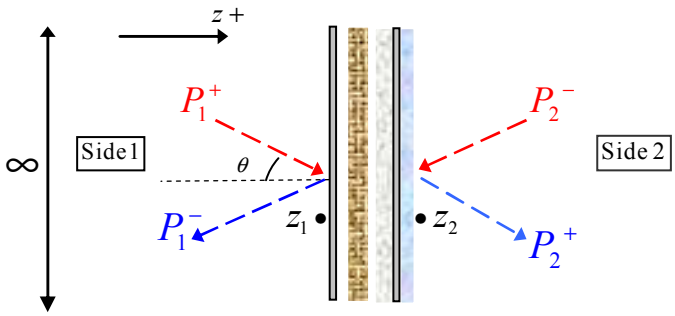

Fig.2-2 The schematic of a passive system with infinite laterally dimensions

Consider a passive system (ex: elastic plate, porous layer…) located between the axial coordinates z_1 on the left side and z_2 on the right side as shown in Fig.2-2, supposing that two plane waves P_1^+, P_2^- excite this system on both sides with the angle θ.

2.1.1 The sound pressure and the normal particle velocity

Suppose the medium (here is air) on both sides of the structure is an ideal fluid and uniform, and the sound propagation is adiabatic. In the Cartesian coordinate $(0,x,z)$ system, the sound pressure in the point $M_1(x,z_1)$, $M_2(x,z_1)$ close to the surface of the structure can be expressed as,

$$P_1 = P_1(x,z_1,t) = (P_1^+ e^{-j(k_z z_1 + k_x x)} + P_1^- e^{j(k_z z_1 + k_x x)}) e^{j\omega t} \tag{2-1}$$

$$P_2 = P_2(x,z_2,t) = (P_2^+ e^{-j(k_z z_2 + k_x x)} + P_2^- e^{j(k_z z_2 + k_x x)}) e^{j\omega t} \tag{2-2}$$

Here, P_1^+ represents the amplitude of the plane wave with the z positive direction on the left side of the structure; P_2^- represents the amplitude of the plane wave with the z negative direction on the right side of the structure; P_1^- represents the amplitude of the plane wave with the z negative direction on the left side of the structure, and it consists of the reflected wave produced by the incident wave P_1^+ and transmitted wave produced by the incident P_2^-; P_2^+ represents the amplitude of the plane wave with the z positive direction on the right side of the structure, and it consists of the reflected wave produced by the incident wave P_2^- and transmitted wave produced by the incident P_1^+; $k = \omega / c_0$ is the total wave number ; $k_z = k\cos\theta$ is the wave number in the direction of z axis; $k_x = k\sin\theta$ is the wave number in the direction of x axis; c_0 is the sound velocity ; ω is the angular frequency.

For the convenience, the simplified expressions can be rewritten as,

$$\begin{aligned} P_1^+ &= P_1^+ e^{-j(k_z z_1 + k_x x)} \\ P_1^- &= P_1^- e^{j(k_z z_1 + k_x x)} \\ P_2^+ &= P_2^+ e^{-j(k_z z_2 + k_x x)} \\ P_2^- &= P_2^- e^{j(k_z z_2 + k_x x)} \end{aligned} \tag{2-3}$$

According to the wave motion equations, the particle velocity at $M_1(x,z_1)$, $M_2(x,z_1)$ can be expressed as,

$$V_1^z = V_1^z(x,z) = Y(P_1^+ - P_1^-) \tag{2-4}$$

$$V_2^z = V_2^z(x,z) = Y(P_2^+ - P_2^-) \tag{2-5}$$

Here, $Y = \dfrac{\cos\theta}{Z_0}$ is the admittance; $Z_0 = \rho_0 c_0$ is the Medium characteristic impedance.

2.1.2 The acoustic matrices

1. The transfer matrix

The transfer matrix **T** reflects the relationship between input and output of linear system. For the double-wall structure, considering the acoustic parameters (sound pressure and particle velocity) in the front of the structure as the input, and that in the back of the structure as the output, the transfer function of this structure based on the transfer matrix can be established and expressed as,

$$\begin{bmatrix} P_1 \\ V_1^z \end{bmatrix} = \mathbf{T} \cdot \begin{bmatrix} P_2 \\ V_2^z \end{bmatrix}, \quad \mathbf{T} = \begin{bmatrix} T_{11} & T_{12} \\ T_{21} & T_{22} \end{bmatrix} \tag{2-6}$$

Here, T_{11}, T_{12}, T_{21}, T_{22} are the elements of the transfer matrix.

2. The scattering matrix

When linear theory is valid, the acoustical behavior of this system can be described completely by its scattering matrix **D** which gives linear relationships between the incoming pressure wave vector $\begin{bmatrix} P_1^+ & P_2^- \end{bmatrix}^T$ and the outgoing pressure wave vector $\begin{bmatrix} P_1^- & P_2^+ \end{bmatrix}^T$:

$$\begin{bmatrix} P_1^- \\ P_2^+ \end{bmatrix} = \mathbf{D} \cdot \begin{bmatrix} P_1^+ \\ P_2^- \end{bmatrix}, \mathbf{D} = \begin{bmatrix} D_{11} & D_{12} \\ D_{21} & D_{22} \end{bmatrix} \tag{2-7}$$

This matrix **D** is independent of the upstream and the downstream acoustic conditions and is filled by four coefficients, and the physical meaning of each coefficient is as follows: D_{11} and D_{21} represents respectively anechoic reflection and transmission coefficients associated with the left side incoming waves; D_{22} and D_{12} represents respectively anechoic reflection and transmission coefficients associated with the right side incoming waves. The superscript '+' and '-' represent the positive and negative direction of *z* axis respectively. If the structure is symmetry, and the mediums on both sides of the structure are same, we have,

$$D_{11} = D_{22}, \quad D_{12} = D_{21} \tag{2-8}$$

3. The impedance matrix and the admittance matrix

The impedance matrix **Z** reflects the relationship between the sound pressure and the normal particle velocity on both sides of the structure, defined as:

$$\begin{bmatrix} P_1 \\ P_2 \end{bmatrix} = \mathbf{Z} \cdot \begin{bmatrix} V_1^z \\ V_2^z \end{bmatrix}, \quad \mathbf{Z} = \begin{bmatrix} Z_{11} & Z_{12} \\ Z_{21} & Z_{22} \end{bmatrix} \tag{2-9}$$

Therefore, the inverse of the impedance matrix is the admittance matrix **Y**, expressed as,

$$\begin{bmatrix} V_1^z \\ V_2^z \end{bmatrix} = \mathbf{Y} \cdot \begin{bmatrix} P_1 \\ P_2 \end{bmatrix}, \quad \mathbf{Y} = \begin{bmatrix} Y_{11} & Y_{12} \\ Y_{21} & Y_{22} \end{bmatrix} \tag{2-10}$$

Seen from the above definition, the scattering matrix is the most direct and clear way to describe the acoustic characteristic of double-wall structure. Its elements directly give the reflection and transmission coefficients under the positive and negative directions of the incident sound wave. Based on the scattering matrix, we can deduce the energy dissipation of the structure, including the transmission loss, the absorption coefficient which directly reflects of the acoustic properties of the structure. Meanwhile, the four matrices are directly determined by the inherent properties of the structure, and independent of the sound source location. Because of the linear relationship between each matrix, when one of the matrices is known, the others can be derived easily.

2.1.3 The transformation of the matrices

1. Transformation between the transfer matrix and the scattering matrix

Eq. (2-6) can be written as,

$$\begin{aligned} P_1 &= T_{11} P_2 + T_{12} V_2^z \\ V_1 &= T_{21} P_2 + T_{22} V_2^z \end{aligned} \tag{2-11}$$

Substituting Eq. (2-1) ~ (2-5) into Eq. (2-6), we get,

$$\begin{aligned} P_1^+ + P_1^- &= T_{11}\left(P_2^+ + P_2^-\right) + T_{12} Y \left(P_2^+ - P_2^-\right) \\ P_1^+ - P_1^- &= \frac{T_{21}}{Y}\left(P_2^+ + P_2^-\right) + T_{22}\left(P_2^+ - P_2^-\right) \end{aligned} \tag{2-12}$$

Eq. (2-12) can be expressed as follows,

$$P_1^+ + P_1^- = X^+ P_2^+ + X^- P_2^- \tag{2-13}$$

$$P_1^+ - P_1^- = W^+ P_2^+ + W^- P_2^- \tag{2-14}$$

Here

$$X^{\pm} = T_{11} \pm Y T_{12} \quad \text{and} \quad W^{\pm} = \frac{T_{21}}{Y} \pm T_{22} \tag{2-15}$$

After simply mathematical operation with Eq. (2-13) and (2-14), we have,

$$P_1^- = \frac{\left(X^+ - W^+\right)}{\left(X^+ + W^+\right)} P_1^+ + \frac{\left(X^+ W^- - W^+ X^-\right)}{\left(X^+ + W^+\right)} P_2^- \tag{2-16}$$

$$P_2^+ = \frac{2}{X^+ + W^+} P_1^+ - \frac{X^- + W^-}{X^+ + W^+} P_2^- \tag{2-17}$$

Eq. (2-16) and (2-17) can be written in a matrix, and the four coefficients of the scattering matrix are expressed in terms of the transfer matrix,

$$\begin{bmatrix} P_1^- \\ P_2^+ \end{bmatrix} = \begin{bmatrix} D_{11} & D_{12} \\ D_{21} & D_{22} \end{bmatrix}_{2\times 2} \cdot \begin{bmatrix} P_1^+ \\ P_2^- \end{bmatrix} \tag{2-18}$$

Here

$$D_{12} = \frac{X^+W^- - W^+X^-}{X^+ + W^+} \tag{2-19}$$

$$D_{11} = \frac{X^+ - W^+}{X^+ + W^+} \tag{2-20}$$

$$D_{21} = \frac{2}{X^+ + W^+} \tag{2-21}$$

$$D_{22} = -\frac{X^- + W^-}{X^+ + W^+} \tag{2-22}$$

2. Transformation between the transfer matrix and the impedance matrix

Eq. (2-6) can be written as:

$$P_1 = Z_{11}V_1^z + Z_{12}V_2^z \tag{2-23}$$

$$P_2 = Z_{21}V_1^z + Z_{22}V_2^z \tag{2-24}$$

After simply mathematical operation with Eq. (2-23) and (2-24), we have,

$$P_1 = \frac{Z_{11}}{Z_{21}}P_2 + \left(Z_{12} - \frac{Z_{22}}{Z_{21}}\right)V_2^z \tag{2-25}$$

$$V_1 = \frac{1}{Z_{21}}P_2 - \frac{Z_{22}}{Z_{21}}V_2^z \tag{2-26}$$

Eq. (2-25) and (2-26) can be written in a matrix, and compared to Eq. (2-6), we get,

$$T_{11} = \frac{Z_{11}}{Z_{21}} \quad T_{12} = Z_{12} - \frac{Z_{22}}{Z_{21}} \tag{2-27}$$

$$T_{21} = \frac{1}{Z_{21}} \quad T_{22} = -\frac{Z_{22}}{Z_{21}} \tag{2-28}$$

2.1.4 The acoustic properties of the double-wall structure

1. Transmission loss

When the structure is excited only by the incident wave from the left side, the transmission loss $TL_{(1)}$ can be obtained by the scattering matrix element D_{21},

$$TL_{(1)} = 10\log\left(\frac{1}{|D_{21}|^2}\right) \tag{2-29}$$

When the structure is excited only by the incident wave from the right side, the transmission loss $TL_{(2)}$ can be obtained by the scattering matrix element D_{12},

$$TL_{(2)} = 10\log\left(\frac{1}{|D_{12}|^2}\right) \tag{2-30}$$

2. Absorption coefficient

When the structure is excited only by the incident wave from the left side, the absorption coefficient $\alpha_{(1)}$ can be obtained by the scattering matrix element D_{11},

$$\alpha_{(1)} = 1 - |D_{11}|^2 \tag{2-31}$$

When the structure is excited only by the incident wave from the right side, the absorption coefficient $\alpha_{(2)}$ can be obtained by the scattering matrix element D_{22},

$$\alpha_{(2)} = 1 - |D_{22}|^2 \tag{2-32}$$

3. Loss power

The energy loss power W_{loss} of the double-wall structure is defined as the difference between the input power W_{in} and the radiating power W_{rad},

$$W_{loss} = W_{in} - W_{rad} \tag{2-33}$$

According to the definition of the sound power, we have,

$$W_{in} = \int_S I_{in}^z dS = \int_S I_{in}^z(z_1, x, y)dS + \int_S I_{in}^z(z_2, x, y)dS \tag{2-34}$$

$$W_{rad} = \int_S I_{rad}^z dS = \int_S I_{rad}^z(z_1, x, y)dS + \int_S I_{rad}^z(z_2, x, y)dS \tag{2-35}$$

Here, $I_{in}^z(z_1, x, y)$, $I_{in}^z(z_2, x, y)$ represent respectively the normal incident sound intensity at the points $M_1(z_1, x, y)$ and $M_2(z_2, x, y)$; $I_{rad}^z(z_1, x, y)$, $I_{rad}^z(z_2, x, y)$ represent respectively the normal radiating sound intensity at the points $M_1(z_1, x, y)$ and $M_2(z_2, x, y)$.

According to the definition of the sound intensity, the normal sound intensity can be expressed by the normal particle velocity and the acoustic pressure,

$$I^z = \frac{1}{2}\mathrm{Re}\left(PV^{z*}\right) \tag{2-36}$$

Hence,

$$I_{in}^{z} = I_{in}^{z}(z_1, x, y) + I_{in}^{z}(z_2, x, y) = \frac{\cos(\theta)}{2\rho_0 c_0}\left(\left|P_1^{+}\right|^2 + \left|P_2^{-}\right|^2\right) \tag{2-37}$$

$$I_{rad}^{z} = I_{rad}^{z}(z_1, x, y) + I_{rad}^{z}(z_2, x, y) = \frac{\cos(\theta)}{2\rho_0 c_0}\left(\left|P_1^{-}\right|^2 + \left|P_2^{+}\right|^2\right) \tag{2-38}$$

In the plane wave excited, the normal sound intensity does not change with x, y,

$$W_{in} = S \cdot I_{in}^{z} = X^2\left(\left|P_1^{+}\right|^2 + \left|P_2^{-}\right|^2\right) \tag{2-39}$$

$$W_{rad} = S \cdot I_{rad}^{z} = X^2\left(\left|P_1^{-}\right|^2 + \left|P_2^{+}\right|^2\right) \tag{2-40}$$

Here, $X = \sqrt{S \cdot \frac{\cos(\theta)}{2\rho_0 c_0}}$; $S = ab$ is the cross-section area of the double-wall structure.

With some mathematical operation, W_{in} and W_{rad} can be rewritten as,

$$W_{in} = \mathbf{\Pi}_{in}{}^{H} \times \mathbf{\Pi}_{in} \tag{2-41}$$

$$W_{rad} = \mathbf{\Pi}_{rad}{}^{H} \times \mathbf{\Pi}_{rad} \tag{2-42}$$

Here, $\mathbf{\Pi}_{in} = X \cdot \begin{bmatrix} P_1^{-} & P_2^{+} \end{bmatrix}^T$; $\mathbf{\Pi}_{rad} = X \cdot \begin{bmatrix} P_1^{+} & P_2^{-} \end{bmatrix}^T$; Subscript H is the conjugate transpose.

Substituting Eq. (2-41) ~ (2-42) into Eq. (2-33), we get,

$$W_{loss} = \mathbf{\Pi}_{in}{}^{H} \times \mathbf{\Pi}_{in} - \mathbf{\Pi}_{rad}{}^{H} \times \mathbf{\Pi}_{rad} \tag{2-43}$$

According to the definition of the scattering matrix, we have,

$$\begin{bmatrix} P_1^{-} \\ P_2^{+} \end{bmatrix} = \mathbf{D} \cdot \begin{bmatrix} P_1^{+} \\ P_2^{-} \end{bmatrix} \Rightarrow \quad \mathbf{\Pi}_{rad} = \mathbf{D} \cdot \mathbf{\Pi}_{in} \tag{2-44}$$

Substituting Eq. (2-44) into Eq. (2-43), we get,

$$W_{loss} = \mathbf{\Pi}_{in}{}^{H} (\mathbf{I} - \mathbf{H}) \cdot \mathbf{\Pi}_{in} \tag{2-45}$$

Here, $\mathbf{H} = \mathbf{D}^{H} \cdot \mathbf{D}$; $\mathbf{I}$ is an unit matrix.

Obviously, $\mathbf{H}$ is a positive definite matrix, then an unit matrix $\mathbf{U}$ can make

$$\mathbf{H} = \mathbf{U} \cdot \begin{bmatrix} \lambda_1 & 0 \\ 0 & \lambda_2 \end{bmatrix} \cdot \mathbf{U}^{H} \tag{2-46}$$

Here, λ_1, λ_2 are the eigenvalues of the matrix $\mathbf{H}$; $\mathbf{U}$ is the eigenvector of the matrix $\mathbf{H}$.

And

$$\mathbf{I} = \mathbf{U} \cdot \mathbf{U}^{H} \tag{2-47}$$

Substituting Eq. (2-46) and (2-47) into Eq. (2-45), we get,

$$W_{loss} = \mathbf{\Pi}_{in}{}^{H}\mathbf{U}\begin{bmatrix} 1-\lambda_1 & 0 \\ 0 & 1-\lambda_2 \end{bmatrix}\mathbf{U}^{H}\mathbf{\Pi}_{in} \tag{2-48}$$

Defining

$$\mathbf{d} = \mathbf{U}^{H}\mathbf{\Pi}_{in} \tag{2-49}$$

Then

$$W_{loss} = \mathbf{d}^{H}\left[diag(1-\lambda_j)\right]\mathbf{d}, \quad j = 1,2 \tag{2-50}$$

Eq. (2-50) can be rewritten as,

$$W_{loss} = \sum_{j=1}^{2}\xi_j \left|d_j\right|^2, \quad \xi_j = 1-\lambda_j \tag{2-51}$$

Defining with decibel (dB),

$$W_{loss} = 10\log\left(\frac{W_{in}}{W_{rad}}\right) \tag{2-52}$$

$$W_{loss} = 10\log\left(\frac{|d_1|^2 + |d_2|^2}{\lambda_1|d_1|^2 + \lambda_2|d_2|^2}\right) \tag{2-53}$$

Eq. (2-53) means that if $\lambda_{j=1,2} < 1$, the double-wall structure has energy dissipation; if $\lambda_{j=1,2} = 1$, it has not energy dissipation.

2.2 The derivations of the transfer matrix

This section presents the transfer matrix of the air layer, the porous material, the elastic plate and the interface between them. Besides, the total transfer matrices of some multilayer systems are given.

2.2.1 The transfer matrix of air layer

A normal plane wave transmits into an air layer with the thickness l (seeing in Fig.2-3), the acoustic waves I and R at the point M_1 respectively are the incident and reflected waves along the z direction. P_1, v_1 represent the total sound pressure and normal velocity at the point M_1; P_2, v_2 represent the total sound pressure and normal velocity at the point M_2.

When the acoustic wave transmits into the air layer from point M_1 to point M_2, we have:

$$\begin{cases} P_1 = I + R \\ v_1 = \dfrac{1}{Z_0}(I - R) \end{cases} \tag{2-54}$$

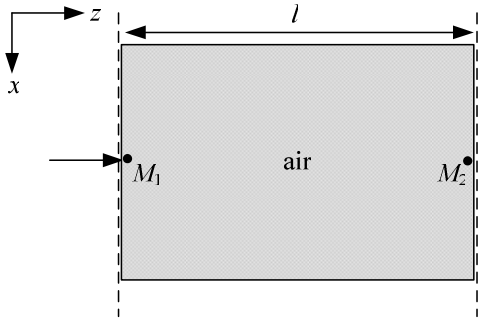

Fig.2-3 The transfer matrix of the air layer

$$\begin{cases} P_2 = I \cdot e^{-jk_0 l} + R \cdot e^{jk_0 l} \\ v_2 = \dfrac{1}{Z_0}(I \cdot e^{-jk_0 l} - R \cdot e^{jk_0 l}) \end{cases} \tag{2-55}$$

Here, $Z_0 = \rho_0 C_0$, $k_0 = \omega / C_0$, ρ_0, C_0 are respectively the density and the sound velocity of the air.

Substituting Eq. (2-55) to (2-54) with mathematic operation, Eq. (2-54) can be expressed as:

$$\begin{cases} P_1 = P_2 \cos k_0 l + jZ_0 v_2 \sin k_0 l \\ v_1 = \dfrac{1}{Z_0}(jP_2 \sin k_0 l + Z_0 v_2 \cos k_0 l) \end{cases} \tag{2-56}$$

Eq. (2-56) is rewritten in the form of a matrix:

$$\begin{bmatrix} P_1 \\ v_1 \end{bmatrix} = \begin{bmatrix} \cos k_0 l & jZ_0 \sin k_0 l \\ j \sin k_0 l / Z_0 & \cos k_0 l \end{bmatrix} \cdot \begin{bmatrix} P_2 \\ v_2 \end{bmatrix} \tag{2-57}$$

Hence

$$\mathbf{T_a} = \begin{bmatrix} \cos k_0 l & jZ_0 \sin k_0 l \\ j \sin k_0 l / Z_0 & \cos k_0 l \end{bmatrix} \tag{2-58}$$

Eq. (2-58) is the transfer matrix of the air layer.

2.2.2 The transfer matrix of porous material

A normal plane wave transmits into a porous material with the thickness l, seeing in Fig.2-4.

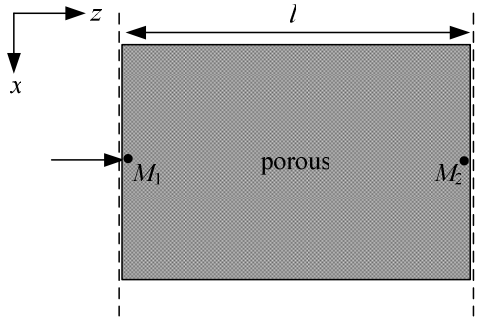

Fig.2-4 The transfer matrix of the porous material

Suppose the porous material is rigid, its transfer matrix can be written as Eq. (2-59) by changing the impedance of the air Z_0 into the impedance of the porous material Z_c, according to Lafarge-Allard's theory [130].

$$\mathbf{T}_{\mathbf{poro}} = \begin{bmatrix} \cos k_c l & jZ_c \sin k_c l \\ j \sin k_c l / Z_c & \cos k_c l \end{bmatrix} \tag{2-59}$$

Here, Z_c, k_c are the impedance and wave number of the porous material respectively, detailed as follows. Eq. (2-59) is the transfer matrix of the porous material.

Herein, the porous material is assumed to behave like a visco-thermal equivalent fluid and supposed to have a rigid frame, either because of its very high density or elasticity modulus or because of its working conditions (when placed on a rigid wall for instance). In this situation the acoustic waves may only propagate in the air contained in the pores of the material. In the reason of thermal and viscous effects occurring in the pores of the medium, some acoustic wave is diffused in heat and sound energy is then absorbed. For obtaining the impedance Z_c and the wave number k_c of the porous medium, Lafarge-Allard's theory [130] requires five intrinsic invariant and independent parameters which are defined below.

When a porous material with fixed thickness e is submitted to a difference of static pressure $\Delta P = P_2 - P_1$, and a macroscopic flow of average velocity v appears through the material, the resistivity is defined by the ratio of the static pressure difference to the product of the velocity and the thickness of the porous sample (Darcy's law):

$$\sigma = \frac{\Delta P}{ve} \tag{2-60}$$

The porosity of a porous material is the ratio of the volume of fluid contained in the pores Vol_{fluid} to the total volume of the material Vol_{tot}:

$$\phi = \frac{Vol_{fluid}}{Vol_{tot}} \tag{2-61}$$

The tortuosity is a dimensional quantity which takes into account the sinuous fluid paths through the porous material.

$$\alpha_\infty = \frac{\int_V |v|^2 \, dV}{\left| \int_V v dV \right|^2} \tag{2-62}$$

Here v is the microscopic velocity and V is a homogenization volume of the material.

The viscous characteristic length Λ has been introduced by Johnson [163] in order to establish a new expression of the effective density taking into account the high frequency viscous and inertial effects.

$$\Lambda = s\left(\frac{8\alpha_\infty \eta}{\phi \sigma} \right)^{1/2} \tag{2-63}$$

The thermal characteristic length Λ', which has been defined by Champoux and Allard [164], describes the thermal exchanges between the material frame and the pore saturating fluid.

$$\Lambda' = s'\left(\frac{8\alpha_\infty \eta}{\phi \sigma} \right)^{1/2} \tag{2-64}$$

Here s and s' are the shape factors, η is the dynamic viscosity of air.

The effective density and bulk modulus frequency dependences in the Lafarge-Allard's theory [130] are expressed as:

$$\rho_e(\omega) = \alpha_\infty \rho_0 \left[1 + \frac{\sigma \phi}{j\omega \rho_0 \alpha_\infty} \left(1 + \frac{4 j \alpha_\infty^2 \eta \rho_0 \omega}{\sigma^2 \Lambda^2 \phi^2} \right)^{1/2} \right] \tag{2-65}$$

$$K(\omega) = \frac{\gamma P_0}{\gamma - (\gamma - 1)\left[1 + \frac{8\eta}{j\omega \Lambda'^2 \, \mathrm{Pr} \, \rho_0} \left(1 + \frac{j \rho_0 \omega \Lambda'^2 \, \mathrm{Pr}}{16\eta} \right)^{1/2} \right]^{-1}} \tag{2-66}$$

Here Pr=0.702 is Prandtl number and γ is the specific heat ratio.

Hence, in the scattering matrix method, the impedance Z_c and the wave number k_c of the porous material is calculated by the effective density $\rho_e(\omega)$ and the bulk modulus $K(\omega)$, expressed as:

$$Z_c(\omega)=\sqrt{\rho_e(\omega)K(\omega)}\,,\qquad k_c(\omega)=\omega\sqrt{\frac{\rho_e(\omega)}{K(\omega)}} \tag{2-67}$$

2.2.3 The transfer matrix of an elastic plate

A normal plane wave transmits through an elastic plate from the point M_1 to the point M_2, seeing in Fig.2-5. P_1, v_1 represent the total sound pressure and normal velocity at the point M_1; P_2, v_2 represent the total sound pressure and normal velocity at the point M_2; Z_p, v_p represent the impedance and normal velocity of the elastic plate.

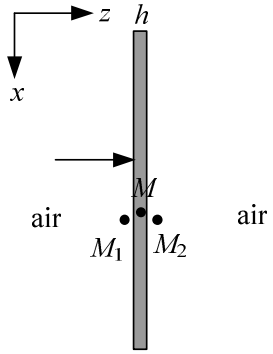

Fig.2-5 The transfer matrix of the elastic plate

According to Newton second law and the continuity of the normal velocity at the interface, we can get the expressions as follows:

$$\begin{cases} P_1-P_2=Z_p v_p \\ v_p=v_1=v_2 \end{cases} \tag{2-68}$$

If this elastic plate is infinite, the mass law is widely used and Z_p is defined as $Z_p=j\rho_s h\omega$, where ρ_s, h are respectively the density and the thickness of the plate. For the plate with finite dimension, therefore, structural modes have to be taken into account. The plate is supposed to be simply supported and only the first mode is considered. The plate impedance becomes $Z_p=\frac{k_s}{j\omega}+j\rho_s h\omega$, where the stiffness k_s is adjusted to get the resonance and the vibrational modes.

Eq. (2-68) can be written in the form of a matrix:

$$\begin{bmatrix} P_1 \\ v_1 \end{bmatrix}=\begin{bmatrix} 1 & Z_p \\ 0 & 1 \end{bmatrix}\cdot\begin{bmatrix} P_2 \\ v_2 \end{bmatrix} \tag{2-69}$$

Hence

$$\mathbf{T}_{\mathbf{a/pl/a}} = \begin{bmatrix} 1 & Z_p \\ 0 & 1 \end{bmatrix} \tag{2-70}$$

Eq. (2-70) is the transfer matrix of the elastic plate.

2.2.4 The transfer matrix between different media

1. Air layer and porous material

A normal plane wave transmits into a porous material with the thickness l from the point M_1 at the air layer to the point M_2 at the porous material, seeing in Fig.2-6. P_1, v_1 represent the total sound pressure and normal velocity at the point M_1; P_2, v_2 represent the total sound pressure and normal velocity at the point M_2; ϕ is the porosity of the porous material.

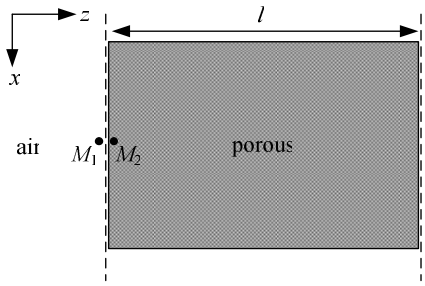

Fig.2-6 The transfer matrix of the interface between air layer and porous material

According to the continuity of the acoustic pressure and the normal velocity at the interface of the air layer and the porous material, we can get the expressions as follows:

$$\begin{cases} P_1 = P_2 \\ v_1 = v_2\phi \end{cases} \tag{2-71}$$

Eq. (2-71) can be written in the form of a matrix:

$$\begin{bmatrix} P_1 \\ v_1 \end{bmatrix} = \begin{bmatrix} 1 & 0 \\ 0 & \phi \end{bmatrix} \cdot \begin{bmatrix} P_2 \\ v_2 \end{bmatrix} \tag{2-72}$$

Hence,

$$\mathbf{T}_{\mathbf{a/poro}} = \begin{bmatrix} 1 & 0 \\ 0 & \phi \end{bmatrix} \tag{2-73}$$

Eq. (2-73) is the transfer matrix of the interface between air layer and porous material.

If the plane wave transmits into an air layer from point M_1 at the porous material to point M_2 at air layer, the transfer matrix of the interface between porous material and air layer can be written as:

$$\mathbf{T}_{\mathbf{poro/a}} = \left(\mathbf{T}_{\mathbf{a/poro}}\right)^{-1} = \begin{bmatrix} 1 & 0 \\ 0 & 1/\phi \end{bmatrix} \tag{2-74}$$

2. Air layer, elastic plate and porous material

A normal plane wave transmits into a porous material from the point M_1 at the air layer to the point M_2 at the porous material by the point M at the elastic plate which is infinite and simply supported, seeing in Fig.2-7. P_1, v_1 represent the total sound pressure and normal velocity at the point M_1; P_2, v_2 represent the total sound pressure and normal velocity at the point M_2; ϕ is the porosity of the porous material; Z_p, v_p represent the impedance and normal velocity of the elastic plate.

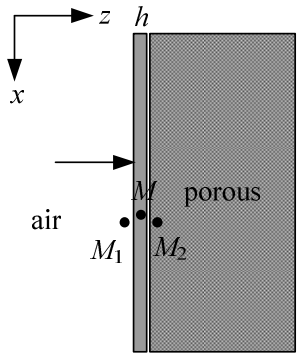

Fig.2-7 The transfer matrix of the interface between air layer, elastic plate and porous material

According to Newton second law and the continuity of the normal velocity at the interface, we can get the expressions as follows:

$$\begin{cases} P_1 - P_2 = Z_p v_p \\ v_p = v_1 = v_2 \phi \end{cases} \tag{2-75}$$

Eq. (2-75) can be written in the form of a matrix:

$$\begin{bmatrix} P_1 \\ v_1 \end{bmatrix} = \begin{bmatrix} 1 & Z_p\phi \\ 0 & \phi \end{bmatrix} \cdot \begin{bmatrix} P_2 \\ v_2 \end{bmatrix} \tag{2-76}$$

Hence

$$\mathbf{T}_{\mathbf{a/pl/poro}} = \begin{bmatrix} 1 & Z_p\phi \\ 0 & \phi \end{bmatrix} \tag{2-77}$$

Eq. (2-77) is the transfer matrix of the interface between the air layer, elastic plate and porous material.

If the plane wave transmits into an air layer from point M_1 at the porous material to point M_2 at air layer by point M at the elastic plate, the transfer matrix of the interface between the porous material, elastic plate and air layer can be written as:

$$\mathbf{T}_{\mathbf{poro/pl/a}} = \left(\mathbf{T}_{\mathbf{a/pl/poro}}\right)^{-1} = \begin{bmatrix} 1 & Z_p \\ 0 & 1/\phi \end{bmatrix} \tag{2-78}$$

2.2.5 The total transfer matrix

The total transfer matrix of the multilayer systems consisting of several layers, such as air layer, porous material and elastic plate, can be calculated by the transfer matrices of each layer and their interfaces. Considering the simple system 'air/porous material/air' (seeing in Fig.2-8), the normal plane wave transmits through a porous material with the thickness l and an air layer with the thickness h from point M_1 at the front of the porous material to point M_2 at the back of the porous material.

The total sound pressure P_1 and normal velocity v_1 at the point M_1 can be expressed as:

$$\begin{bmatrix} P_1 \\ v_1 \end{bmatrix} = \mathbf{T}_{\mathbf{a/poro}} \cdot \mathbf{T}_{\mathbf{poro}} \cdot \mathbf{T}_{\mathbf{poro/a}} \cdot \begin{bmatrix} P_2 \\ v_2 \end{bmatrix} \tag{2-79}$$

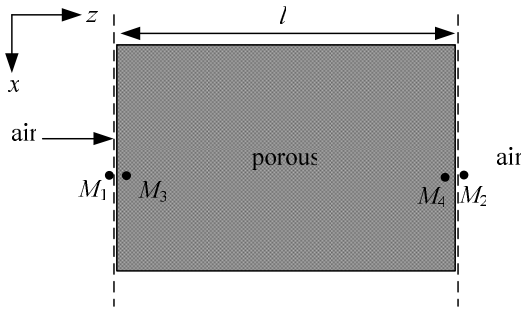

Fig.2-8 The total transfer matrix of the air/porous material/air

Then the total transfer matrix can be written as:

$$\begin{aligned} \mathbf{T}_{\mathbf{total}} &= \mathbf{T}_{\mathbf{a/poro}} \cdot \mathbf{T}_{\mathbf{poro}} \cdot \mathbf{T}_{\mathbf{poro/a}} \\ &= \begin{bmatrix} 1 & 0 \\ 0 & \phi \end{bmatrix} \cdot \begin{bmatrix} \cos k_c l & jZ_c \sin k_c l \\ j \sin k_c l / Z_c & \cos k_c l \end{bmatrix} \cdot \begin{bmatrix} 1 & 0 \\ 0 & 1/\phi \end{bmatrix} \end{aligned} \tag{2-80}$$

Considering the system 'porous material/air/plate' (seeing in Fig.2-9), the normal plane wave transmits through the porous material (thickness l), air gap (thickness e), and an elastic plate (thickness h, simply supported) from point M_1 at the front of the l to point M_2 at the back of the elastic plate.

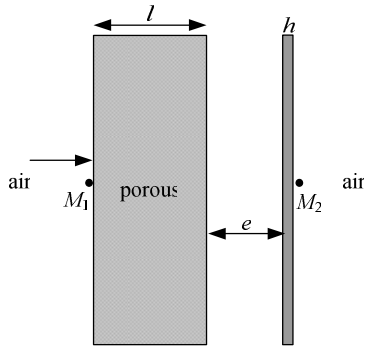

Fig.2-9 The total transfer matrix of the porous material/air/plate

The total transfer matrix between the point M_1 and the point M_2 can be expressed as:

$$\mathbf{T}_{\mathbf{total}} = \mathbf{T}_{\mathbf{a/poro}} \cdot \mathbf{T}_{\mathbf{poro}} \cdot \mathbf{T}_{\mathbf{poro/a}} \cdot \mathbf{T}_{\mathbf{a}} \cdot \mathbf{T}_{\mathbf{a/pl/a}} \tag{2-81}$$

Considering the system 'plate/porous material/plate' (seeing in Fig.2-10), the normal plane wave transmits through an elastic plate 1 (thickness h_1, simply supported), a porous material (thickness l), and an elastic plate 2 (thickness h_2, simply supported) from point M_1 at the front of the elastic plate 1 to point M_2 at the back of the elastic plate 2.

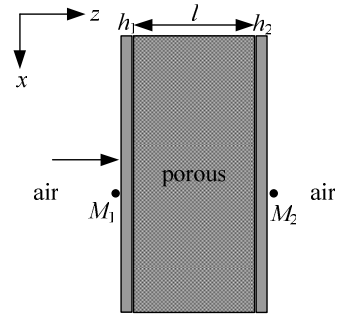

Fig.2-10The total transfer matrix of the plate/porous material/plate

The total transfer matrix between the point M_1 and the point M_2 can be expressed as:

$$\mathbf{T}_{\mathbf{total}} = \mathbf{T}_{\mathbf{a/pl/poro}} \cdot \mathbf{T}_{\mathbf{poro}} \cdot \mathbf{T}_{\mathbf{poro/pl/a}} \tag{2-82}$$

Considering the system 'porous material/air/plate/air/porous material/air/plate' (seeing in Fig.2-11), the normal plane wave transmits through a porous material (thickness l), an air layer (thickness e_1), an elastic plate 1 (thickness h_1, simply supported), an air layer (thickness e_2), a porous material (thickness l), an air layer (thickness e_3), and an elastic plate 2 (thickness h_2, simply supported) from point M_1 at the front of the porous material to point M_2 at the back of the elastic plate 2.

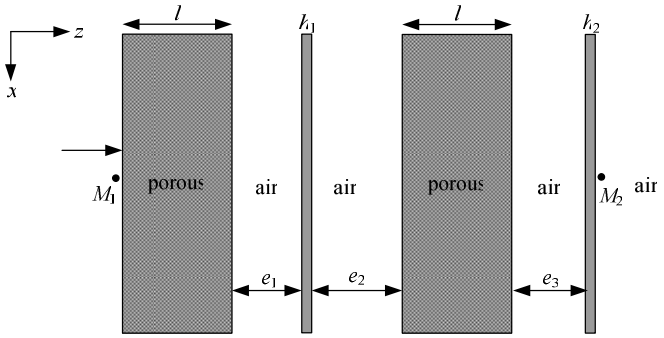

Fig.2-11 The total transfer matrix of the porous material/air/plate/air/porous material/air/plate

The total transfer matrix between the point M_1 and the point M_2 can be expressed as:

$$\mathbf{T}_{\text{total}} = \mathbf{T}_{\text{a/poro}} \cdot \mathbf{T}_{\text{poro}} \cdot \mathbf{T}_{\text{poro/a}} \cdot \mathbf{T}_{\text{a}} \cdot \mathbf{T}_{\text{pl}} \cdot \mathbf{T}_{\text{a}} \cdot \mathbf{T}_{\text{a/poro}} \cdot \mathbf{T}_{\text{poro}} \cdot \mathbf{T}_{\text{poro/a}} \cdot \mathbf{T}_{\text{a}} \cdot \mathbf{T}_{\text{pl}} \tag{2-83}$$

2.3 Numerical examples

In this section, some examples of double-wall acoustic absorbent or/and insulation structures are modeled by the transfer matrix method, and their absorption coefficient and transmission loss are calculated. The transfer matrices of the total structures are obtained through the expressions in section 2.2. The elastic plates and the porous materials used in these structures are simply supported.

2.3.1 Sound absorbent system

The structure shown in Fig.2-9 is actually the $\lambda/4$ resonance absorber, whose absorption peak appears in the condition that the distance between the reflective surface and porous material is equivalent to $\lambda/4$ or odd multiple of $\lambda/4$. Table.2-1 gives the physical parameters of the used materials, in which the parameters of the porous materials have been obtained from the Ref. [162]. According to Eq. (2-81) derived in the previous section and the relationship between the transfer matrix and the scattering matrix, the total scattering matrix of this structure can be obtained, and its absorption coefficient and transmission loss can be calculated.

Table.2-1 The physical parameters of the materials

Elastic thin plate	
Section area	66×66 mm
Thickness	0.2 mm
Mass density	7700 kg/m^3
Young's modulus	2.16e11 N/m^2
Stiffness	3.2e6 N/m^3
Poisson's ratio	0.27
Porous material (felt)	
Thickness	20 mm
Porosity	0.95
Resistivity	30000 rayls/m
Mass density	100 kg/m^3
Tortuosity	1.1
Viscous length	37 μm
Thermal length	196 μm

Fig.2-12a describes the absorption coefficient of the $\lambda/4$ resonance absorber with different thickness of air layer, respectively 30mm, 60mm, and 90mm, under a normal incident plane wave excitation. The curves show that the frequency of the first absorption peak decreases with the increase of the air layer's thickness: 2800Hz, 1400Hz, and 950Hz. Thus, to enhance the absorption coefficient in low frequency, we must increase the thickness of the air, for example, when the required frequency is as low as 500Hz the thickness of the air layer is up to 170mm. Fig.2-12b describes the transmission loss of the $\lambda/4$ resonance absorber with different thickness of air layer, respectively 30mm, 60mm, and 90mm. The curves show that its transmission loss exceeds 40dB over 1000Hz, while quickly decreases lower than 1000Hz. When the frequency is equal to 400Hz, the structure resonance appears.

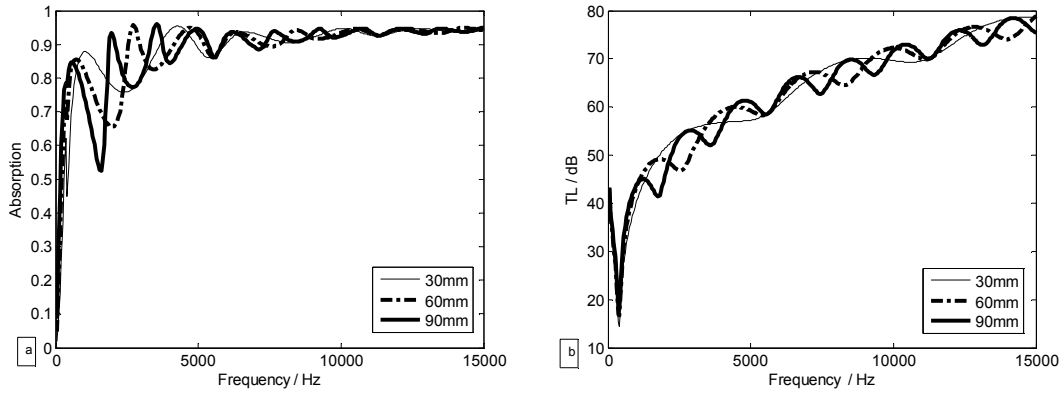

Fig.2-12 Acoustic performance of the $\lambda/4$ resonance absorber; a) absorption; b) transmission loss

Fig.2-13 shows the loss power of the $\lambda/4$ resonance absorber with different thickness of air layer. The curves show that there is energy dissipation in the $\lambda/4$ resonance absorber, and it is increased with the frequency. for the existence of energy loss, and an upward trend with increasing frequency. In the peak of the absorption coefficient, the loss power is up to maximum, which means the radiating power achieves minimum and the more energy is dissipated by the structure itself.

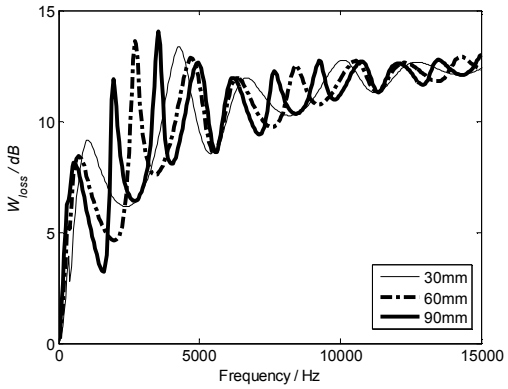

Fig.2-13 Loss power of the $\lambda/4$ resonance absorber

2.3.2 Sound insulation system

A typical double-wall sound insulation structure is shown in Fig.2-10, in which the core can be an air gap, a porous material or their combination. The physical parameters of the used materials are given in Table.2-1, and the thickness of the air gap is 20mm. Fig.2-14 describes the absorption coefficient and transmission loss of three kinds of the double-wall sound insulation structures: plate-air-plate, plate-porous-plate, and plate-air-porous-air-plate. The curves show that the absorption coefficient of these sound insulation systems is very weak, but their transmission loss is perfect in whole frequency band except in the resonance frequencies. Besides, in the condition of the same elastic plate used, the first resonance frequency of the double-wall structure will not be changed with different cores, 230Hz, which is also the resonance frequency of the elastic plate. However, the second resonance frequency changes with the core: 530Hz, 480Hz, and 350Hz, which are the resonance frequencies of the total structures.

Moreover, it has been concluded that the system with a porous material core can improve the transmission performance in first resonance frequency obviously, comparing to the one with an air gap core, due to the porous media dissipates the wave energy by producing friction in pore and radiating heat. Besides, because of the acoustical wave attenuation in air, the system with several layers of air gap and porous medium can insulate more sound transmission in whole frequencies.

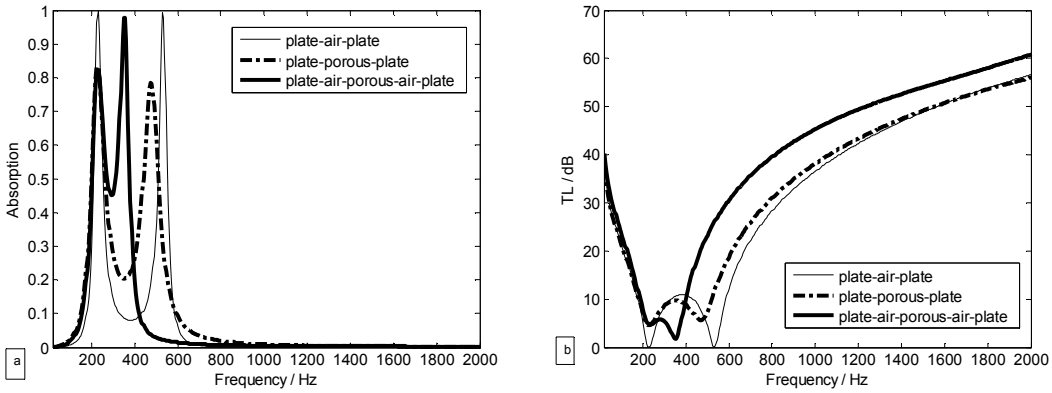

Fig.2-14 Acoustic performance of different sound insulation systems; a) absorption; b) transmission loss

Fig.2-15 describes the loss power of the double-wall sound insulation structures with different cores. The curves show that there is energy dissipation in the sound insulation structures near the resonance frequency; no energy dissipation exists in other frequency band, but the transmission loss is great, which means the incident sound power is entirely reflected. Besides, in the peak of the absorption coefficient, the loss power is up to maximum, which means the radiating power achieves minimum and the more energy is dissipated by the structure itself.

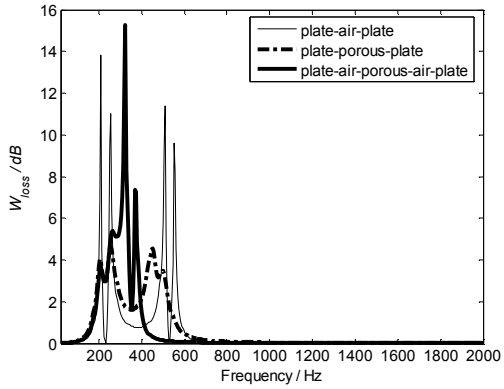

Fig.2-15 Loss power of the different sound insulation systems

2.3.3 Sound absorbent and insulation system

The structure shown in Fig.2-11 is a double-wall sound absorbent and insulation structure, and the porous material located at the front of the elastic plate enhance the absorption coefficient of the structure. The physical parameters of the used materials are given in Table.2-1, and the thickness of the air gap is successively 30mm, 10mm, 15mm. Fig.2-16 describes the absorption coefficient and transmission loss of this structure. The curves show

that the absorption coefficient of this structure is excellent, and it is up to 0.6 over 600Hz; its transmission loss is also perfect in whole frequency band except in the resonance frequencies. Besides, the first resonance frequency of this structure is still 230Hz, which is also the resonance frequency of the elastic plate; the second resonance frequency is 365Hz, which is the resonance frequency of the total structure.

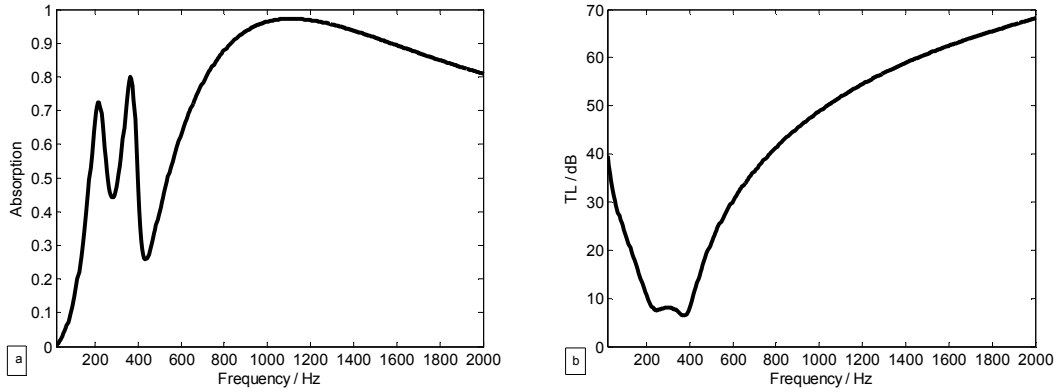

Fig.2-16 Acoustic performance of the sound absorbent and insulation system; a) absorption coefficient; b) transmission loss

Fig.2-17 describes the loss power of the double-wall sound absorbent and insulation structure. The curves show that there is energy dissipation in the structure in whole analysis frequency. Besides, in the peak of the absorption coefficient, the loss power is up to maximum, which means the radiating power achieves minimum and the more energy is dissipated by the structure itself. Compared to Fig.2-15, the energy dissipation is still great in the no-resonance frequency, which means the porous material located at the front of the elastic plate eliminates the reflected energy.

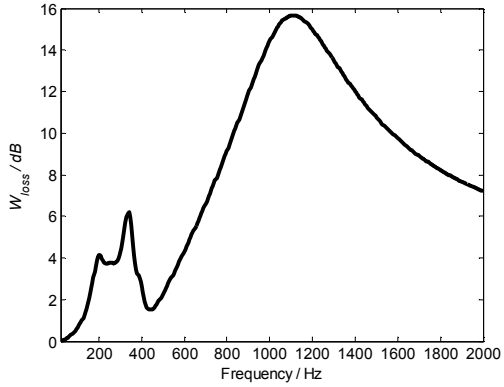

Fig.2-17 Loss power of the sound absorbent and insulation system

2.4 Conclusions

In this chapter, the transfer matrix method is applied to analyze the acoustic characteristic of the double-wall passive acoustic structure. Firstly, the definition of the transfer matrix and scattering matrix are given in the acoustic structure, and the relationship between them is also expressed. Based on the sound propagation principle, the transfer matrix of the elastic simply supported plate, the air gap, the rigid porous material and the interface between each layer are modeled and then deduced to establish the total transfer matrix of the double-wall structure. Lastly, the absorption coefficient and transmission loss of the double-wall passive acoustic structure are calculated and analyzed with some numerical examples.

Chapter 3

Acoustic performance analysis of hybrid active acoustic structure by scattering matrix method

In the preceding chapter, the acoustic performance of the double-wall passive structure is analyzed by the transfer matrix method, and some examples of sound absorbent or/and insulation systems are given. However, when the double-wall structures are hybrid (including active control), the transfer matrix method is not suitable to model the problem since calculations become complicate. Moreover, even if the structure is passive, the acoustic characteristics of the structure can not be directly expressed by the transfer matrix. Therefore, a concept of the scattering matrix [126] is proposed.

According to the definition of the scattering matrix, when the structure is excited only by the incident wave from the left side, the elements D_{11} and D_{21} of the scattering matrix respectively represent the reflection and transmission coefficients under the incident wave excitation from the left side; when the structure is excited only by the incident wave from the right side, the elements D_{22} and D_{12} of the scattering matrix respectively represent the reflection and transmission coefficients under the incident wave excitation from the right side. Thus, the acoustic characteristics of the structure can be directly expressed by the scattering matrix.

For the passive structure, the scattering matrix can be directly derived by the transfer matrix based on the principle of sound wave propagation; when the structure is with active control, the unit having the secondary source should be analyzed separately. Similar to the transfer matrix method, the scattering matrix of total hybrid active structure can also be

obtained by multiplying the scattering matrix of each layer due to the continuity nature of the sound pressure and velocity.

This chapter aims at analyzing the acoustic characteristic of the hybrid active structure and to developing a hybrid active acoustic structure having good performance on both absorption and acoustic insulation for a wide frequency range. These hybrid active structures combine passive and active means by using passive layers and active plate, respectively. Passive layers include absorbent material (porous layer or/and micro-perforate plate) located in the emission side to increase absorption. The active plate consisting of two piezoelectric patches bonded to an elastic thin plate acts as a secondary source in order to improve acoustic insulation at low and resonances frequencies. By analogy with duct systems, the active plate in hybrid active acoustic structure is modeled as a two-port source. Using the scattering matrix method, it can be completely described in form of a scattering matrix and a source strength vector which represents respectively the passive and active proprieties of this plate. When systems or layers are passive, such as porous layers, elastic thin plate etc, only the scattering matrix is sufficient to characterize completely their acoustical behavior. Simulation of active control of hybrid systems is carried out by introducing a source vector for the secondary source in order to minimize the sound pressure level at the control point. The acoustic performance of hybrid active structures, transmission loss and absorption, are then deduced from the secondary source vector and the scattering matrices of all layers or elements composing the hybrid system.

3.1 Theoretical basis and analytical simulation

3.1.1 The acoustical behavior of an active plate

The secondary source in the hybrid active structure is produced by gluing the piezoelectric ceramics onto both sides of an elastic plate simply supported, and then imposing an opposite voltage on the piezoelectric ceramics. The elastic plate with the piezoelectric ceramics can be called the active plate shown in Fig.3-1. The secondary source generated by the active plate is not directional, and it radiates sound waves not only to the left side of the structure but also to the right side of the structure. Suppose that the primary source is located at the left side of the structure, the sound wave radiated by the active plate which transmits to the left side of the structure will interfere with the primary source and produce the ‘acoustic feedback’ phenomenon. Therefore, this phenomenon should be taken into account when modeling the active plate.

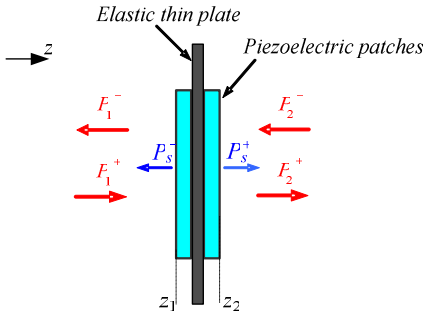

Fig.3-1 The active plate

This active plate can be modeled as a two-port source in form of a radiated source vector $\mathbf{P_S}$ and a scattering matrix $\mathbf{D^s}$. The relationship between the incoming pressure wave vector $\left[P_1^+(z_1) \quad P_2^-(z_2)\right]^T$ and the outgoing pressure wave vector $\left[P_1^-(z_1) \quad P_2^+(z_2)\right]^T$ are written as:

$$\begin{bmatrix} P_1^-(z_1) \\ P_2^+(z_2) \end{bmatrix} = \mathbf{D^s} \cdot \begin{bmatrix} P_1^+(z_1) \\ P_2^-(z_2) \end{bmatrix} + \mathbf{P_S}, \quad \mathbf{P_S} = \begin{bmatrix} P_S^-(z_1) \\ P_S^+(z_2) \end{bmatrix} \tag{3-1}$$

Here, P_S^+ and P_S^- are the pressure radiated by the active plate in the right and the left side, respectively. The scattering matrix $\mathbf{D^s}$ describes the acoustical behavior of the active plate, while $\mathbf{P_S}$ represents its active behavior. When this plate is acting as a secondary source of an active control system, $\mathbf{P_S}$ depends of external acoustic conditions (incident pressures, external discontinuities…).

3.1.2 The active sound absorbent structure

As described in Chapter 2, the $\lambda/4$ resonance absorber is an absorbent system in which the porous material is placed at a distance equal to a quarter of a wavelength from the rigid wall, in order that the pressure vanishes at the back face, i.e. $P_2 = 0$, shown in Fig.3-2(a). According to Ref. [162], $P_2 = 0$ means the surface impedance Z_s ($Z_s = \sigma e$ in Darcy's law) of the porous material matches the characteristic impedance of air, that is $Z_s = \sigma e = \rho_0 c_0$, therefore the maximum absorption coefficient is obtained under normal incidence. Herein, ρ_0, c_0 are the air density and velocity, σ, e are the resistivity and thickness of the porous material. However, this passive absorber raises two major problems: (1) The required air gap for a low frequency becomes very large (e.g., $\lambda/4 = 0.17m$ in air at 500 Hz); (2) This system is only effective in narrow frequency bands, especially for low frequencies.

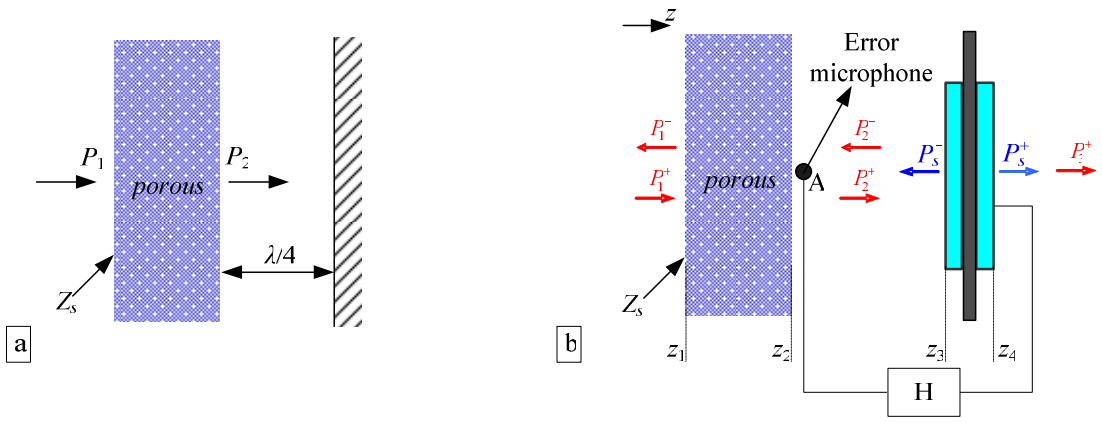

Fig.3-2 The absorbent systems; (a) the λ/4 resonance absorber; (b) the active absorber

Hence, an active absorber appears to be particularly efficient in avoiding these drawbacks: the air gap can be replaced by an active control loop which minimizes the pressure $P_2(z_2)$ (Fig.3-2(b)). The secondary source generates a pressure wave, which cancels the primary one by destructive interference at the microphone location (point A), just behind the porous layer, and then produces a pressure release condition at the back surface of the layer. Thus, broadband excitations can be controlled with a reduced absorbent thickness. This active absorber, called 'an equivalent of the $\lambda/4$ resonance absorber', also offers the advantage of separating the control system from a hostile environment (air flow or hot stream for instance).

The scattering matrix $\mathbf{D^1}$ of the porous material layer located between axial coordinates z_1 and z_2 leads to relationships between $\left[P_1^+(z_1) \quad P_2^-(z_2)\right]^T$ and $\left[P_1^-(z_1) \quad P_2^+(z_2)\right]^T$:

$$\begin{bmatrix} P_1^-(z_1) \\ P_2^+(z_2) \end{bmatrix} = \mathbf{D^1} \cdot \begin{bmatrix} P_1^+(z_1) \\ P_2^-(z_2) \end{bmatrix} \tag{3-2}$$

The scattering matrix $\mathbf{D^2}$ of the air gap layer located between z_2 and z_3 leads to the following relations:

$$\begin{bmatrix} P_2^-(z_2) \\ P_2^+(z_3) \end{bmatrix} = \mathbf{D^2} \cdot \begin{bmatrix} P_2^+(z_2) \\ P_2^-(z_3) \end{bmatrix} \tag{3-3}$$

In the case of anechoic upstream acoustic conditions $\left(P_3^-(z_3)=0\right)$, the scattering matrix $\mathbf{D^S}$ of the active plate located between z_3 and z_4 gives the following equations systems:

$$\begin{bmatrix} P_2^-(z_3) \\ P_3^+(z_4) \end{bmatrix} = \mathbf{D^S} \cdot \begin{bmatrix} P_2^+(z_3) \\ 0 \end{bmatrix} + \begin{bmatrix} P_S^-(z_3) \\ P_S^+(z_4) \end{bmatrix} \tag{3-4}$$

To simulate the active control of the error sensor position at z_2, the pressure $P_S^-(z_3)$ radiated by the active plate in the left side must be introduced in computations in order to minimize the acoustic pressure $P_2(z_2)$. This is possible only if the value of the pressure $P_S^+(z_4)$ radiated in the right side is known or related with $P_S^-(z_3)$ by a given relationship. However, the used active plate has symmetrical geometry and symmetrical material proprieties. Hence, radiated pressures P_S^- and P_S^+ are related by the following equation:

$$\left|P_S^-(z_3)\right| = \left|P_S^+(z_4)\right| \qquad and \qquad \varphi_S^- = -\varphi_S^+ \tag{3-5}$$

Here, φ_S^-, φ_S^+ are respectively the phases of the radiating sound waves.

From Eq. (3-2) ~ (3-5), we can calculate $P_2(z_2)$ as well as the reflected and transmitted pressures $P_1^-(z_1)$ and $P_3^+(z_4)$ at the emission and the transmission side respectively:

$$P_2(z_2) = a_1 P_1^+(z_1) + a_2 P_S^+(z_4) \tag{3-6}$$

$$P_1^-(z_1) = a_3 P_1^+(z_1) + a_4 P_S^+(z_4) \tag{3-7}$$

$$P_3^+(z_4) = a_5 P_1^+(z_1) + a_6 P_S^+(z_4) \tag{3-8}$$

Here,

$$A_1 = \frac{D_{21}^2}{1 - D_{22}^2 D_{11}^S} \qquad B_1 = \frac{D_{22}^2}{1 - D_{22}^2 D_{11}^S} \qquad A_2 = D_{11}^S A_1 \qquad B_2 = D_{11}^S B_1 + 1$$

$$A_3 = D_{11}^2 + D_{12}^2 A_2 \qquad B_3 = D_{12}^2 B_2 \qquad A_4 = \frac{D_{21}^1}{1 - D_{22}^1 A_3} \qquad B_4 = \frac{D_{22}^1 B_3}{1 - D_{22}^1 A_3}$$

$$A_5 = A_3 A_4 \qquad B_5 = A_3 B_4 + B_3$$

$$a_1 = A_4 + A_5 \qquad a_2 = B_4 + B_5 \qquad a_3 = D_{11}^1 + D_{12}^1 A_5$$

$$a_4 = D_{12}^1 B_5 \qquad a_5 = D_{21}^S A_1 A_4 \qquad a_6 = D_{21}^S A_1 B_4 + D_{21}^S B_1 + 1$$

D_{ij}^1, D_{ij}^2, D_{ij}^S, $i, j = 1,2$, are the elements of the scattering matrices $\mathbf{D^1}$, $\mathbf{D^2}$, $\mathbf{D^S}$. These scattering matrices are deduced from analytical transfer matrices $\mathbf{T_{a/poro/a}}$, $\mathbf{T_a}$, and $\mathbf{T_{a/pl/a}}$ (Chapter 2) associated respectively to the porous material, the air gap and the active plate.

It must be noted that $\mathbf{T_{a/pl/a}}$ is the passive transfer matrix of the active plate (when $P_S^- = P_S^+ = 0$). In active control, the pressure P_2 vanishes, thus

$$P_2(z_2) = 0 \quad \Rightarrow P_S^+(z_3) = -\frac{a_1}{a_2} P_1^+(z_1) \tag{3-9}$$

We can define a factor χ for describing the active control degree, its expression as follows:

$$\chi = \begin{cases} 0 \\ \chi, \ (0 < \chi < 1) \\ 1 \end{cases} \tag{3-10}$$

$$P_S^+(z_3) = -\chi \cdot \frac{a_1}{a_2} P_1^+(z_1) \tag{3-11}$$

Here, $\chi = 1$ means that the pressure at z_2 is to zero, and all noise is completely reduced by active control; $\chi = 0$ means that there is just passive control, and active control doesn't work; if χ is between 0 and 1, it means active control just half-operates. We can adjust the active control degree by changing the value of χ according to the practical application.

Its reflection and transmission coefficients at z_1 and z_4, respectively, are determined from Eqs. (3-7) ~ (3-9) and (3-11):

$$R(\chi) = P_1^-(z_1) / P_1^+(z_1) = \left(a_3 - \chi \cdot \frac{a_1 a_4}{a_2} \right) \tag{3-12}$$

$$\tau(\chi) = P_3^+(z_4) / P_1^+(z_1) = \left(a_5 - \chi \cdot \frac{a_1 a_6}{a_2} \right) \tag{3-13}$$

The absorption coefficient α and the transmission loss TL of the hybrid active acoustic structure are finally deduced from Eq. (3-12) and (3-13):

$$\alpha(\chi) = 1 - |R(\chi)|^2, \qquad TL(\chi) = 10 \lg \left(1 / |\tau(\chi)|^2 \right) \tag{3-14}$$

3.1.3 The active sound insulation structure

Another multilayer active structure on the noise insulation aims to improve the acoustic attenuation and transmission loss of sound waves. As a particular example of such systems, a double-wall structure is made up of two elastic plates (called 'active plate' and 'radiating plate' respectively) and a core such as an air gap or highly dissipative medium. Nevertheless, it is well known that such double-wall passive packages are sufficiently efficient at medium and high frequencies but exhibit poor performance at low frequencies, where the resonance inherent to the layer distribution occurs, discussed in Section 2.3.2. Therefore, a double-wall active acoustic structure concept is proposed to improve the acoustical transmission performance at resonance frequencies by active control technique. Fig.3-3 shows the configuration of a typical double-wall active system, where the system (1) includes absorbing element such as: air cavity, porous material, or porous material coupled with air

cavities…The secondary source generates a pressure wave, which make the pressure vanish at the error microphone location (point B), $P_3(z_3)=0$.

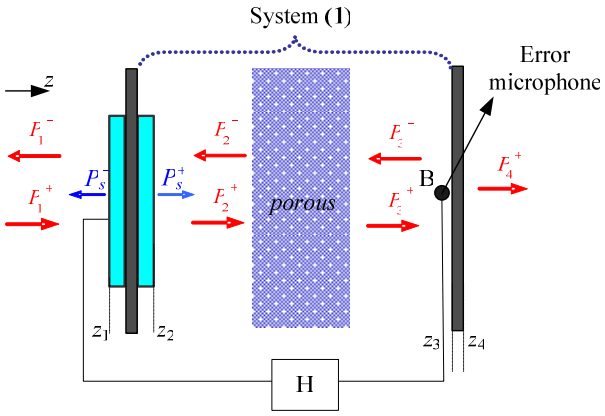

Fig.3-3 The double-wall active system

Via the analogical analysis in the above section, the pressure P_2 vanishes in active control, and the pressure of the secondary source, the reflection coefficient, and the transmission coefficient can be expressed as follows,

$$P_S^+(z_2)=-\chi\cdot\frac{b_1}{b_2}P_1^+(z_1) \tag{3-15}$$

$$R(\chi)=P_1^-(z_1)/P_1^+(z_1)=\left(b_3-\chi\cdot\frac{b_1b_4}{b_2}\right) \tag{3-16}$$

$$\tau(\chi)=P_4^+(z_4)/P_1^+(z_1)=\left(b_5-\chi\cdot\frac{b_1b_6}{b_2}\right) \tag{3-17}$$

Here, $b_1,\cdots,b_6$ are given in **Appendix**.

It has been noted that, the above analysis is based on the control objective of $P_3(z_3)=0$, which is equal to $P_4^+(z_4)=0$, seeing the expressions of $P_3(z_3)$ and $P_4^+(z_4)$ in **Appendix**. The reason for locating the error sensor at the point B is to prevent the error sensor from exposing in the environment and losing the control effect.

3.1.4 The active sound absorbent and insulation structure

1. Active control with one error sensor based on sound insulation

Hybrid active acoustic structures modeled in this work must be efficient on both absorption and acoustic insulation for a wide frequency range. One general combination

which reaches this goal is the system given in Fig.3-4, with one error sensor in active control. This system consists of a system (1) located in the emission side in order to reduce reflection, and an active cell in order to insure high acoustic insulation. The system (1) includes absorbing elements such as: poroelastic layers coupled with air cavities, and/or a micro perforate plate…The active cell consists of two plates coupled with the system (2) which can be: an air or porous layer, or air/porous/air. The active plate vibrates in order to reduce the pressure level at the error microphone located at z_4 (point B), $P_4(z_4)=0$.

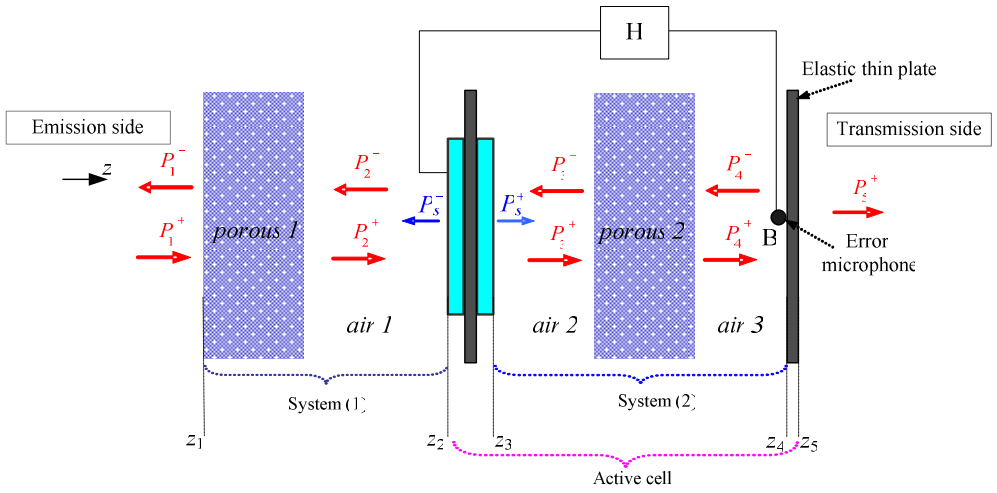

Fig.3-4 General configuration of the multilayer hybrid active acoustic structures

Similarly, the pressure P_4 vanishes in active control, and the pressure of the secondary source, the reflection coefficient, and the transmission coefficient can be expressed as follows,

$$P_S^+(z_3)=-\chi\cdot\frac{g_1}{g_2}P_1^+(z_1) \tag{3-18}$$

$$R(\chi)=P_1^-(z_1)/P_1^+(z_1)=\left(g_3-\chi\cdot\frac{g_1g_4}{g_2}\right) \tag{3-19}$$

$$\tau(\chi)=P_5^+(z_5)/P_1^+(z_1)=\left(g_5-\chi\cdot\frac{g_1g_6}{g_2}\right) \tag{3-20}$$

Here, $g_1,\cdots,g_6$ are given in **Appendix**.

2. Active control with one error sensors based on sound absorption

Another hybrid active acoustic structure with one error senor for improving sound absorption performance with active control is shown in Fig.3-5, in which the error sensor (point A) makes the system (1) as an equivalent of the $\lambda/4$ resonance absorber, $P_2(z_1')=0$.

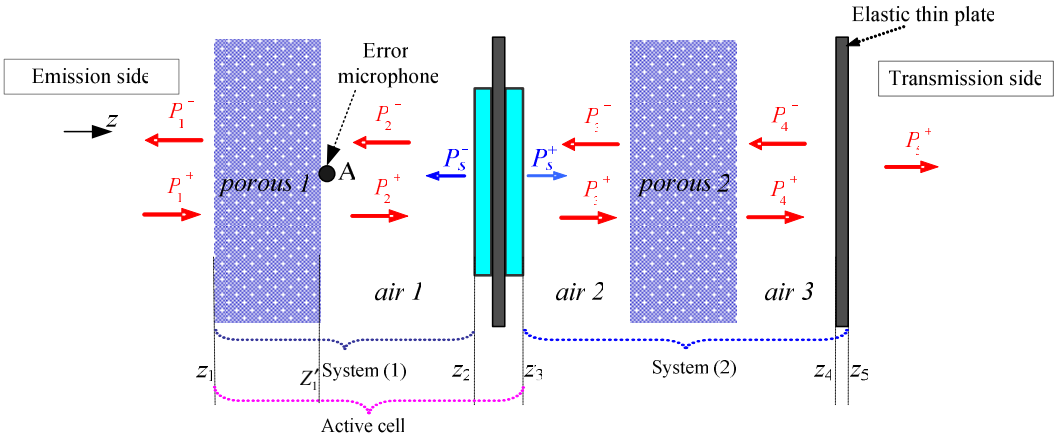

Fig.3-5 The hybrid system in active control with two error sensor

Similarly, the pressure $P_1^{'}$ vanishes in active control, and the pressure of the secondary source, the reflection coefficient, and the transmission coefficient can be expressed as follows,

$$P_S^+(z_3) = -\chi \cdot \frac{e_1}{e_2} P_1^+(z_1) \tag{3-21}$$

$$R(\chi) = P_1^-(z_1)/P_1^+(z_1) = \left(e_5 - \chi \cdot \frac{e_1 e_6}{e_2} \right) \tag{3-22}$$

$$\tau(\chi) = P_5^+(z_5)/P_1^+(z_1) = \left(e_7 - \chi \cdot \frac{e_1 e_8}{e_2} \right) \tag{3-23}$$

Here, $e_1, \cdots, e_6$ are given in **Appendix**.

3. Active control with two error sensors

A hybrid active acoustic structure with two error sensors in active control is shown in Fig.3-6, in which the combination of the active cells makes the system (1) as an equivalent of the $\lambda/4$ resonance absorber and the system (2) as a sound insulation system. In this case, the control objective is written as,

$$J = \left|P_2(z_1')\right|^2 + \left|P_4(z_4)\right|^2 = P_2(z_1')P_2^*(z_1') + P_4(z_4)P_4^*(z_4) \tag{3-24}$$

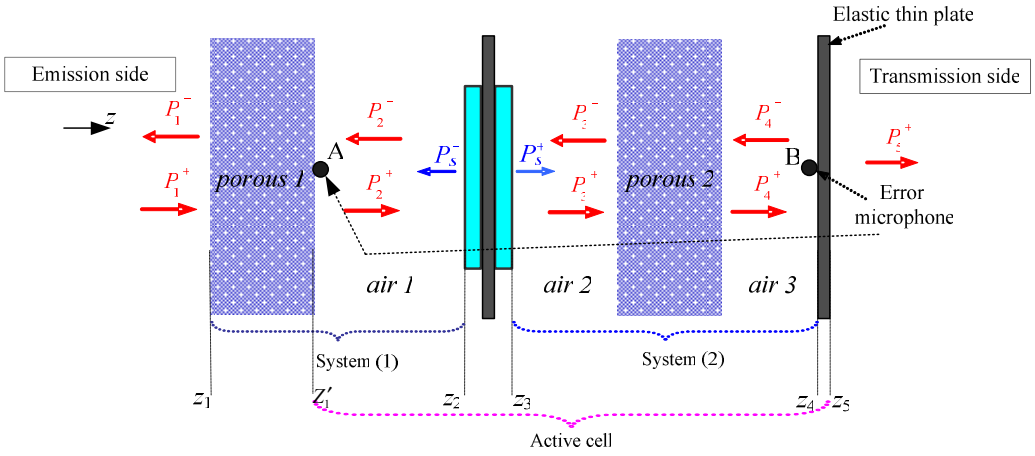

Fig.3-6 The hybrid system in active control with two error sensors

Then, the reflection coefficient, and the transmission coefficient can be expressed as follows, detailed in **Appendix**,

$$P_S^+(z_3) = -\chi \cdot \frac{b}{2a} e^{j\varphi_s} \tag{3-25}$$

$$R(\chi) = P_1^-(z_1)/P_1^+(z_1) = \left(e_5 - \chi \cdot \frac{be_6}{2a\left|P_1^+\right|} e^{-j\Delta\varphi} \right) \tag{3-26}$$

$$\tau(\chi) = P_5^+(z_5)/P_1^+(z_1) = \left(e_7 - \chi \cdot \frac{be_8}{2a\left|P_1^+\right|} e^{-j\Delta\varphi} \right) \tag{3-27}$$

3.2 Numerical examples

3.2.1 Sound absorbent system

In this section, the absorption coefficient and transmission loss of the active absorber shown in Fig.3-2(b) have been calculated with or without active control. The physic parameters of each layer are given in Table.2-1 and Table.3-1. In this configuration, the acoustic excitation is a normal plane wave with pressure amplitude 1Pa. The piezo-ceramics patch with a cross section 50mm × 50mm is glued to the center of the active plate, and all layers including porous materials have a cross section of 66mm × 66mm. The thicknesses of the air gap between the active plate and porous material is 30mm, which makes this absorber not too thick (about 51mm). The scattering matrices of each part are deducted from the transfer matrix of the related part according the formula mentioned in Chapter 2. Worthy of saying, the transfer matrix of porous material is attained by its impedance and complex

propagation constant calculated with effective density $\rho_e(\omega)$ and bulk modulus $K(\omega)$, mentioned in Refs. [115] and [130].

Fig.3-7(a) shows the absorption coefficient α with $\chi = 0,\ 0.2,\ 0.5,\ 0.8,\ 1$. The improvement of α is significant after the deployment of active control. Comparison between active and passive control shows a more efficient improvement of the absorption with active control in the frequencies less than 500Hz. Besides, with different active control degree ($\chi = 0.2 \sim 1$), the absorption of the active absorber has been improved obviously less than 400Hz, which is the resonance of the active plate. Fig.3-7(b) shows the transmission loss TL with $\chi = 0,\ 0.2,\ 0.5,\ 0.8,\ 1$. Comparing the results of the active and passive control in Fig.3-7(b), the transmission loss with active control has been decreased in all-range frequency (except for $\chi = 0.2$ in resonance frequency), and the more the control degree is, the lower the transmission loss is, because the active plate is a two-port source which can produce a transmitting wave in downstream side. Therefore, this active absorber is an efficient sound absorbent system, where it is not noise insulation structure.

Table.3-1 Physic parameters of piezoelectric ceramic

Thickness	0.5 mm
Mass density	7760 kg/m^3
Young's modulus	9.6e10
Poisson's ratio	0.34

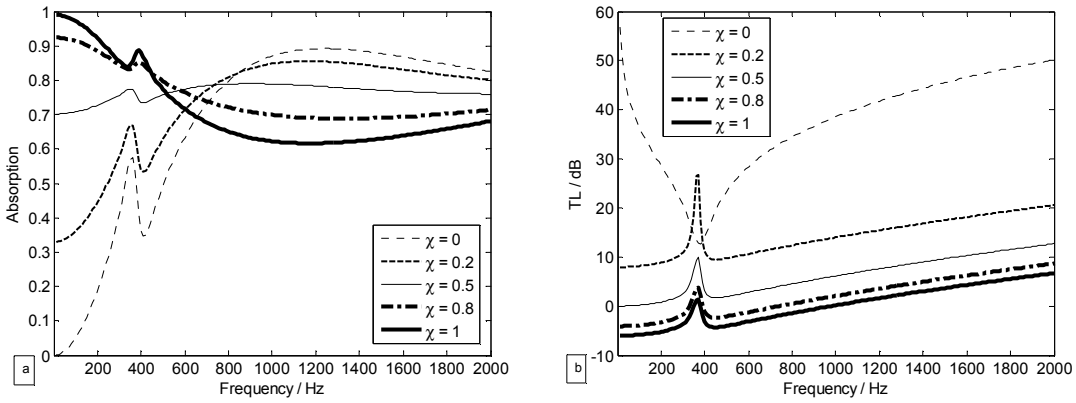

Fig.3-7 Acoustic performance of the active absorber with different control degree; a) absorption; b) transmission loss

3.2.2 Sound insulation system

In this structure, three kinds of the system (1) in Fig.3-3 are modeled: a) an air cavity with 20mm in thickness, b) a porous material layer with 20mm in thickness, and c) a porous material of 20mm in thickness coupled with two air cavities: 10mm and 15mm in thickness. The acoustic performances of the sound insulation structure in different system (1) are simulated for finding an optimal insulation system, seeing the numerical results in Fig.3-8 ~ Fig.3-10.

Fig.3-8(a) shows the absorption coefficient α with $\chi = 0,\ 0.5,\ 1$ of the plate-air-plate system (about 21mm in thickness). The improvement of α is significant after the deployment of active control. In passive control ($\chi = 0$ in Fig.3-8 (a)), the first sharp in absorption curve is the resonance of the active plate, where the second sharp in curve is the resonance of the total system. Comparison between active and passive control shows a more efficient improvement of the absorption with active control in low-frequency range. However, with different active control degree ($\chi = 0.5$ and $\chi = 1$), the absorption of the double-wall system has not improved obviously. Fig.3-8(b) shows the transmission loss TL of this system with $\chi = 0,\ 0.5$. Because of the pressure-release condition with $\chi = 1$, the incident wave is completely reduced, thus the TL with $\chi = 1$ is not given here. From the results in Fig.3-8(b) with and without active control, the transmission loss can be increased with active control in all-range frequency and approximately 10dB obtained around the resonance frequency.

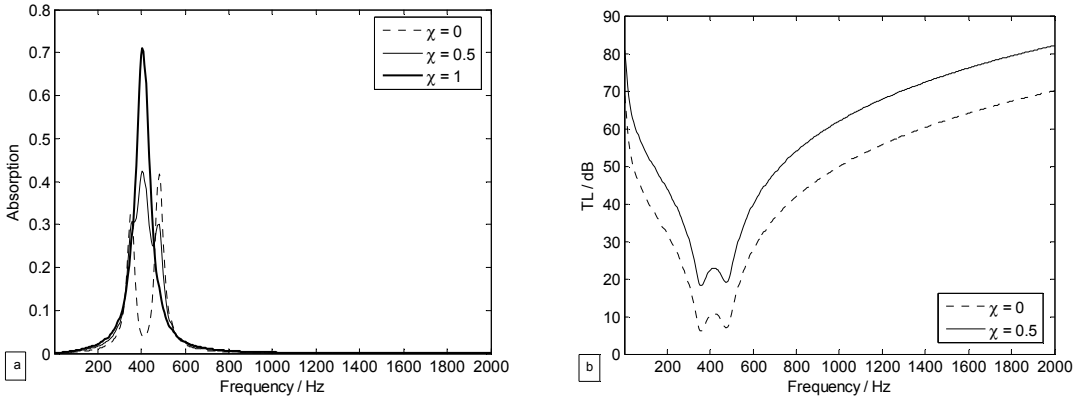

Fig.3-8 Acoustic performance of the plate-air-plate system with different control degree; a) absorption; b) transmission loss

Fig.3-9(a) shows the absorption coefficient α with $\chi = 0,\ 0.5,\ 1$ of the plate-porous-plate system (about 21mm in thickness). The improvement of α is significant after the deployment of active control. Comparison between active and passive control shows a more efficient improvement of the absorption with active control in low-frequency range. Fig.3-9(b) shows the transmission loss TL of this system with $\chi = 0,\ 0.5$. Similarly, because of the pressure-release condition with $\chi = 1$, the incident wave is completely reduced, thus the TL with $\chi = 1$ is not given here. Comparing active and passive control in Fig.3-9(b), the transmission loss can be increased with active control in all-range frequency and approximately 8dB obtained around the resonance frequency.

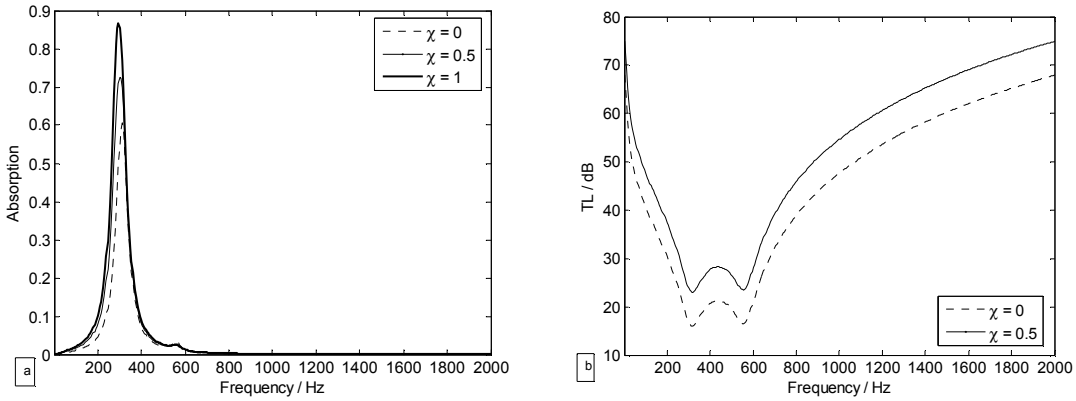

Fig.3-9 Acoustic performance of the plate-porous-plate system with different control degree; a) absorption; b) transmission loss

Fig.3-10(a) shows the absorption coefficient α with $\chi = 0,\ 0.5,\ 1$ of the plate-air-porous-air-plate system (about 46mm in thickness). The improvement of α is significant after the deployment of active control. Comparison between active and passive control shows a more efficient improvement of the absorption with active control in low-frequency range. Fig.3-10(b) shows the transmission loss TL of this system with $\chi = 0,\ 0.5$. Similarly, because of the pressure-release condition with $\chi = 1$, the incident wave is completely reduced, thus the TL with $\chi = 1$ is not given here. Comparing active and passive control in Fig.3-10(b), the transmission loss can be increased with active control in all-range frequency and approximately 15dB obtained around the resonance frequency.

From the numerical results and discussions in above section, it can be seen that these double-wall systems have a good transmission performance, but lack in efficient absorption characteristic. Besides, the simulation results show that the transmission loss can be enhanced in whole analysis frequency; however, the active control only improves the transmission loss

in low frequency range in engineering application, in order to prevent the piezoelectric ceramics from being destroyed.

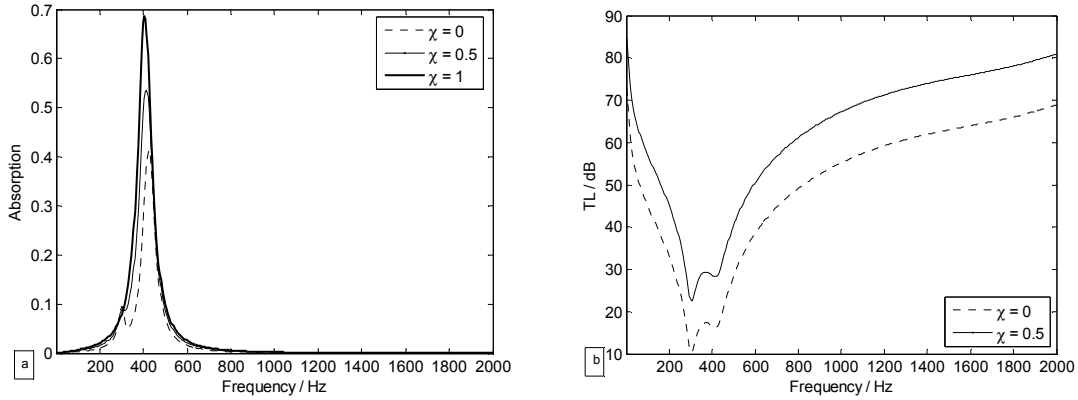

Fig.3-10 Acoustic performance of the plate-air-porous-air-plate system with different control degree; a) absorption; b) transmission loss

3.2.3 Hybrid systems

In this part, the absorption coefficient and transmission loss of the hybrid system with one error sensor shown in Fig.3-4 have been calculated with or without active control. Fig.3-11(a) shows the absorption coefficient α with $\chi = 0,\ 0.5,\ 1$ of this hybrid system (about 96mm in thickness) based on the pressure-release condition at the front surface of the elastic plate. The absorption coefficient α has been very slight changed with or without active control; however, it has been improved clearly comparing that of the sound insulation systems: exceeding 0.6 over 500Hz.

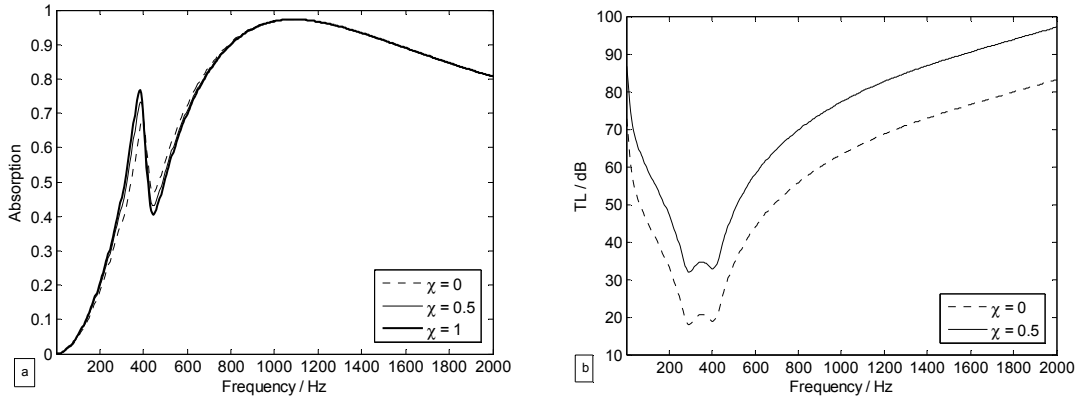

Fig.3-11 Acoustic performance of the hybrid system with an error sensor at point B; a) absorption; b) transmission loss

Fig.3-11(b) shows the transmission loss TL of this system with $\chi = 0,\ 0.5$. Once again, the incident wave is completely reduced due to the pressure-release condition with $\chi = 1$, thus the TL with $\chi = 1$ is not given here. Comparing the results in Fig.3-11(b), the transmission loss can be increased with active control in all-range frequency and approximately 15dB obtained around the resonance frequency.

Fig.3-12(a) exhibits the absorption coefficient α with $\chi = 0,\ 0.5,\ 1$ of this hybrid system shown in Fig.3-5 based on the pressure-release condition at the back surface of the porous material. The absorption coefficient α has an obvious improvement with active control in the frequencies lower than 600Hz, while it reduces slightly with active control over 800Hz. Whatever, it has been improved clearly comparing that of the hybrid system in Fig.3-4: exceeding 0.7 in all-range frequency with completely active control. Fig.3-12(b) shows the transmission loss TL of this system with $\chi = 0,\ 0.5,\ 1$. Nevertheless, the transmission loss has been deceased with active control in all-range frequency, because the radiating pressure of the active plate enhances the acoustical wave energy in the transmission side.

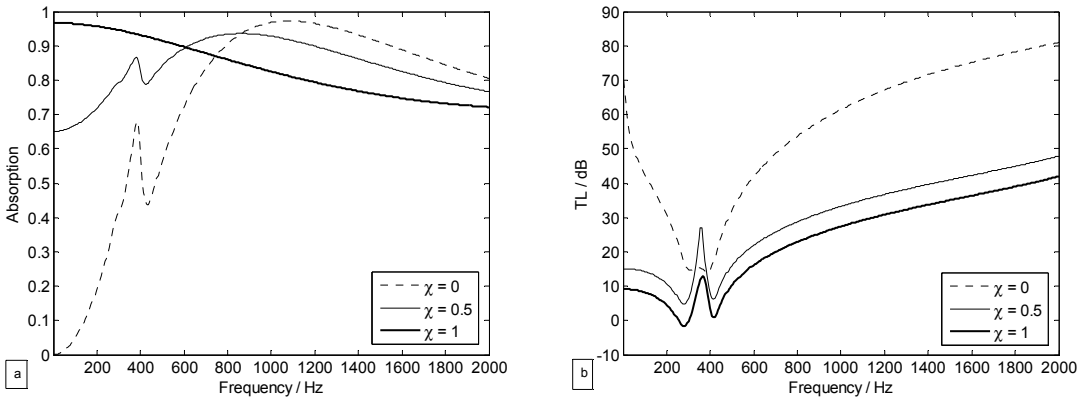

Fig.3-12 Acoustic performance of the hybrid system with one error sensor at point A; a) absorption; b) transmission loss

Lastly, the absorption coefficient and transmission loss of the hybrid system with two error sensor shown in Fig.3-6 have been calculated with or without active control. Fig.3-13(a) shows the absorption coefficient α with $\chi = 0,\ 0.5,\ 1$ of this hybrid system based on minimizing the sound power energy. The absorption coefficient α has an obvious improvement with active control in the frequencies lower than 500Hz, while it has nearly no change with active control over 600Hz: exceeding 0.6 over 500Hz. Fig.3-13(b) shows the transmission loss TL of this system with $\chi = 0,\ 0.5,\ 1$. However, the transmission loss has been decreased with active control in all-range frequency.

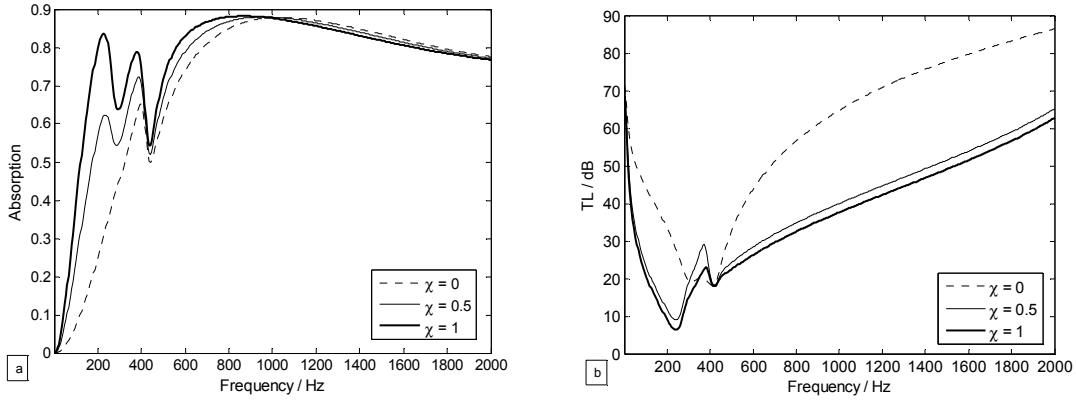

Fig.3-13 Acoustic performance of the hybrid system with two error sensor; a) absorption; b) transmission loss

According to the above analysis, it can be concluded that: (1) with one error sensor controlling the pressure at the front surface of the elastic plate, the hybrid system has excellent acoustic performance in sound absorption and insulation; (2) with one error sensor controlling the pressure at the back surface of the porous material, the hybrid system has the best sound absorption coefficient in all-range frequency, but results in the worst transmission loss; (3) with two error sensor controlling the sound power energy, the hybrid system obtains an obvious improvement in the sound absorption, while its transmission loss has also been reduced. Hence, the hybrid system shown in Fig.3-4 is the suitable choice for improving the acoustic performance, and it is the one that we focus on in the full text.

3.3 Influence factor of acoustic performance in hybrid systems

3.3.1 The porous material layers

In this part, based on active control with $\chi = 0.5$ the parameters of each layer have been changed for finding the important factor which influences the performance of the hybrid system with one error sensor controlling the pressure at the front surface of the elastic plate. Some results of porous materials are shown in Fig.3-14~Fig.3-18. Fig.3-14 shows the absorption coefficient α with the porosity of the porous mediums located respectively at both sides of the active plate: ϕ= 75% (dotted line), 85% (solid line), and 95% (bold line). It has been shown that the porosity of the porous medium at the front of the active plate is more important to the absorption of the hybrid system. The bigger it is, the better the absorption is in the frequencies over 1000Hz. However, the absorption of this hybrid system is independent on the porosity of another porous material. The transmission loss is not affected clearly in all cases, thus it is not given here.

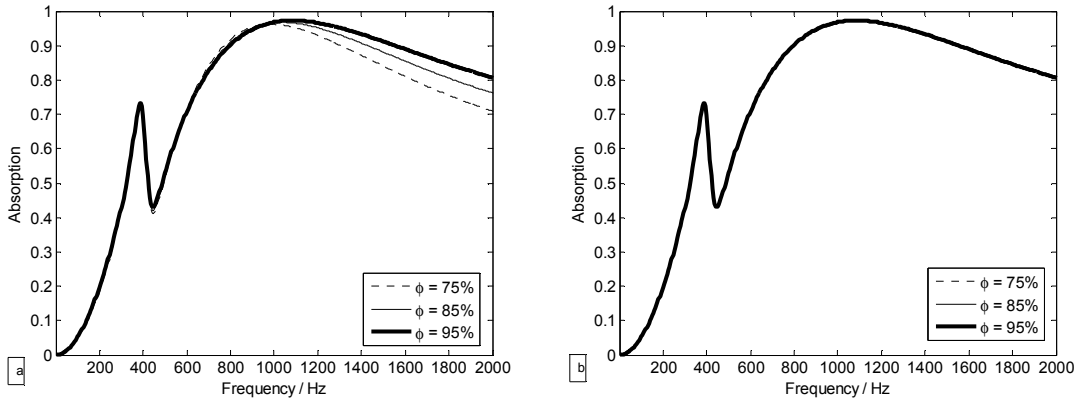

Fig.3-14 Absorption coefficient of the hybrid system with different porous porosities; (a) α with the different porosity of the porous material 1; (b) α with the different porosity of the porous material 2

Then the influence of the thickness of porous materials is given in Fig.3-15 and Fig.3-16. Fig.3-15 shows the absorption coefficient and transmission loss of the hybrid system with different thicknesses of the porous material 1 located at the front of the active plate: 10mm (dotted line), 20mm (solid line), 40mm (bold line), and 14mm (dashed and bold line). To be noted, when the thickness of the porous material 1 is equal to 14mm, the surface impedance Z_s of this porous material is equal to $\rho_0 c_0$. For this porous material, the bigger thickness has a better transmission loss in all frequency ranges, but no improvement in very low frequencies. However, the absorption of the hybrid system is affected obviously by the thickness of this porous material. In lower than the resonance frequency, its absorption is improved by the increased thickness, while it is decreased in some range over the resonance frequency.

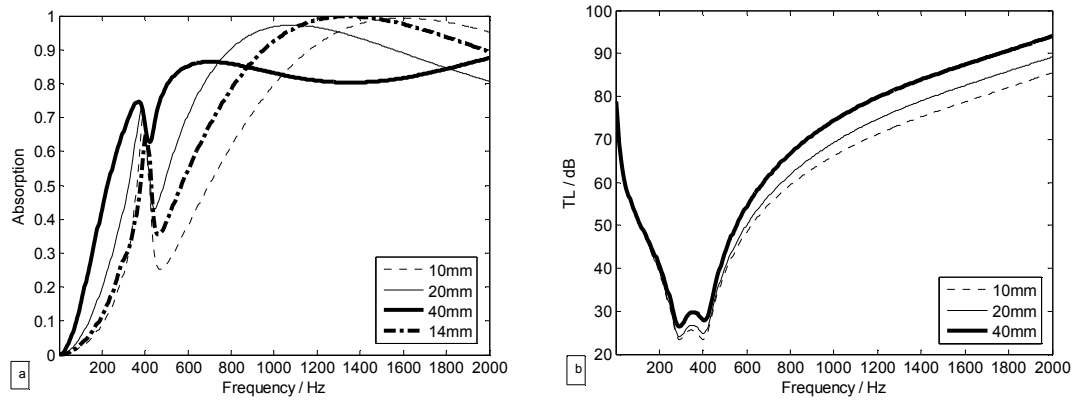

Fig.3-15 Acoustic performance of the hybrid system in different thicknesses of porous material 1; (a) absorption coefficient**;** (b) transmission loss

Fig.3-16 shows the absorption coefficient and transmission loss of the hybrid system with different thicknesses of the porous material 2 located at the back of the active plate: 10mm (dotted line), 20mm (solid line) and 40mm (bold line). For this porous material, similarly, the bigger thickness has a better transmission loss in all frequency ranges, but no improvement in very low frequencies. Nevertheless, the absorption is not changed distinctly with the increased thickness.

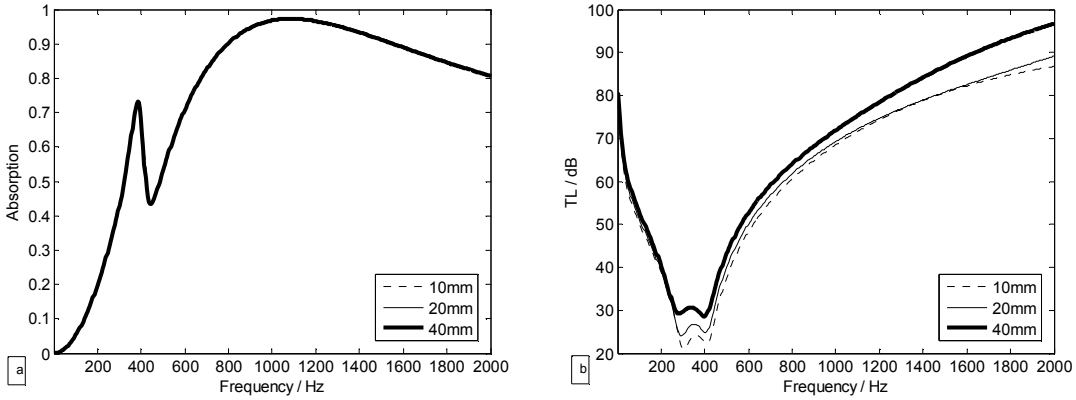

Fig.3-16 Acoustic performance of the hybrid system in different thicknesses of porous material 2; (a) absorption coefficient**;** (b) transmission loss

Lastly, the influence of the resistivity of porous materials is shown in Fig.3-17 and Fig.3-18. Fig.3-17 shows the absorption coefficient and transmission loss of the hybrid system with different resistivity of the porous materials located at the front of the active plate: 14750 (dotted line), 30000 (solid line) and 50000 (bold line). For this porous material, the higher resistivity has a better transmission loss in all frequency ranges, but no improvement in very low frequencies. However, the absorption of the hybrid system is affected obviously by the resistivity of this porous material. In lower than the resonance frequency, its absorption is improved by the increased resistivity, while it is decreased over the resonance frequency.

Fig.3-18 shows the absorption coefficient and transmission loss of the hybrid system with different resistivity of the porous materials located at the back of the active plate: 14750 (dotted line), 30000 (solid line) and 50000 (bold line). For this porous material, similarly, the bigger thickness has a better transmission loss in the frequency over 1000Hz, but no improvement in low frequencies. Nevertheless, the absorption is not changed distinctly with the increased resistivity. Therefore, it can be concluded that designing a hybrid system, more attention should be paid to the porous material located at the front of the active plate and the proper thickness, porosity and resistivity should be chosen for getting better acoustic performance.

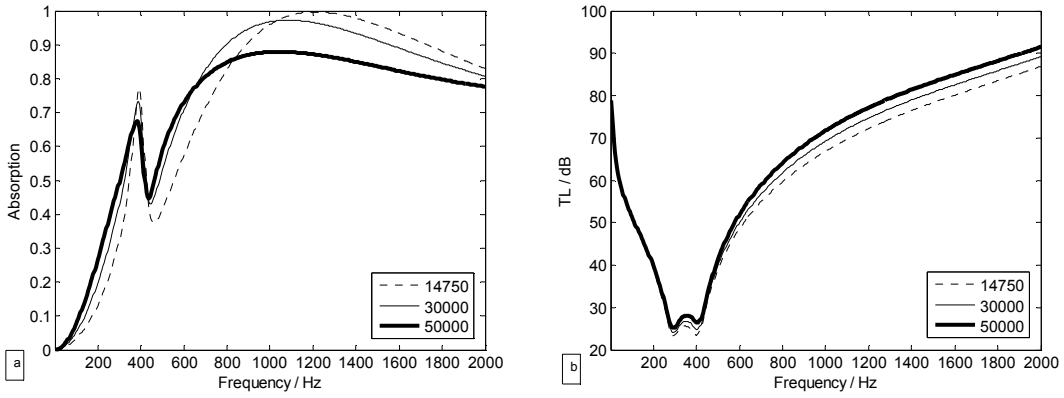

Fig.3-17 Acoustic performance of the hybrid system in different resistivity of porous material 1; (a) absorption coefficient α; (b) transmission loss TL

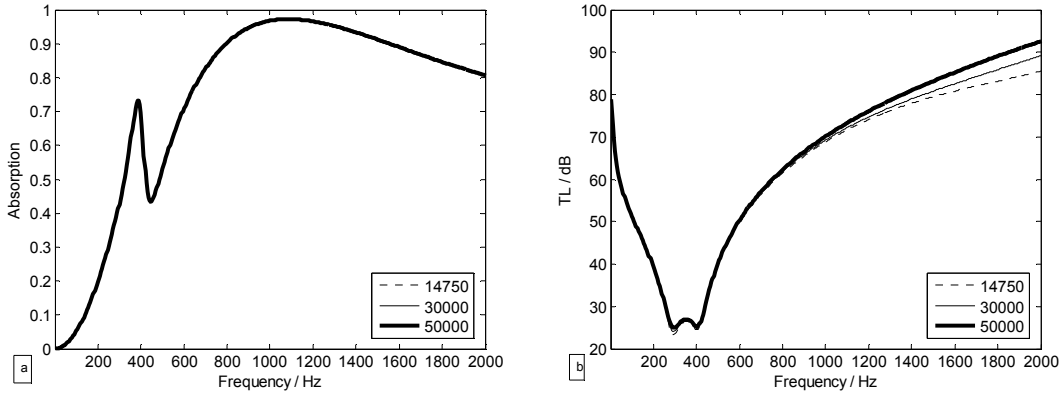

Fig.3-18 Acoustic performance of the hybrid system in different resistivity of porous material 2; (a) absorption coefficient α; (b) transmission loss TL

3.3.2 The air gap layers

In this part, the influence of the thickness of air gaps has been shown in Fig.3-19~Fig.3-21 based on active control with $\chi = 0.5$. For the air gap 1 (15mm (dotted line), 30mm (solid line), 60mm (bold line)), the increased thickness improves the absorption of the hybrid system in the frequencies lower than 800Hz, but exhibits a lack over 800Hz. For the air gap 2 (5mm (dotted line), 10mm (solid line), 20mm (bold line)) and the air gap 3 (7mm (dotted line), 15mm (solid line), 30mm (bold line)), the absorption is not influenced distinctly with the increased thickness. Besides, for all air gaps, the transmission loss has a little improvement with the increased thickness. Therefore, it can be concluded that for designing a hybrid system, more attention should be paid to the air gap located at the front of the active plate.

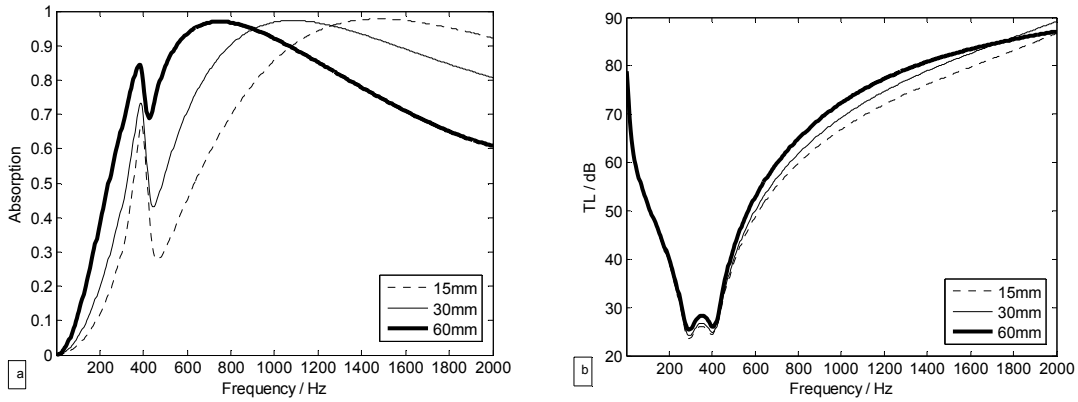

Fig.3-19 Acoustic performance of the hybrid system in different thicknesses of air gap 1; (a) absorption coefficient**;** (b) transmission loss.

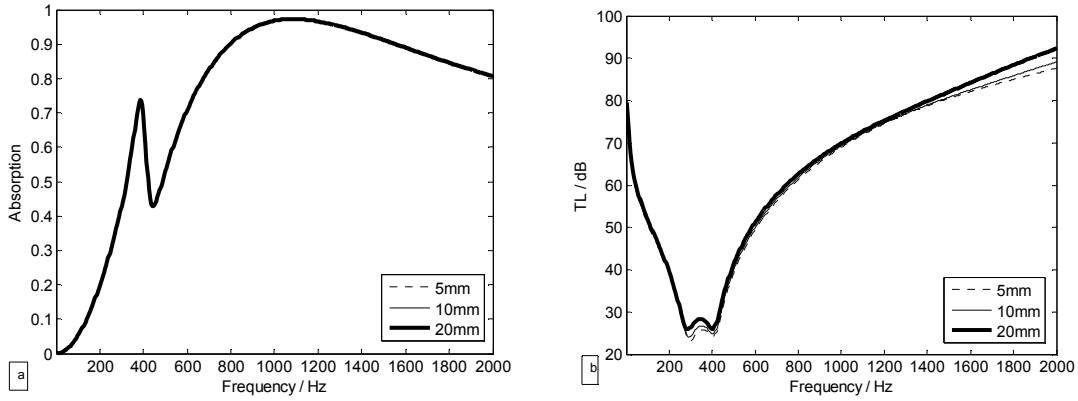

Fig.3-20 Acoustic performance of the hybrid system in different thicknesses of air gap 2; (a) absorption coefficient**;** (b) transmission loss

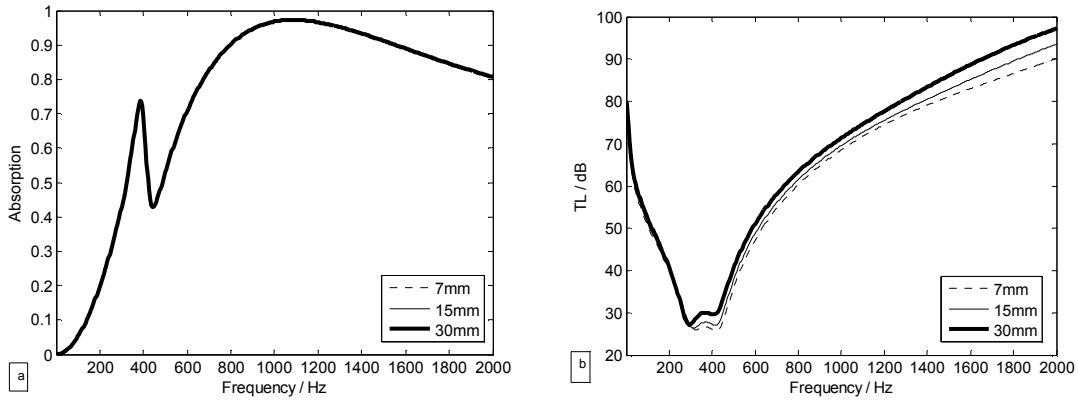

Fig.3-21 Acoustic performance of the hybrid system in different thicknesses of air gap 3; (a) absorption coefficient**;** (b) transmission loss

3.4 Conclusions

In this chapter, a hybrid active acoustic structure allowing good acoustic insulation and absorption for a wide frequency range have been modeled by the scattering matrix method. These hybrid active acoustic structures combine passive and active means by using passive layers and active plate, respectively. It is a combination of a sound absorbent system as 'an equivalent of the $\lambda/4$ resonance absorber', and a sound insulation system for improving the transmission loss. The secondary source is realized by an active plate consisting of two piezoelectric patches bonded to an elastic thin plate in order to improve acoustic insulation at low and resonances frequencies.

In the scattering matrix method, the active plate has been completely described in form of a scattering matrix and a source strength vector which represents respectively the passive and active proprieties of this plate. In active control, the source strength vector of the active plate is calculated in order to minimize the sound pressure or power at the location of the error sensor. The acoustic performances of the hybrid system, the absorption coefficient and transmission loss, are then deduced from the secondary source vector and the scattering matrix coefficients of all layers or elements composing this system. The simulation results show that a significant gain on transmission loss (higher than 15 dB) has been obtained by active control around the resonance frequency. Meanwhile, the absorption coefficient of this hybrid system exceeds 0.6 over 500Hz.

Lastly, the influence factors which affect the acoustic performance of the hybrid system have been investigated by simulation on different parameters of each layer. It can be concluded that more attention should be paid to the layers located at the front of the active plate when designing a hybrid system. The appropriate thickness, porosity and resistivity of the porous material and the air gap's thickness should be chosen for getting much better acoustic performance of the hybrid system.

In conclusion, the scattering matrix approach is an efficient tool for modeling or optimizing multilayered hybrid systems because of its simplicity. Indeed, when the elements of hybrid systems cannot be modeled by analytical methods (ex: complex boundary conditions, geometries…), numerical data in form of scattering-coefficients or radiated pressures can easily be incorporated in the computation program. That allows a smaller computation time compared with other numerical methods modeling the whole structure at the same time. However, this approach is not a perfect method when the porous material is elastic or coupled with an elastic plate. Due to the biphasic nature of the porous material, the elasticity of the skeleton should be considered, and the strong coupling between the solid and

fluid phases cannot be ignored. Hence, a new method for modeling the poroelastic medium should be proposed, described in the next chapter.

Chapter 4

Finite element study of hybrid active acoustic structure with poroelastic materials based on the (u, p) formulation

In the preceding chapter, the acoustic performance of the hybrid active acoustic structure is calculated by the scattering matrix method, in which the porous material is supposed as an equivalent fluid with effective density and bulk modulus [129]. This type of modeling applies to porous materials having a rigid skeleton, i.e., motionless or a very limp skeleton. In this case, only one compression wave propagates in the air-saturated medium, and five important parameters are needed to define the equivalent density and the equivalent impedance: porosity, resistivity, tortuosity, viscous, and thermal length [129]. Hence, Helmholtz's equation is a governing equation in the porous material.

However, when the porous material is elastic (called 'poroelastic'), or it is attached to an elastic plate, this hypothesis is no more suitable. In this case, the porous material is subject to three basic waves propagating simultaneously in the solid and fluid phase: two compressions and one shearing waves. Therefore, the elasticity of the skeleton should be considered, and the strong coupling between the solid and fluid phases cannot be ignored. Biot's theory of fluid saturated media is widely applied to describe the waves propagating in geophysics materials and to establish its mechanical behavior. For several decades, many authors have extended this theory to sound-absorbing materials, such as glass wool and polymer foams. Based on their progresses, a (*u, p*) formulation described by the displacement in the solid phase and the pressure in the fluid phase is developed with Biot's theory to model the acoustic behavior of the poroelastic material. This (*u, p*) formulation makes the scattering matrix

method complicate and inconvenient for modeling the hybrid active acoustic structure with poroelastic medium. Hence, a new method for modeling this hybrid system should be proposed.

This chapter aims to develop a finite element model of hybrid active acoustic structure with the (*u, p*) formulation in the Comsol environment. The partial differential equation of porous materials is described with the Comsol formulation, and the couplings between each layer are formulated in the Comsol environment. This model is validated by describing the normal surface impedance for the analytically solved case of a one-dimensional porous material with three boundary conditions: bonded into a rigid wall, attached with a layer of air, and an active control condition with zero pressure in the rear of the porous medium. Besides, the dynamic responses of some hybrid active acoustic structure are studied, in which piezoelectric patches are added onto the excited plate behaving as a secondary vibrational source, thus enhancing the effectiveness at low and/or resonance frequencies. The properties of different layers in these hybrid systems are calculated in the Comsol environment and the acoustic performance of the hybrid systems is validated by the numerical results of the scattering matrix method.

4.1 The Biot's theory of sound propagation in poroelastic material

4.1.1 The (u, p) formulation for poroelastic medium

Suppose the poroelastic material behaves like a visco-thermal equivalent fluid and has a rigid frame, good precision can be obtained when incident wave is in high frequency, but it is not appropriate in much low frequency because of the strong coupling between elastic solid and fluid. A classical displacement-displacement formulation (u,U) is proposed by Biot [131], seeing Eq. (4-1).

$$\begin{aligned} \nabla\cdot\boldsymbol{\sigma}^{\mathbf{s}} &= \rho_{11}\ddot{\mathbf{u}}^{\mathbf{s}} + \rho_{12}\ddot{\mathbf{U}}^{\mathbf{f}} + \tilde{b}(\dot{\mathbf{u}}^{\mathbf{s}} - \dot{\mathbf{U}}^{\mathbf{f}}) \\ \nabla\cdot\boldsymbol{\sigma}^{\mathbf{f}} &= \rho_{22}\ddot{\mathbf{U}}^{\mathbf{f}} + \rho_{12}\ddot{\mathbf{u}}^{\mathbf{s}} - \tilde{b}(\dot{\mathbf{u}}^{\mathbf{s}} - \dot{\mathbf{U}}^{\mathbf{f}}) \end{aligned} \tag{4-1}$$

Here, $\mathbf{u}^{\mathbf{s}}$ and $\mathbf{U}^{\mathbf{f}}$ stand for the frame and fluid displacements respectively; $\boldsymbol{\sigma}^{\mathbf{s}}$ and $\boldsymbol{\sigma}^{\mathbf{f}}$ stand for the frame and fluid stress tensor respectively. $\boldsymbol{\sigma}^{\mathbf{f}}$ depends on the pressure of fluid, and $\boldsymbol{\sigma}^{\mathbf{f}} = -\phi p\cdot\mathbf{I}$. ρ_{11} and ρ_{22} represent the relative densities of the frame and fluid, whereas ρ_{12} stands for a strong inertial coupling between the frame and fluid. $\tilde{b} = \sigma\phi^2\left(1+\frac{4j\alpha_\infty^2\eta\rho_0\omega}{\sigma^2\Lambda^2\phi^2}\right)^{1/2}$ is viscous damping coefficient depending on frequency. $\mathbf{I}$ is a unit diagonal matrix. The relations between ρ_{11}, ρ_{22}, ρ_{12} as follows:

$$\rho_{11} = \rho_s - \rho_{12}$$

$$\rho_{22} = \phi\rho_0 - \rho_{12}$$

$$\rho_{12} = -\phi\rho_0(\alpha_\infty - 1)$$

Here, ρ_s is the material density of poroelastic medium, and ρ_0 is air density.

Suppose this porous material is uniformity, and incident wave is a time-harmonic plane wave, Eq. (4-1) can be rewritten by eliminating the factor $e^{j\omega t}$:

$$\omega^2\tilde{\rho}_{11}\mathbf{u}^s + \omega^2\tilde{\rho}_{12}\mathbf{U}^f + \nabla\cdot\boldsymbol{\sigma}^s = 0 \tag{4-2}$$

$$\omega^2\tilde{\rho}_{22}\mathbf{U}^f + \omega^2\tilde{\rho}_{12}\mathbf{u}^s - \phi\nabla p = 0 \tag{4-3}$$

Here

$$\tilde{\rho}_{11} = \rho_{11} + \tilde{b}/j\omega$$

$$\tilde{\rho}_{22} = \rho_{22} + \tilde{b}/j\omega$$

$$\tilde{\rho}_{12} = \rho_{12} - \tilde{b}/j\omega$$

From Eq. (4-3), $\mathbf{U}^f$ can be described by $\mathbf{u}^s$:

$$\mathbf{U}^f = \frac{\phi}{\omega^2\tilde{\rho}_{22}}\nabla p - \frac{\tilde{\rho}_{12}}{\tilde{\rho}_{22}}\mathbf{u}^s \tag{4-4}$$

A. Solid phase motion equation in (u, p) formulation

Substituting Eq. (4-4) to (4-2)

$$\omega^2\tilde{\rho}\mathbf{u}^s + \phi\frac{\tilde{\rho}_{12}}{\tilde{\rho}_{22}}\nabla p + \nabla\cdot\boldsymbol{\sigma}^s = 0 \tag{4-5}$$

Here $\tilde{\rho} = \tilde{\rho}_{11} - (\tilde{\rho}_{12})^2 / \tilde{\rho}_{22}$.

It is to be noted that $\boldsymbol{\sigma}^s = \boldsymbol{\sigma}^s(\mathbf{u}^s, \mathbf{U}^f)$ still depends on the fluid displacement $\mathbf{U}^f$, therefore a mathematic operation is carried out according to the stress-strain relation [130] based on Biot theory:

$$\boldsymbol{\sigma}^s(\mathbf{u}^s, \mathbf{U}^f) = A\nabla\cdot\mathbf{u}^s + 2N\boldsymbol{\varepsilon}^s + Q\nabla\cdot\mathbf{U}^f \tag{4-6}$$

$$-\phi p\cdot\mathbf{I} = R\nabla\cdot\mathbf{U}^f + Q\nabla\cdot\mathbf{u}^s \tag{4-7}$$

Here

$$A = K_b + \frac{(1-\phi)^2}{\phi}K_f - \frac{2}{3}N$$

$$Q = (1-\phi)K_f$$

$$R = \phi K_f$$

N is the shear modulus of poroelastic medium; K_b and K_f are the bulk modulus of the solid phase in vacuum and the fluid phase with the solid phase in motionless, $K_b = \frac{2N(\mu+1)}{3(1-2\mu)}$, $K_f = K(\omega)$; μ is Poisson ratio of solid phase.

Substituting Eq. (4-7) to (4-6):

$$\boldsymbol{\sigma}^{\mathbf{s}}(\mathbf{u}^{\mathbf{s}}, \mathbf{U}^{\mathbf{f}}) = \left(A - \frac{Q^2}{R}\right)\nabla \cdot \mathbf{u}^{\mathbf{s}} + 2N\boldsymbol{\varepsilon}^{\mathbf{s}} - \phi\frac{Q}{R}p \cdot \mathbf{I} \tag{4-8}$$

Define

$$\begin{aligned}\hat{\boldsymbol{\sigma}}^{\mathbf{s}}(\mathbf{u}^{\mathbf{s}}) &= \left(A - \frac{Q^2}{R}\right)\nabla \cdot \mathbf{u}^{\mathbf{s}} + 2N\boldsymbol{\varepsilon}^{\mathbf{s}} \\ &= \left(K_b - \frac{2}{3}N\right)\nabla \cdot \mathbf{u}^{\mathbf{s}} + 2N\boldsymbol{\varepsilon}^{\mathbf{s}}\end{aligned} \tag{4-9}$$

Then

$$\boldsymbol{\sigma}^{\mathbf{s}}(\mathbf{u}^{\mathbf{s}}, \mathbf{U}^{\mathbf{f}}) = \hat{\boldsymbol{\sigma}}^{\mathbf{s}}(\mathbf{u}^{\mathbf{s}}) - \phi\frac{Q}{R}p \cdot \mathbf{I} \tag{4-10}$$

Substituting Eq. (4-10) to (4-5):

$$\nabla \cdot \hat{\boldsymbol{\sigma}}^{\mathbf{s}}(\mathbf{u}^{\mathbf{s}}) + \omega^2\tilde{\rho}\mathbf{u}^{\mathbf{s}} + \tilde{\gamma}\nabla p = 0 \tag{4-11}$$

Here, $\tilde{\gamma} = \phi\left(\frac{\tilde{\rho}_{12}}{\tilde{\rho}_{22}} - \frac{Q}{R}\right)$. Equation (4-11) is the solid motion equation in (u, p) formulation.

B. Fluid phase motion equation in (u, p) formulation

Taking a divergence to Eq. (4-4):

$$\nabla \cdot \mathbf{U}^{\mathbf{f}} = \frac{\phi}{\omega^2\tilde{\rho}_{22}}\nabla^2 p - \frac{\tilde{\rho}_{12}}{\tilde{\rho}_{22}}\nabla \cdot \mathbf{u}^{\mathbf{s}} \tag{4-12}$$

Substituting Eq. (4-12) to Eq. (4-7):

$$\nabla^2 p + \omega^2\frac{\tilde{\rho}_{22}}{R}p - \omega^2\frac{\tilde{\rho}_{22}\tilde{\gamma}}{\phi^2}\nabla \cdot \mathbf{u}^{\mathbf{s}} = 0 \tag{4-13}$$

Equation (4-13) is the fluid motion equation in (u, p) formulation.

Equation (4-11) and (4-13) are the (u, p) formulation for poroelastic medium. The two terms in Eq. (4-11) mean the solid vibration characteristic in vacuum, whereas the two terms in Eq. (4-13) mean the acoustic wave propagation in fluid with motionless solid. The third term in the two equations is the coupling correction between the solid and fluid phase.

4.1.2 Coupling boundary conditions

The couplings between poroelastic/air, poroelastic/elastic and poroelastic /poroelastic are presented in this part. Simpler boundary conditions (a rigid wall, imposed pressure, imposed displacements) can be directly derived from these formulations described below.

A. Poroelastic/air coupling

In the case of a poroelastic medium linked to an acoustic medium, Eq. (4-14) states the continuity of the total normal stress, acoustic pressure and fluid flow [142].

$$\begin{aligned} \boldsymbol{\sigma}^{\mathbf{t}} \cdot \mathbf{n} &= -p^a \cdot \mathbf{n} \\ p &= p^a \\ (1-\phi)\mathbf{u}^{\mathbf{s}} \cdot \mathbf{n} + \phi \mathbf{U}^{\mathbf{f}} \cdot \mathbf{n} &= \frac{1}{\rho_0 \omega^2} \nabla p^a \cdot \mathbf{n} \end{aligned} \tag{4-14}$$

Here p^a is the pressure in the acoustic medium, $\boldsymbol{\sigma}^{\mathbf{t}}$ is the total stress tensor in the poroelastic material, and $\mathbf{n}$ is the outward normal unit vector.

$$\begin{aligned} \boldsymbol{\sigma}^{\mathbf{t}} &= \boldsymbol{\sigma}^{\mathbf{t}}(\mathbf{u}^{\mathbf{s}}, \mathbf{U}^{\mathbf{f}}) = \boldsymbol{\sigma}^{\mathbf{s}}(\mathbf{u}^{\mathbf{s}}, \mathbf{U}^{\mathbf{f}}) + \boldsymbol{\sigma}^{\mathbf{f}}(\underline{u}^{s}, \mathbf{U}^{\mathbf{f}}) \\ &= \hat{\boldsymbol{\sigma}}^{\mathbf{s}}(\mathbf{u}^{\mathbf{s}}) - \phi\left(1 + \frac{\underline{Q}}{R}\right) p \end{aligned} \tag{4-15}$$

Substituting Eq. (4-15) to (4-14):

$$\begin{aligned} \hat{\boldsymbol{\sigma}}^{\mathbf{s}}(\mathbf{u}^{\mathbf{s}}) \cdot \mathbf{n} &= -\left[1 - \phi\left(1 + \frac{\underline{Q}}{R}\right)\right] p^a \cdot \mathbf{n} \\ \nabla p \cdot \mathbf{n} &= \nabla p^a \cdot \mathbf{n} = 0 \\ p - p^a &= 0 \end{aligned} \tag{4-16}$$

By substituting p for $\mathbf{U}^{\mathbf{f}}$ using Eq. (4-4), the correct normal acceleration can be obtained, as written in Eq. (4-17).

$$\frac{1}{\rho_0} \nabla p^a \cdot \mathbf{n} = \omega^2 \left[\mathbf{u}^{\mathbf{s}} \cdot \mathbf{n} \left(1 - \phi \left(1 + \frac{\tilde{\rho}_{12}}{\tilde{\rho}_{22}} \right) \right) \right] + \frac{\phi^2}{\tilde{\rho}_{22}} \nabla p \cdot \mathbf{n} \tag{4-17}$$

B. Poroelastic/elastic coupling

Suppose the poroelastic material is bonded onto an elastic solid, which encompasses total continuity between the solid phase and elastic displacements, the continuity of the total normal stress, displacement and no fluid flow at the interface are conserved as follows [142]:

$$\begin{aligned} \boldsymbol{\sigma}^{\mathrm{t}} \cdot \mathbf{n} &= \boldsymbol{\sigma}^{\mathrm{e}} \cdot \mathbf{n} \\ \mathbf{u}^{\mathrm{s}} &= \mathbf{u}^{\mathrm{e}} \\ \mathbf{U}^{\mathrm{f}} \cdot \mathbf{n} - \mathbf{u}^{\mathrm{s}} \cdot \mathbf{n} &= \mathbf{0} \end{aligned} \tag{4-18}$$

Here $\boldsymbol{\sigma}^{\mathrm{e}}$ is the total stress tensor in the poroelastic material

Equation (4-18) can be rewritten as follows according to Eq. (4-4) and (4-15):

$$\begin{aligned} \hat{\boldsymbol{\sigma}}^{\mathrm{s}}(\mathbf{u}^{\mathrm{s}}) \cdot \mathbf{n} &= \phi\left(1+\frac{Q}{R}\right) p \cdot \mathbf{n} + \boldsymbol{\sigma}^{\mathrm{e}} \cdot \mathbf{n} \\ \nabla p \cdot \mathbf{n} &= \frac{\omega^2}{\phi}\left(\tilde{\rho}_{12} + \tilde{\rho}_{22}\right) \mathbf{u}^{\mathrm{s}} \cdot \mathbf{n} \\ \mathbf{u}^{\mathrm{e}} - \mathbf{u}^{\mathrm{s}} &= 0 \end{aligned} \tag{4-19}$$

C. Poroelastic/poroelastic coupling

In the case of a poroelastic medium linked to another poroelastic medium, the continuity of the total normal stress, displacement of solid and fluid phase, and fluid flow can be described by Eq. (4-20).

$$\begin{aligned} \boldsymbol{\sigma}_{\mathbf{1}}^{\mathbf{t}} \cdot \mathbf{n} &= \boldsymbol{\sigma}_{\mathbf{2}}^{\mathbf{t}} \cdot \mathbf{n} \\ \mathbf{u}_{\mathbf{1}}^{\mathbf{s}} &= \mathbf{u}_{\mathbf{2}}^{\mathbf{s}} \\ p_1^s &= p_2^s \\ \phi_1\left(\mathbf{U}_{\mathbf{1}}^{\mathbf{f}} \cdot \mathbf{n} - \mathbf{u}_{\mathbf{1}}^{\mathbf{s}} \cdot \mathbf{n}\right) &= \phi_2\left(\mathbf{U}_{\mathbf{2}}^{\mathbf{f}} \cdot \mathbf{n} - \mathbf{u}_{\mathbf{2}}^{\mathbf{s}} \cdot \mathbf{n}\right) \end{aligned} \tag{4-20}$$

Substituting Eq. (4-4) and (4-15) into (4-20), for poroelastic medium 1:

$$\begin{aligned} \hat{\boldsymbol{\sigma}}_{\mathbf{1}}^{\mathbf{s}}(\mathbf{u}_{\mathbf{1}}^{\mathbf{s}}) \cdot \mathbf{n} &= \hat{\boldsymbol{\sigma}}_{\mathbf{2}}^{\mathbf{s}}(\mathbf{u}_{\mathbf{2}}^{\mathbf{s}}) \cdot \mathbf{n} + \left[\phi_1\left(1+\frac{Q_1}{R_1}\right) - \phi_2\left(1+\frac{Q_2}{R_2}\right)\right] p_1 \cdot \mathbf{n} \\ \nabla p_1 \cdot \mathbf{n} &= \omega^2 \frac{\phi_2^2}{\phi_1^2} \nabla p_2 \cdot \mathbf{n} + \omega^2 \left(\frac{\tilde{\rho}_{12}^{(1)} + \tilde{\rho}_{12}^{(1)}}{\phi_1^2} - \frac{\tilde{\rho}_{12}^{(2)} + \tilde{\rho}_{12}^{(2)}}{\phi_2^2}\right) \mathbf{u}_{\mathbf{1}}^{\mathbf{s}} \cdot \mathbf{n} \end{aligned} \tag{4-21}$$

For poroelastic medium 2:

$$\begin{aligned} \hat{\boldsymbol{\sigma}}_{\mathbf{2}}^{\mathbf{s}}(\mathbf{u}_{\mathbf{2}}^{\mathbf{s}}) \cdot \mathbf{n} &= \hat{\boldsymbol{\sigma}}_{\mathbf{1}}^{\mathbf{s}}(\mathbf{u}_{\mathbf{1}}^{\mathbf{s}}) \cdot \mathbf{n} + \left[\phi_2\left(1+\frac{Q_2}{R_2}\right) - \phi_1\left(1+\frac{Q_1}{R_1}\right)\right] p_2 \cdot \mathbf{n} \\ \nabla p_2 \cdot \mathbf{n} &= \omega^2 \frac{\phi_1^2}{\phi_2^2} \nabla p_1 \cdot \mathbf{n} + \omega^2 \left(\frac{\tilde{\rho}_{12}^{(2)} + \tilde{\rho}_{12}^{(2)}}{\phi_2^2} - \frac{\tilde{\rho}_{12}^{(1)} + \tilde{\rho}_{12}^{(1)}}{\phi_1^2}\right) \mathbf{u}_{\mathbf{2}}^{\mathbf{s}} \cdot \mathbf{n} \end{aligned} \tag{4-22}$$

4.2 Finite element method for modeling hybrid active structure

4.2.1 Passive process

A finite element method is used to analyze the acoustic wave propagation in hybrid active acoustic structure based on Comsol environment. Comsol provides powerful applications modes for acoustic, piezoelectric and elastic problems, but it does not currently provide a specific application mode for poroelastic medium. Since the coupling between the fluid and the solid phases occurs in poroelastic medium, the partial differential equations (PDE mode) provided by Comsol is chosen for modeling the poroelastic material [147]. The partial differential equation is rewritten here in Eq. (4-23).

$$\begin{aligned} \boldsymbol{\Gamma}\cdot\nabla &= \mathbf{F} \\ -\boldsymbol{\Gamma}\cdot\mathbf{n} &= \mathbf{G}+\left(\frac{\partial \mathbf{L}}{\partial \mathbf{U}}\right)^{T} l \\ 0 &= \mathbf{L} \end{aligned} \tag{4-23}$$

$\mathbf{U}$ is the vector of unknowns and $\boldsymbol{\Gamma}, \mathbf{F}, \mathbf{G}, \mathbf{L}$ are PDE coefficients depending on $\mathbf{U}$ or its differentiation, $\mathbf{L}$ is the 'Dirichlet' vector, and $\mathbf{G}$ is the 'Neumann' vector; l denotes the Lagrange multiplier; $\mathbf{n}$ is the outward normal unit vector.

In cartesian coordinate system, the displacement of solid phase is presented by $\mathbf{u^s}=(u,v,w)$, whereas the pressure of fluid phase is described by p. Compared the first term to Eq. (4-11) and (4-13), $\boldsymbol{\Gamma}$ and $\mathbf{F}$ can be written as follows:

$$\boldsymbol{\Gamma}=\begin{bmatrix}\Gamma_{ij}\\ \Gamma_{4j}\end{bmatrix}=\begin{bmatrix}\hat{\boldsymbol{\sigma}}^{\mathbf{s}}(\mathbf{u^s})\\ \nabla p\end{bmatrix} \tag{4-24}$$

$$\mathbf{F}=\begin{bmatrix}F_i\\ F_4\end{bmatrix}=\begin{bmatrix}-\omega^2\tilde{\rho}\mathbf{u^s}-\tilde{\gamma}\nabla p\\ -\omega^2\dfrac{\tilde{\rho}_{22}}{R}p+\omega^2\dfrac{\tilde{\rho}_{22}\tilde{\gamma}}{\phi^2}\nabla\cdot\mathbf{u^s}\end{bmatrix} \tag{4-25}$$

According to the formulation of $\hat{\boldsymbol{\sigma}}^{\mathbf{s}}(\mathbf{u^s})$, and defining $u^s_{k,k}=\nabla\cdot\mathbf{u^s}=\dfrac{\partial u}{\partial x}+\dfrac{\partial v}{\partial y}+\dfrac{\partial w}{\partial z}=u_x+v_y+w_z$, $\boldsymbol{\Gamma}$ and $\mathbf{F}$ can be rewritten in details:

$$\boldsymbol{\Gamma}=\begin{bmatrix}2Nu_x+\hat{A}u^s_{k,k} & N(u_y+v_x) & N(u_z+w_x)\\ N(u_y+v_x) & 2Nv_y+\hat{A}u^s_{k,k} & N(w_y+v_z)\\ N(u_z+w_x) & N(v_z+w_y) & 2Nw_z+\hat{A}u^s_{k,k}\\ p_x & p_y & p_z\end{bmatrix} \tag{4-26}$$

$$\mathbf{F}=\begin{bmatrix} -\omega^2\tilde{\rho}u-\tilde{\gamma}p_x \\ -\omega^2\tilde{\rho}v-\tilde{\gamma}p_y \\ -\omega^2\tilde{\rho}w-\tilde{\gamma}p_z \\ -\omega^2\dfrac{\tilde{\rho}_{22}}{R}p+\omega^2\dfrac{\tilde{\rho}_{22}\tilde{\gamma}}{\phi^2}u^s_{k,k} \end{bmatrix} \tag{4-27}$$

Here, $\hat{A}=A-\dfrac{Q^2}{R}$, subscript $'x'$, $'y'$, $'z'$ represent the derivation of x, y, z.

Compared the last two terms of Eq. (4-23) to (4-16)~(4-22), some PDE coefficients can be obtained.

1) Poroelastic/air coupling

$$\mathbf{G}=\begin{bmatrix} \left[1-\phi\left(1+Q/R\right)\right]p^a n_x \\ \left[1-\phi\left(1+Q/R\right)\right]p^a n_y \\ \left[1-\phi\left(1+Q/R\right)\right]p^a n_z \\ 0 \end{bmatrix},\qquad \mathbf{L}=\begin{bmatrix} 0 \\ 0 \\ 0 \\ p-p^a \end{bmatrix} \tag{4-28}$$

2) Poroelastic/elastic coupling

$$\mathbf{G}=\begin{bmatrix} -\phi\left(1+Q/R\right)pn_x-\left(\sigma^e_{xx}n_x+\sigma^e_{xy}n_y+\sigma^e_{xz}n_z\right) \\ -\phi\left(1+Q/R\right)pn_y-\left(\sigma^e_{xy}n_x+\sigma^e_{yy}n_y+\sigma^e_{yz}n_z\right) \\ -\phi\left(1+Q/R\right)pn_z-\left(\sigma^e_{xz}n_x+\sigma^e_{yz}n_y+\sigma^e_{zz}n_z\right) \\ -\left(\omega^2/\phi\right)\left(\tilde{\rho}_{12}+\tilde{\rho}_{22}\right)\left(un_x+vn_y+wn_z\right) \end{bmatrix},\qquad \mathbf{L}=\begin{bmatrix} u^e-u^s \\ v^e-v^s \\ w^e-w^s \\ 0 \end{bmatrix} \tag{4-29}$$

3) Poroelastic/poroelastic coupling

$$\mathbf{G_1}=-\mathbf{A_1}\boldsymbol{\Gamma}_2\cdot\mathbf{n}-\mathbf{B_1},\qquad \mathbf{G_2}=-\mathbf{A_2}\boldsymbol{\Gamma}_1\cdot\mathbf{n}-\mathbf{B_2} \tag{4-30}$$

Here

$$\mathbf{A_1}=\begin{bmatrix} 1 \\ 1 \\ 1 \\ \omega^2\phi_2^2/\phi_1^2 \end{bmatrix}^T,\qquad \mathbf{B_1}=\begin{bmatrix} \left[\phi_1\left(1+Q_1/R_1\right)-\phi_2\left(1+Q_2/R_2\right)\right]p_1n_x \\ \left[\phi_1\left(1+Q_1/R_1\right)-\phi_2\left(1+Q_2/R_2\right)\right]p_1n_y \\ \left[\phi_1\left(1+Q_1/R_1\right)-\phi_2\left(1+Q_2/R_2\right)\right]p_1n_z \\ \omega^2\left((\tilde{\rho}^{(1)}_{12}+\tilde{\rho}^{(1)}_{12})/\phi_1^2-(\tilde{\rho}^{(2)}_{12}+\tilde{\rho}^{(2)}_{12})/\phi_2^2\right)\left(u_1n_x+v_1n_y+w_1n_z\right) \end{bmatrix}$$

$$\mathbf{A_2}=\begin{bmatrix} 1 \\ 1 \\ 1 \\ \omega^2\phi_1^2/\phi_2^2 \end{bmatrix}^T,\qquad \mathbf{B_2}=\begin{bmatrix} \left[\phi_2\left(1+Q_2/R_2\right)-\phi_1\left(1+Q_1/R_1\right)\right]p_2n_x \\ \left[\phi_2\left(1+Q_2/R_2\right)-\phi_1\left(1+Q_1/R_1\right)\right]p_2n_y \\ \left[\phi_2\left(1+Q_2/R_2\right)-\phi_1\left(1+Q_1/R_1\right)\right]p_2n_z \\ \omega^2\left((\tilde{\rho}^{(2)}_{12}+\tilde{\rho}^{(2)}_{12})/\phi_2^2-(\tilde{\rho}^{(1)}_{12}+\tilde{\rho}^{(1)}_{12})/\phi_1^2\right)\left(u_2n_x+v_2n_y+w_2n_z\right) \end{bmatrix}$$

$$\mathbf{L_1} = -\mathbf{L_2} = \begin{bmatrix} u_1 - u_2 \\ v_1 - v_2 \\ w_1 - w_2 \\ p_1 - p_2 \end{bmatrix} \tag{4-31}$$

Based on the above analysis, the unknown displacement $\mathbf{u}^s = (u, v, w)$ of the solid phase and the pressure of the fluid phase p in porous materials can be obtained, and then the pressure at both sides of the hybrid active structure can be calculated in Comsol environment. According to the sound propagation principle of the plane wave, the transmission loss TL and absorption coefficient α of the structure can be expressed,

$$TL = 10\lg(W_i / W_t) \qquad \alpha = 1 - \left(p_r / p_i\right)^2 \tag{4-32}$$

Here, W_i , W_t represent respectively the incident and transmitted sound power, and $W_i = \frac{p_i^2}{2\rho_0 c_0^2} S$, $W_t = \frac{p_t^2}{2\rho_0 c_0^2} S$; p_i , p_r , p_t denote respectively the amplitudes of the incident, reflected and transmitted sound waves; ρ_0 , c_0 are the air density and velocity; S is the cross-section of the structure.

4.2.2 Active control

In Comsol environment, a piezo solid mode is used to model the piezoelectric patches glued to both sides of active plate. Suppose P_{imp} is the pressure of the incident acoustic wave, V_{imp} is the voltage imposed on the piezoelectric patches, simulation of the active behavior of the hybrid active acoustic structure is obtained in three steps in the condition that this active acoustic structure is a linear system. Fig.4-1 shows the transfer function schematic of the hybrid active acoustic structures.

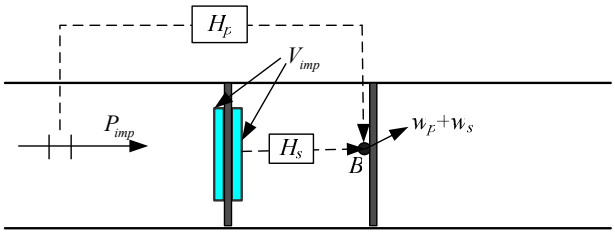

Fig.4-1 The transfer function schematic

1) $P_{imp} = P_0$, $V_{imp} = 0$

The pressure P_{imp} of the incident acoustic wave is impose to P_0 , and the voltage V_{imp} is zero, that is, the active control is turned off. The displacement at the center of the radiating

plate or the pressure of the acoustic wave at radiating side can be calculated, represented in $w_p(\omega)$. Then the first transfer function of incident wave can be written in Eq. (4-31).

$$H_p(\omega) = \frac{w_p(\omega)}{P_0} \tag{4-33}$$

2) $P_{imp} = 0$, $V_{imp} = V_0$

In this step, no more incident wave transmits in hybrid active acoustic structure, and the active plate is excited by an electric potential V_0 applied to the piezoelectric patches. Once again, the displacement at the center of the radiating plate or the pressure of the acoustic wave at radiating side can be calculated, represented in $w_s(\omega)$. Then the second transfer function of secondary sound source can be written in Eq. (4-34).

$$H_s(\omega) = \frac{w_s(\omega)}{V_0} \tag{4-34}$$

3) $P_{imp} = P_1$, $V_{imp} = V_s$

Finally, the pressure P_{imp} of the incident acoustic wave is impose to P_1, and the optimal voltage exciting active plate is calculated by Eq. (4-35).

$$V_s(\omega) = -\frac{H_p(\omega)}{H_s(\omega)} P_1 \tag{4-35}$$

Therefore, the displacement of the radiating plate or the pressure of the acoustic wave at radiating side can be reduced obviously.

4.3 Numerical results and validations

In this section, the properties of different layers in these hybrid systems are calculated in the Comsol environment and the acoustic performance of the hybrid systems is validated by the numerical results of the scattering matrix method.

4.3.1 The radiating plate

The radiating plate used in the hybrid active acoustic structure is an elastic thin plate in steel with a thickness of 0.2mm, and its physics parameters are given in Table.2-1. In the Comsol environment, only a quarter of this simply supported plate is modeled because of its symmetry, which reduces the memory storage and calculation time. Some shape deformations of the radiating plate are drawn in Fig.4-2 by Comsol environment, lower than the simulation frequencies.

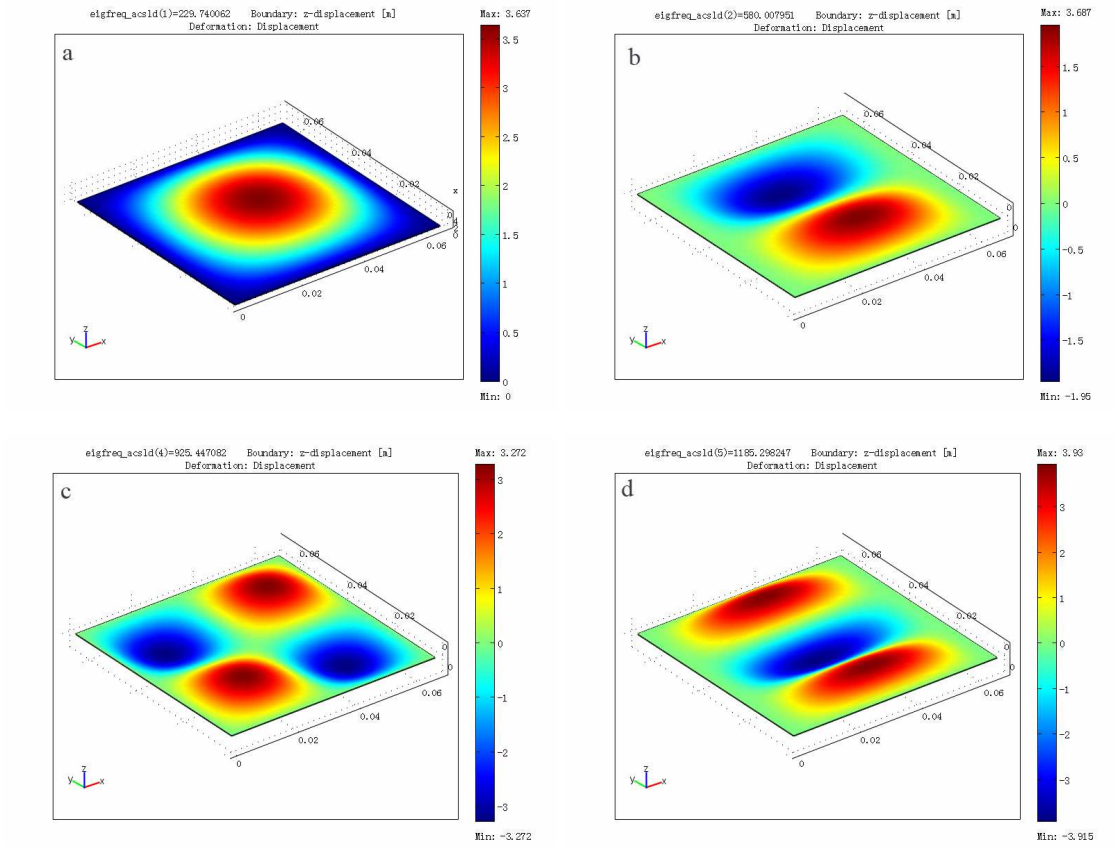

Fig.4-2 Deformations of the radiating plate a) 1-1 shape mode; b) 1-2 shape mode; c) 2-2 shape mode; d) 1-3 shape mode.

Theoretically, the *mn* th eigenfrequency of a simple supported plate can be calculated by the expression:

$$f_{mn} = \frac{\pi}{2}\sqrt{\frac{Eh^2}{12(1-\mu^2)\rho}}\left[\left(\frac{m}{l_x}\right)^2 + \left(\frac{n}{l_y}\right)^2\right] \tag{4-36}$$

Here, E, μ, ρ are the Yong's modulus, Poisson ratio, and density respectively; h, l_x, l_y are the dimension parameters: thickness, length and width. The comparison between the eigenfrequency calculated by Eq. (4-36) and Comsol software is given in Table.4-1. The former six shape modes are respectively in 226Hz, 567Hz, 567Hz, 907Hz, 1134Hz, 1134Hz in the theoretical calculation and in 229Hz, 580 Hz, 580 Hz, 925Hz, 1185Hz, 1185Hz in Comsol environment. The relative errors in each mode are 1%, 2%, 2%, 2%, 4% and 4%, that is because the plate in Comsol is divided into 10×10 meshes. In fact, the more meshes it is divided into, the more precise the eigenfrequency is.

Table.4-1 Comparison of the eigenfrequency in theoretical and Comsol results

	1-1 mode	1-2 mode	2-1 mode	2-2 mode	1-3 mode	3-1 mode
Eq. (4-36)	226 Hz	567 Hz	567 Hz	907 Hz	1134 Hz	1134 Hz
Comsol	229 Hz	580 Hz	580 Hz	925 Hz	1185 Hz	1185 Hz
Relative error	1%	2%	2%	2%	4%	4%

Fig.4-3 shows the transmission loss of this radiating plate in simulation results: the scattering matrix method and the finite element method in Comsol. The two results show the first resonance frequency of the radiating plate is adjacent to 230Hz, and good agreement can be obtained for low frequencies. Unfortunately, the second peak of transmission loss cannot be displayed in the scattering matrix method because only the first vibration mode is used to calculate the transfer matrix of this plate.

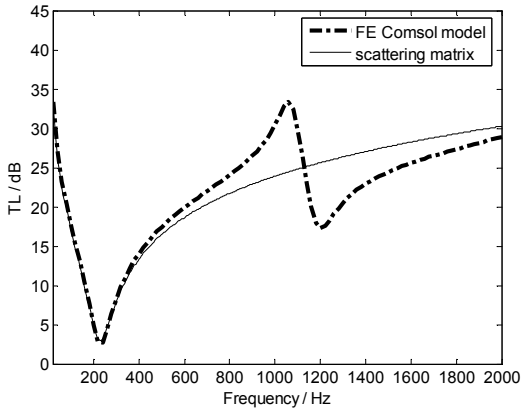

Fig.4-3 The transmission loss of the radiating plate with simple support

4.3.2 The active plate

The active plate used in the hybrid active acoustic structure is the elastic thin steel plate bonded on piezoelectric patches with a thickness of 0.5mm on both sides, and its physics parameters are given in Table.3-1. The configuration of this active plate is shown in Fig.4-4. In the Comsol environment, a quarter of the active plate is modeled with 10×10 meshes. Some shape deformations of the active plate are drawn in Fig.4-5 by Comsol environment, lower than the simulation frequencies. The former six shape modes are respectively in 317Hz, 612 Hz, 612 Hz, 1095Hz, 1374Hz and 1690Hz in Comsol environment, which has an obvious shift compared to the six shape modes of the radiating plate, due to the piezoelectric patches

change the vibrational property of this plate. Besides, the piezoelectric patches bonded on both sides of the active plate make the maximum vibrational amplitudes of each shape mode moving to the edges of the piezoelectric patches except the 1-1 mode compared to that of the radiating plate in Fig.4-2. That is because the boundary condition of the piezoelectric patches is free in Comsol environment.

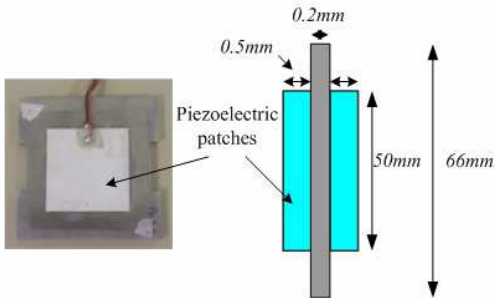

Fig.4-4 The configuration of the active plate

Fig.4-6 represents the transmission loss of this active plate on the condition of no excitation on the piezoelectric patches in simulation results: the scattering matrix method and the finite element method in Comsol. The two results show the first resonance frequency of the active plate is adjacent to 320Hz, and good agreement can be obtained for low frequencies. Nevertheless, the second peak of transmission loss also cannot be displayed in the scattering matrix method because only the first vibration mode is used to calculate the transfer matrix of this plate. Fig.4-7 gives the comparison between the transmission loss of the radiating plate and the active plate, and an obvious improvement can be obtained in the all-range frequency because of the piezoelectric patches.

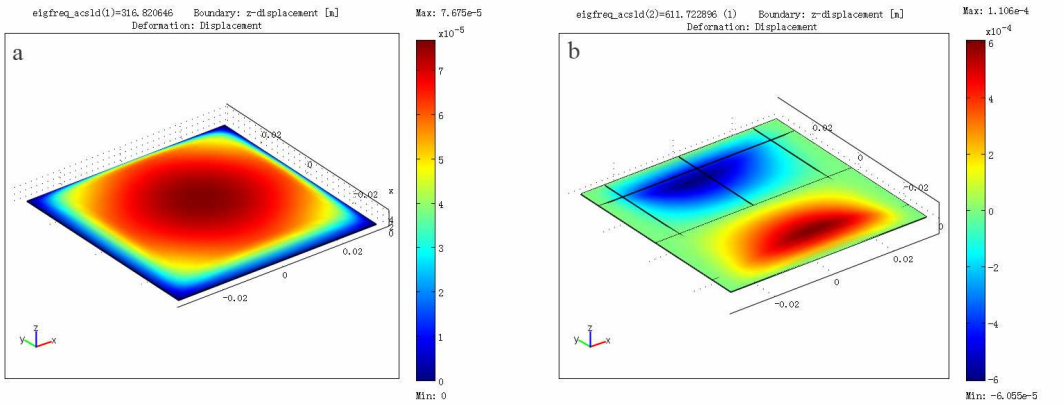

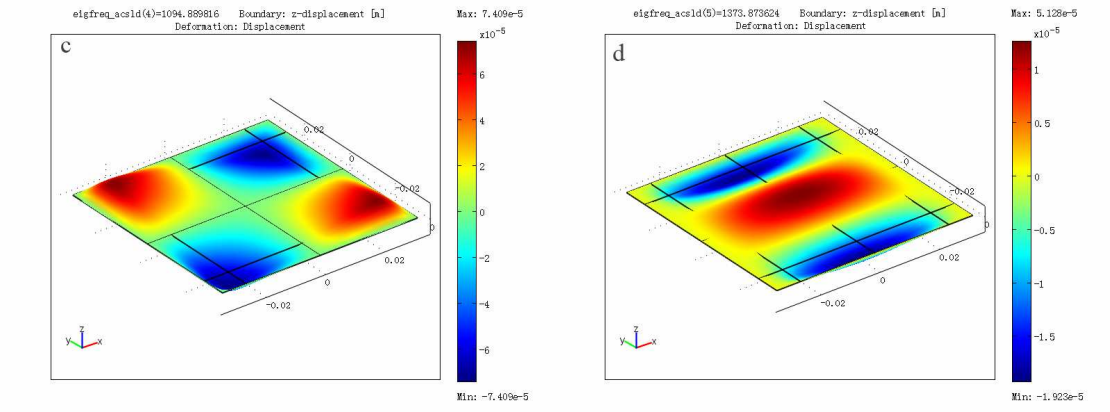

Fig.4-5 Deformations of the active plate a) 1-1 shape mode; b) 1-2 shape mode; c) 2-2 shape mode; d) 1-3 shape mode.

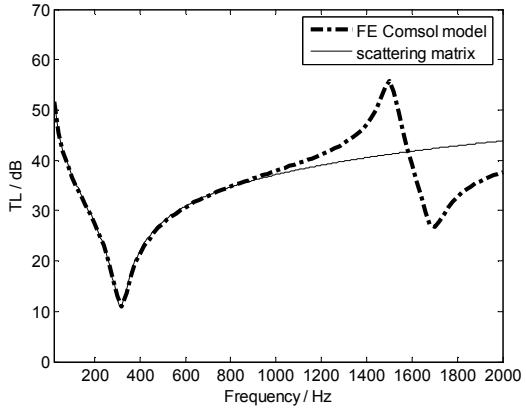

Fig.4-6 The transmission loss of the active plate with simple support

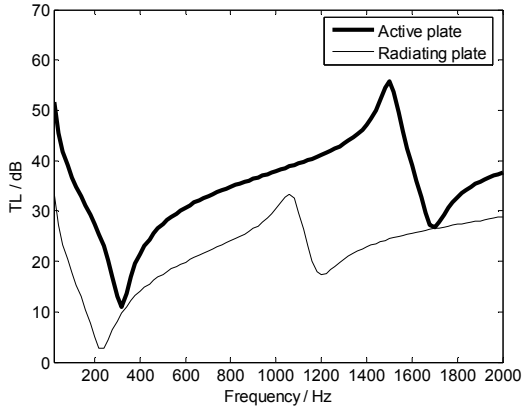

Fig.4-7 Comparison between the transmission loss of the active plate and the radiating plate

4.3.3 Porous material

In the Comsol environment, a PDE model is used to model the poroelastic material. The surface impedance Z_s at normal incidence is calculated for three types of boundary condition as shown in Fig.4-8: with a rigid wall, with a layer of air and active control condition, that is, zero pressure at the rear of the poroelastic medium. In the Biot-Allard theory, the surface impedance is calculated with Eq. (4-37)-(4-39). Z_c, k and Z_0, k_0 are the impedances and wave numbers of the porous material and air layer respectively.

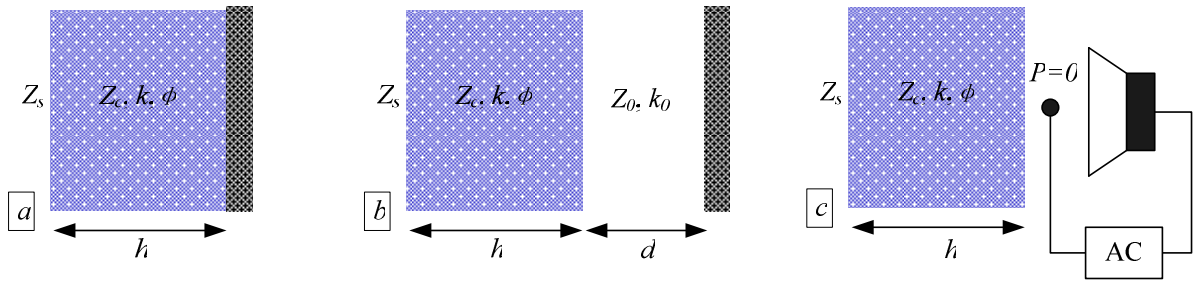

Fig.4-8 Porous material with three boundary conditions a) with a rigid wall; b) with a layer of air; c) active condition

1) with rigid wall, Fig.4-8(a)

$$Z_s = -j\frac{Z_c}{\phi}\cot(kh) \tag{4-37}$$

2) with a layer of air, Fig.4-8(b)

$$Z_s = \frac{Z_c}{\phi}\frac{-jZ_a\cot(kh)+Z_c}{Z_a - jZ_c\cot(kh)} \tag{4-38}$$

Here, $Z_a = -jZ_0\cot(k_0 d)$.

3) active control condition, Fig.4-8(c)

$$Z_s = \frac{Z_c}{\phi}\tan(kh) \tag{4-39}$$

However, in the Comsol environment Z_s is defined as the ratio of the acoustic pressure and total velocity at the impinged face, and can be stated as

$$Z_s(\omega) = \frac{p}{j\omega\left(\phi U_3^f + (1-\phi)u_3^s\right)}$$

$$= p \cdot \left\{ j\omega \left[\phi p_z / \omega^2 \tilde{\rho}_{22} + \left(1 - \phi\left(1 + \tilde{\rho}_{12} / \tilde{\rho}_{22}\right)\right) w \right] \right\}^{-1} \tag{4-40}$$

For confirming that the PDE model modeling this poroelastic material is valid in Comsol, we calculate the ratios of the surface impedance and the air impedance Z_s / Z_0 by applying Biot-Allard theory to some examples given in Table.4-2, which have been validated with experimental measurements [162]. Comparing to the results obtained in Comsol with the finite element method, good agreement can be noted for the three boundary conditions as shown in Fig.4-9.

Table.4-2 Parameters of porous materials (felt)

Thickness	25 cm
Porosity	0.93
Resistivity	23150 rayls/m
Young's modulus	12000 Pa
Mass density	50 kg/m^3
Tortuosity	1.1
Viscous length	44μm
Thermal length	121μm
Poisson ratio	0.06

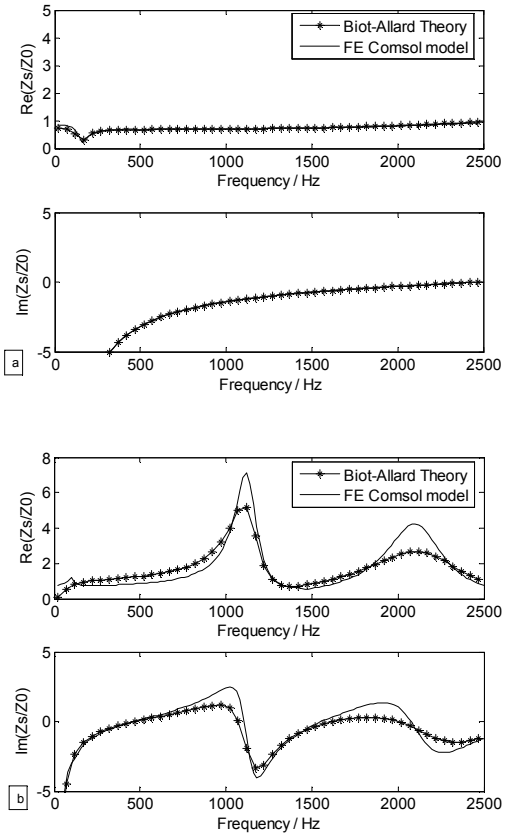

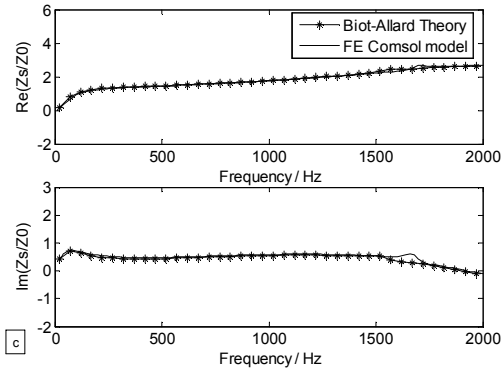

Fig.4-9 Comparison between the surface impedance in Biot-Allard theory and FE Comsol model a) with rigid wall; b) with a layer of 12cm air; c) active condition

In this chapter, the properties of the porous material used in the hybrid active acoustic structure are shown in Table.2-1. The acoustic performance of this porous material is plotted in Fig.4-10 with simulation results: the scattering matrix method and the finite element method in Comsol. In Comsol environment, the first resonance frequency of this material is about 360Hz, and its absorption coefficient is excellent, more than 0.8 over the range of frequencies of interest, whereas its transmission loss is less than 7dB. However, no resonance frequency can be obtained in the scattering matrix method, due to this porous material is elastic which makes an equivalent fluid with a rigid frame unsuitable to model this material.

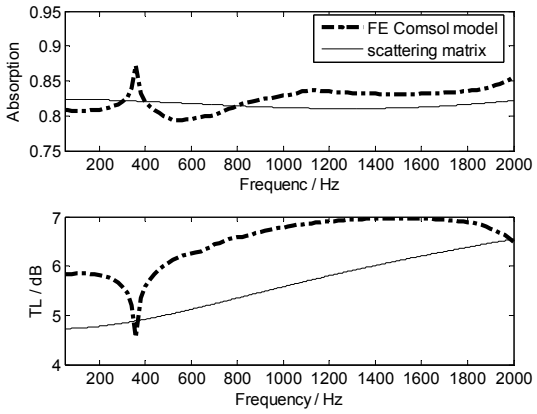

Fig.4-10 The acoustic performance of the porous material

4.3.4 Hybrid active acoustic structure

Some examples of the hybrid active acoustic structure with different cores will be presented in this section. The transmission loss of these packages is given in Comsol environment and the scattering matrix method, and the two results show that obvious improvements can be obtained with active control.

A. A double-wall structure with air gap

A configuration of the double-wall active acoustic structure with air gap of 20mm thickness is shown in Fig.4-11. An error sensor is positioned in point A.

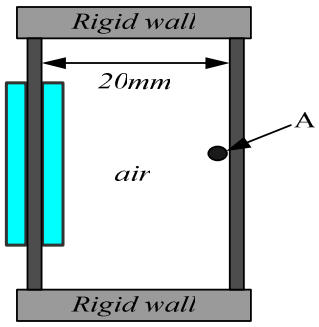

Fig.4-11 The configuration of the double-wall structure with air gap

In the Comsol environment, the 5×5×1, 5×5×2, and 4×4×1 3D meshes are applied respectively to the plate, the air gap and the piezoelectric patches. The transmission loss of this double-wall structure without active control is shown in Fig.4-12 with numerical results: the scattering matrix method and the finite element method. The resonance frequencies of the double-wall structure are 340Hz and 460Hz in Comsol environment, and 350Hz and 470Hz in the scattering matrix method; the relative error of the resonance frequency between the two methods is less than 3%. Besides, the transmission loss in the two methods has a good agreement lower than 600Hz: less than 5dB in difference. However, more differences in the transmission loss has been displayed over 600Hz, that is because only the first vibration mode is used to calculate the transfer matrix of the radiating plate and active plate. Fig.4-13 gives the transmission loss of this double-wall structure in Comsol environment with control the pressure in point A. It shows that the active control is valid until 1660Hz, and about 15dB of the transmission loss can be improved at the resonance frequencies.

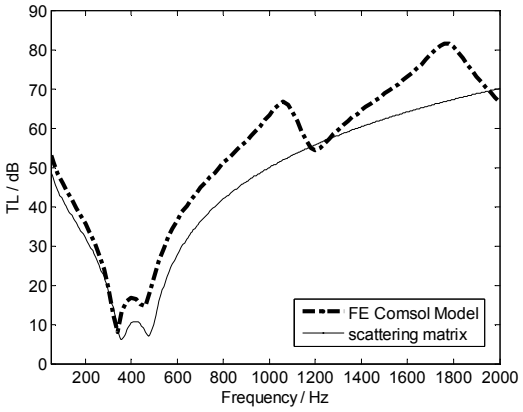

Fig.4-12 The transmission loss of a double-wall structure with air gap without active control

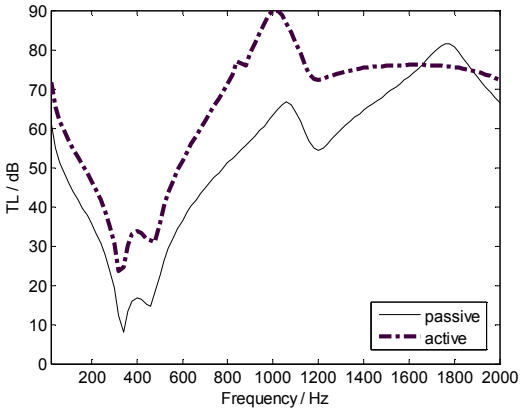

Fig.4-13 The transmission loss of a double-wall structure with air gap with passive and active control

Fig.4-14 shows the displacements of the radiating and active plates in this double-wall structure with or without active control in some frequencies: 100Hz, 340Hz, 460Hz, 600Hz, 1660Hz, and 1800Hz. The upper panel represents the radiating plate, and the down one is the active plate. Fig.4-14(a) and (d) display respectively the displacements in 100Hz and 600Hz of the two plates before and after active control. With active control, their displacements have been obviously reduced. Fig.4-14(b) and (c) display the displacements in the resonance frequencies of the two plates before and after active control, in which the two plates vibrate most strongly compared to other situations, and their displacements have complete attenuation after active control. Fig.4-14(e) represents the displacements in 1660Hz of the two plates before and after active control, in which the active control works weakly and their displacements cannot be reduced. Fig.4-14(f) represents the displacements in 1800Hz of the

two plates before and after active control, in which the active control makes the active plate vibrating more strongly than passive control.

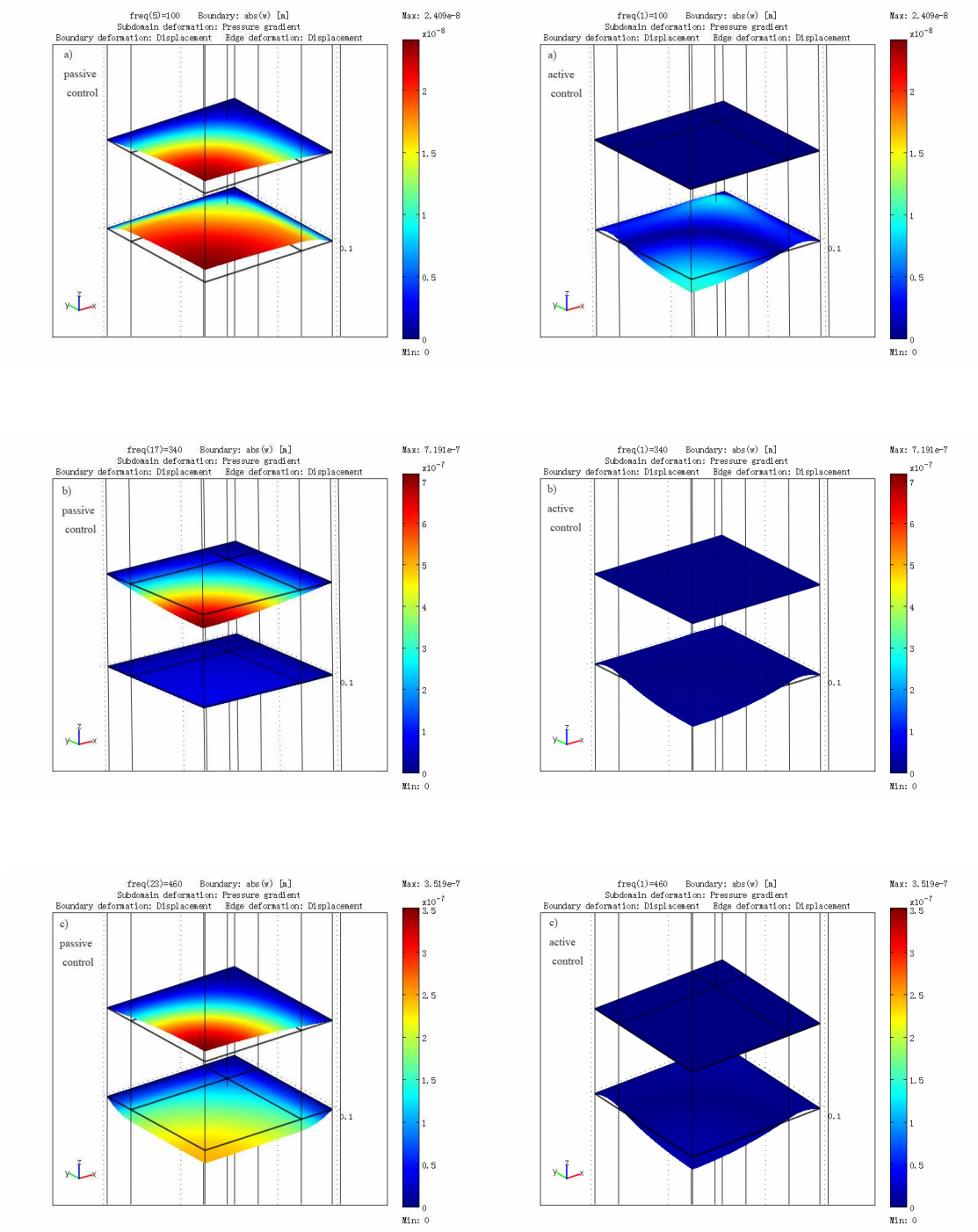

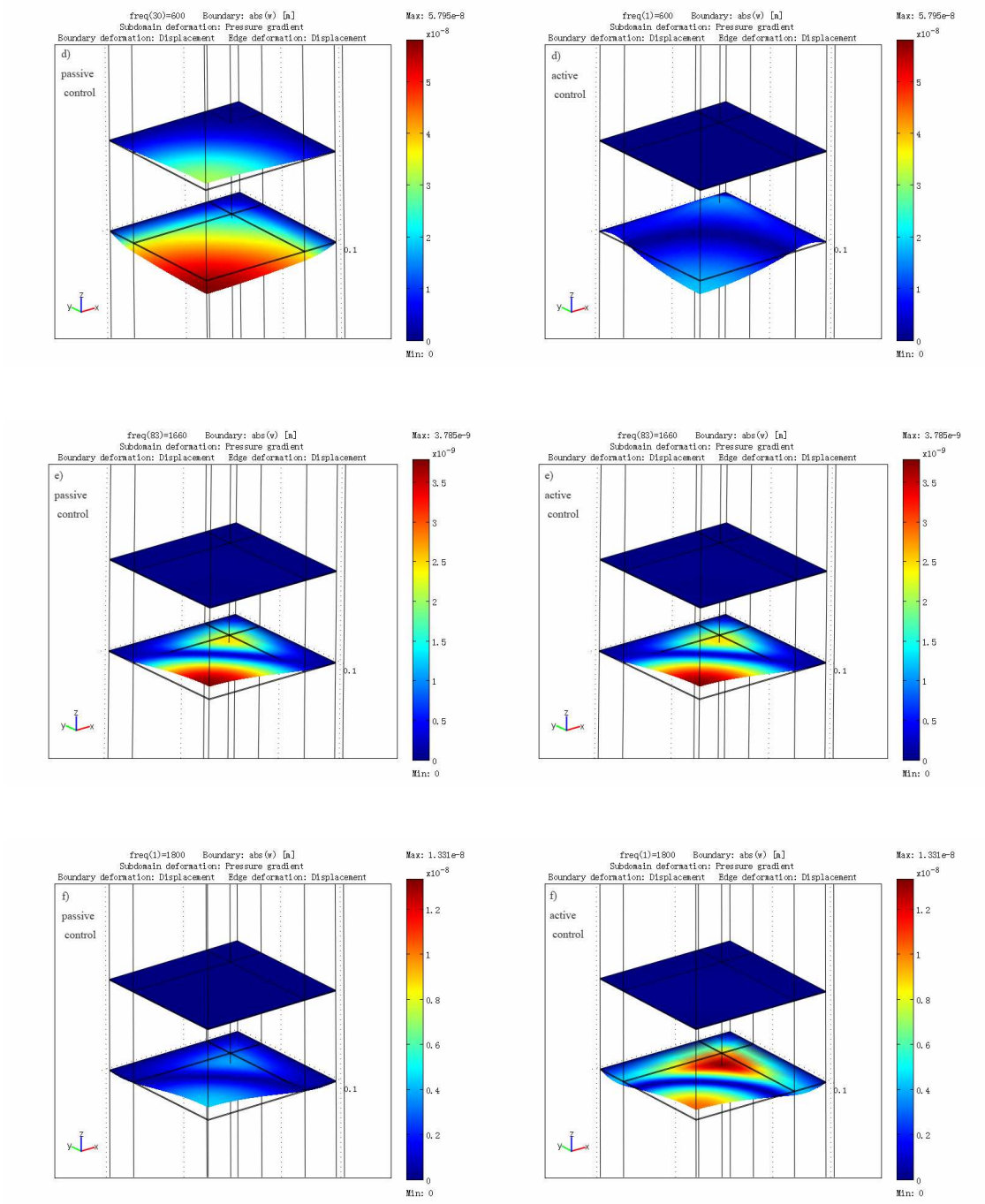

Fig.4-14 The displacement comparison of the radiating and active plates in the double-wall structure with air gap in passive and active control a) 100Hz; b) 340Hz; c) 460Hz; d) 600Hz; e) 1660Hz; f) 1800Hz.

B. A double-wall structure with porous material

Changing the air gap to a porous material core with the same thickness, the transmission loss of this double-wall structure without active control is shown in Fig.4-15 with numerical results: the scattering matrix method and the finite element method. The same meshes are

applied to the layers in Comsol environment. The resonance frequencies of this double-wall structure are 340Hz and 540Hz in Comsol environment, and 320Hz and 560Hz in the scattering matrix method; the relative error of the resonance frequency between the two methods is less than 6%. Besides, the transmission loss in the two methods has a good agreement lower than 800Hz: less than 2dB in difference. However, more differences in the transmission loss has been displayed over 800Hz, that is because the porous material is coupled with the elastic plates and it cannot be considered as an equivalent fluid with a rigid frame.

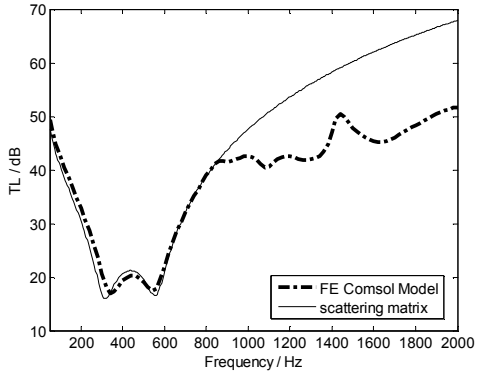

Fig.4-15 The transmission loss of a double-wall structure with air gap without active control

Fig.4-16 gives the transmission loss of this double-wall structure in Comsol environment with controlling the pressure in point A. It shows that the active control is valid until 840Hz, and about 10dB of the transmission loss can be improved at the resonance frequencies. In addition, the numerical results for passive control show that the transmission loss of the double-wall structure has been obviously improved with a porous material core at resonance frequencies, compared to that with an air gap core.

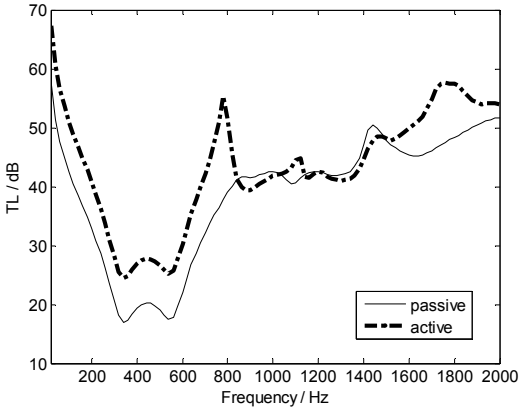

Fig.4-16 The transmission loss of a double-wall structure with porous with passive and active control

Fig.4-17 shows the displacements of the radiating and active plates in this double-wall structure with or without active control in some frequencies: 100Hz, 340Hz, 540Hz, 600Hz, 840Hz, and 900Hz. Fig.4-17(a) and (d) display respectively the displacements in 100Hz and 600Hz of the two plates before and after active control. With active control, their displacements have been obviously reduced. Fig.4-17(b) and (c) display the displacements in the resonance frequencies of the two plates before and after active control, in which the two plates vibrate most strongly compared to other situations, and their displacements have complete attenuation after active control. Fig.4-17(e) represents the displacements in 840Hz of the two plates before and after active control, in which the active control works weakly and their displacements cannot be reduced. Fig.4-17(f) represents the displacements in 900Hz of the two plates before and after active control, in which the active control makes the active plate vibrating more strongly than passive control.

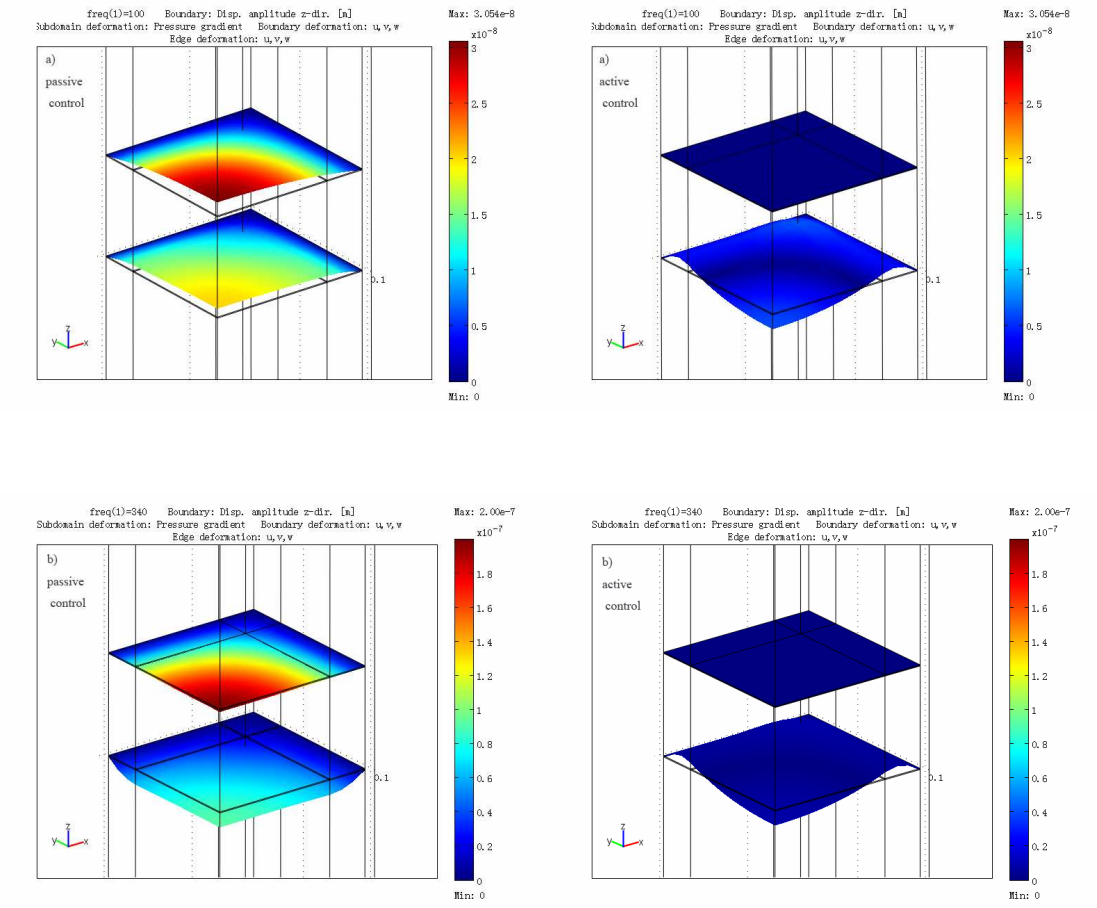

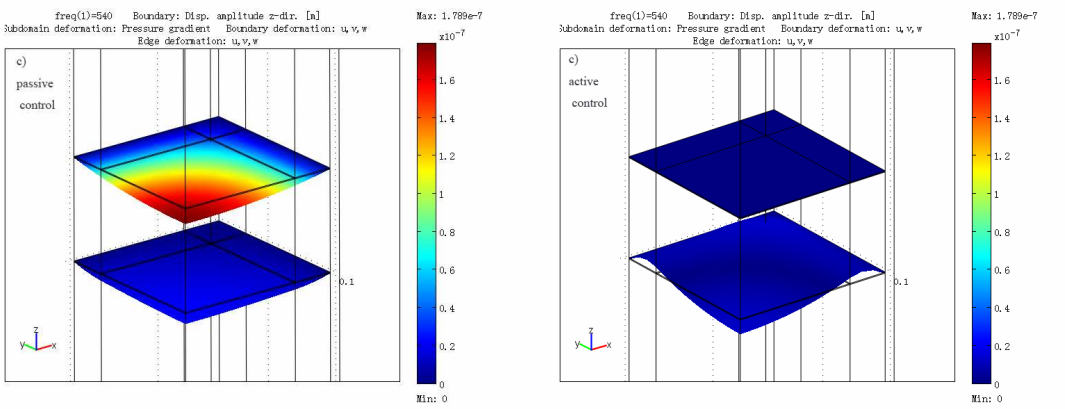
freq(1)=540 Boundary: Disp. amplitude z-dir. [m]
Subdomain deformation: Pressure gradient Boundary deformation: u, v, w
Edge deformation: u, v, w
c)
passive
control
Max: 1.789e-7
x10^-7
1.6
1.4
1.2
1
0.8
0.6
0.4
0.2
0
Min: 0
0.1
freq(1)=540 Boundary: Disp. amplitude z-dir. [m]
Subdomain deformation: Pressure gradient Boundary deformation: u, v, w
Edge deformation: u, v, w
c)
active
control
Max: 1.789e-7
x10^-7
1.6
1.4
1.2
1
0.8
0.6
0.4
0.2
0
Min: 0
0.1

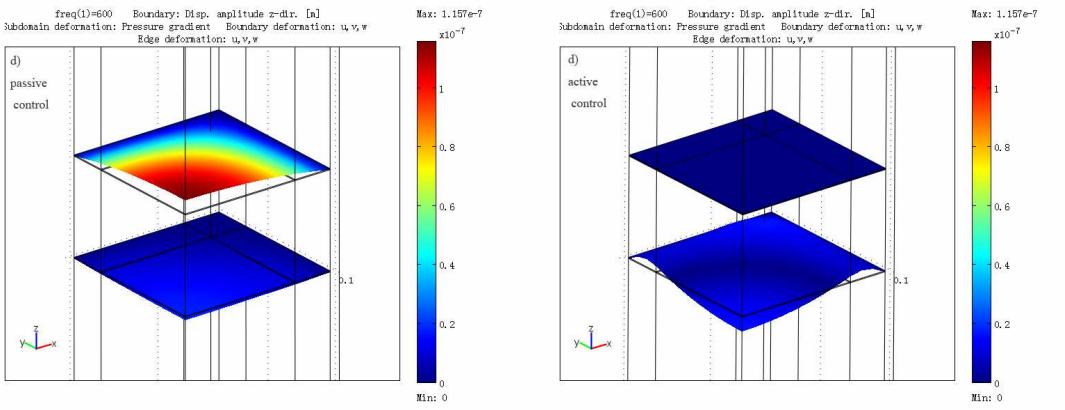
freq(1)=600 Boundary: Disp. amplitude z-dir. [m]
Subdomain deformation: Pressure gradient Boundary deformation: u, v, w
Edge deformation: u, v, w
d)
passive
control
Max: 1.157e-7
x10^-7
1
0.8
0.6
0.4
0.2
0
Min: 0
0.1
freq(1)=600 Boundary: Disp. amplitude z-dir. [m]
Subdomain deformation: Pressure gradient Boundary deformation: u, v, w
Edge deformation: u, v, w
d)
active
control
Max: 1.157e-7
x10^-7
1
0.8
0.6
0.4
0.2
0
Min: 0
0.1

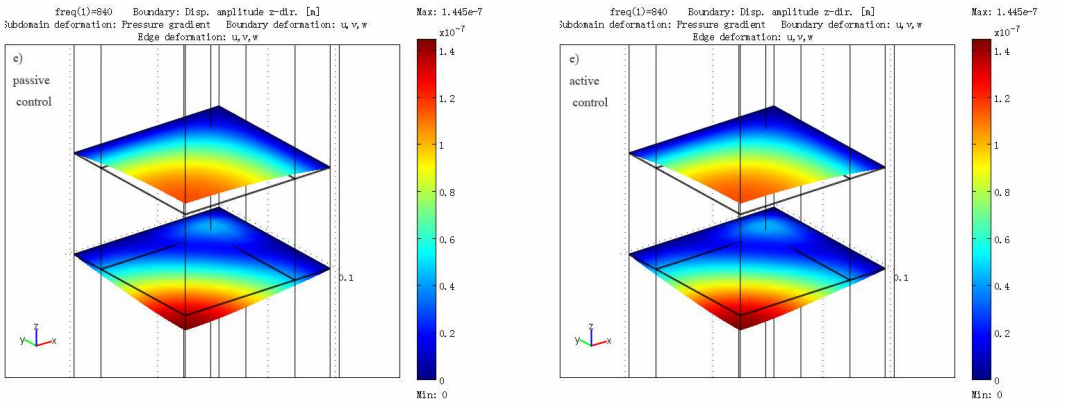
freq(1)=840 Boundary: Disp. amplitude z-dir. [m]
Subdomain deformation: Pressure gradient Boundary deformation: u, v, w
Edge deformation: u, v, w
e)
passive
control
Max: 1.445e-7
x10^-7
1.4
1.2
1
0.8
0.6
0.4
0.2
0
Min: 0
0.1
freq(1)=840 Boundary: Disp. amplitude z-dir. [m]
Subdomain deformation: Pressure gradient Boundary deformation: u, v, w
Edge deformation: u, v, w
e)
active
control
Max: 1.445e-7
x10^-7
1.4
1.2
1
0.8
0.6
0.4
0.2
0
Min: 0
0.1

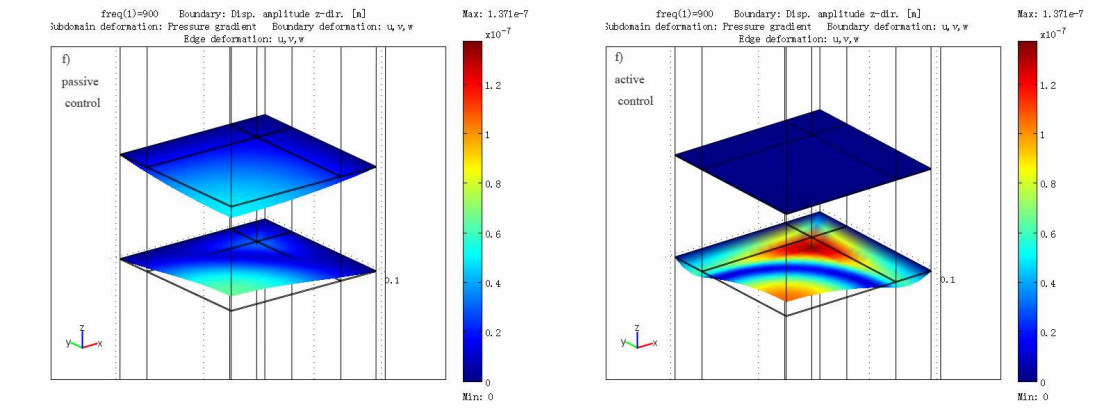

Fig.4-17 The displacement comparison of the radiating and active plates in the double-wall structure with porous material in passive and active control a) 100Hz; b) 340Hz; c) 540Hz; d) 600Hz; e) 840Hz; f) 900Hz.

C. A hybrid structure with several layers

A complex hybrid structure with several air gaps and porous materials, discussed in chapter 3, is presented in this section, named 'Cell A' (Fig.4-18). The reason for choosing these layers lies in the fact that this composition is efficient in absorption and insulation cases, detailed in chapter 3.

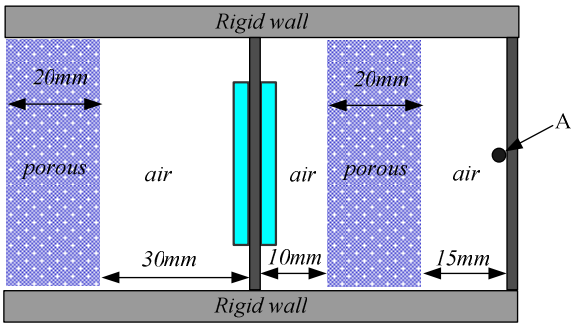

Fig.4-18 The configuration of Cell A

The transmission loss and absorption coefficient of this hybrid structure without active control is shown in Fig.4-19 with numerical results: the scattering matrix method and the finite element method. The same meshes are applied to the layers in Comsol environment. The resonance frequencies of this hybrid structure are 320Hz and 420Hz in Comsol environment, and 300Hz and 400Hz in the scattering matrix method; the relative error of the resonance frequency between the two methods is less than 6%. Besides, the transmission loss in the two methods has a good agreement lower than 600Hz: less than 5dB in difference. However, more differences in the transmission loss has been displayed over 600Hz, that is

because the porous medium is poroelastic and cannot be considered as an equivalent fluid with a rigid frame. The absorption coefficient of this hybrid structure in the two methods matches each other very well, and the absolute error doesn't exceed 0.1 in analysis frequencies.

Fig.4-20 gives the transmission loss of this hybrid structure in Comsol environment with control the pressure in point A. It shows that the active control is valid until 600Hz, and the transmission loss can be improved by a maximum of 20dB in the range of 300~500Hz. Besides, the absorption coefficient with or without active control exceeds 0.6 for the frequencies over 500Hz. It can be concluded that this hybrid structure has excellent sound absorption and transmission performance.

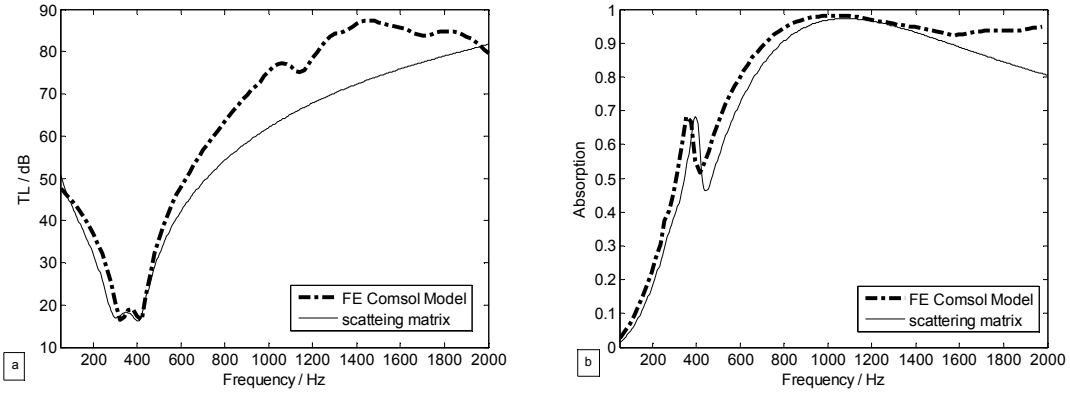

Fig.4-19 The acoustic performance of Cell A in Comsol without active control a) transmission loss; b) absorption coefficient

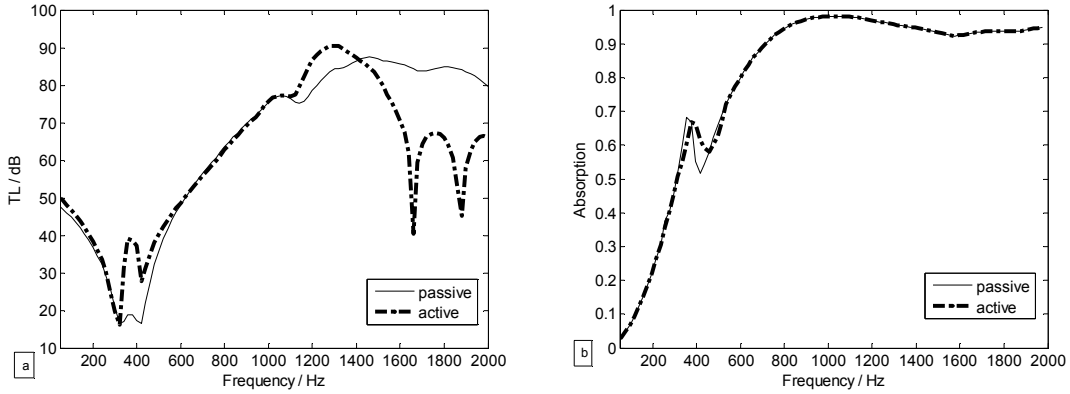

Fig.4-20 The acoustic performance of Cell A in Comsol a) transmission loss; b) absorption coefficient

Fig.4-21 shows the displacements of the radiating and active plates in this hybrid structure with or without active control in some frequencies: 100Hz, 320Hz, 360Hz and 1600Hz. Fig.4-21(a) displays the displacements in 100Hz of the two plates before and after active control. With active control, their displacements have been weakly reduced. Fig.4-21(b) display the displacements in the first resonance frequency of the two plates before and after active control, in which the two plates vibrate most strongly compared to other situations, and their displacements have no attenuation after active control, shown equally in Fig.4-20(a). Fig.4-21(c) represents the displacements in 360Hz of the two plates before and after active control, in which the active control works strongly and the displacement of the radiating plate has been reduced obviously. Fig.4-21(d) represents the displacements in 1600Hz of the two plates before and after active control, in which the active control makes the active plate vibrating more strongly than passive control.

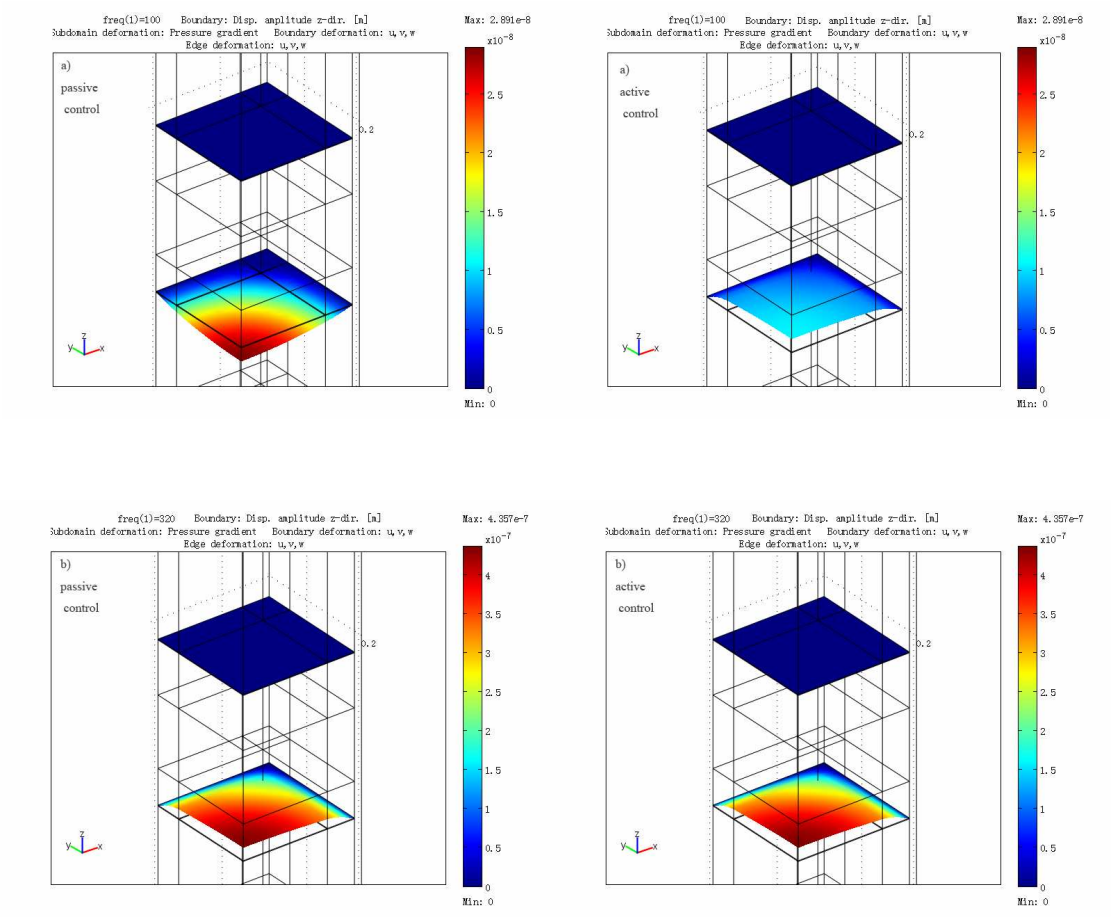

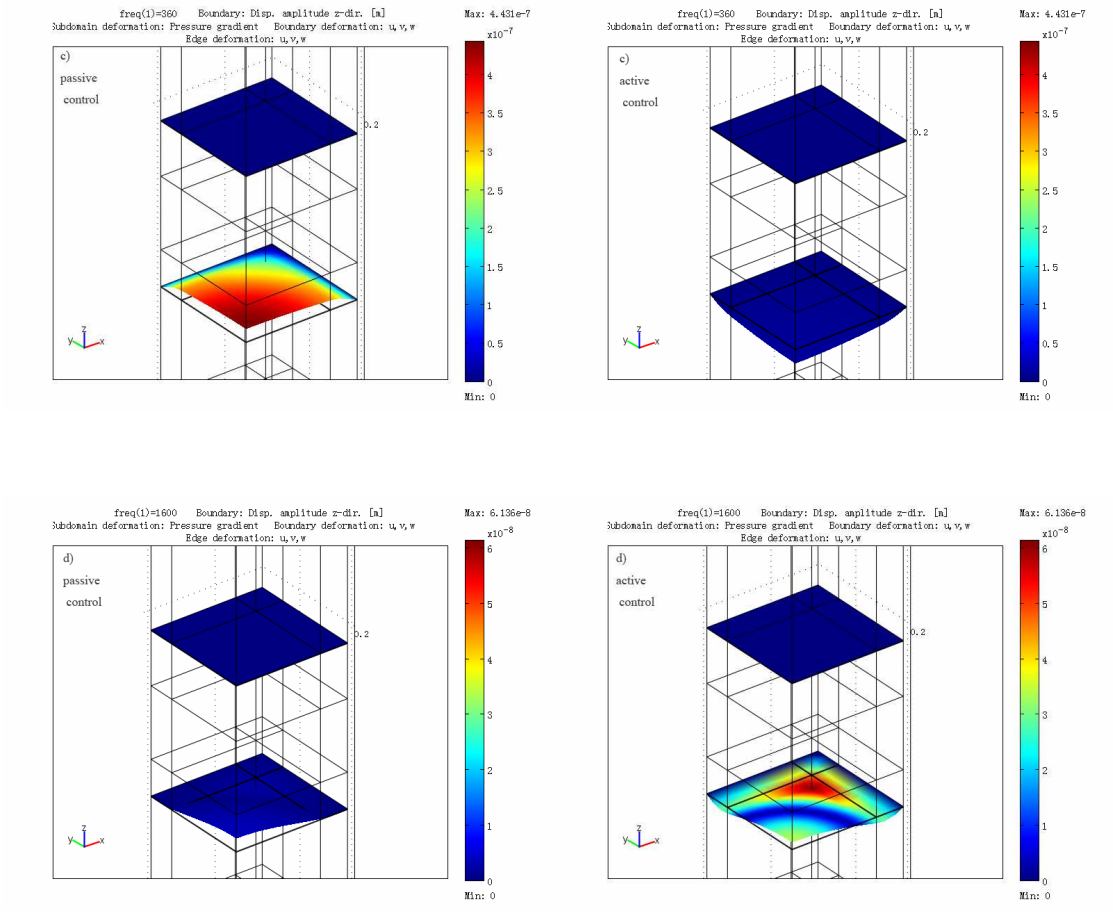

Fig.4-21 The displacement comparison of the radiating and active plates in Cell A with passive and active control a) 100Hz; b) 320Hz; c) 360Hz; d) 1600Hz.

4.4 Conclusions

In this chapter, a finite element model of hybrid active acoustic structure is developed with the (*u, p*) formulation in the Comsol environment. This model has considered the elasticity of the skeleton of the poroelastic material and the strong coupling between the solid and fluid phases. Besides, the boundary conditions on the coupling surface of the elastic, poroelastic and air layers were formulated in Comsol modes. In active control, a piezo solid mode in Comsol environment is applied to model the piezoelectric patches glued to both sides of active plate, and the optimal voltage of the secondary sound source is calculated by the transfer functions of incident and secondary sound wave.

Some examples have been considered to illustrate the numerical results in the Comsol environment. Firstly, the validity of the transmission loss of the radiating and active plates in the hybrid structures has been demonstrated. The numerical results show that the first

resonance frequencies and the transmission loss of the radiating and active plates are in good agreement in the scattering matrix method and the finite element model in Comsol environment. However, the second peak of transmission loss cannot be displayed in the scattering matrix method because only the first vibration mode is applied to calculate the transfer matrix of the two plates. Secondly, the surface impedance of the porous materials was validated by Biot's theory for different boundary conditions. Nevertheless, the results in the scattering matrix method doesn't agree well with that in Comsol environment, due to the elastic behavior of the porous material which makes an equivalent fluid with a rigid frame unsuitable to model this material.

Lastly, the dynamic responses of some hybrid active acoustic structure have been studied under plane wave excitation, in which piezoelectric patches are added onto the excited plate behaving as a secondary vibrational source. The resonance frequencies of these hybrid structures have been calculated by the scattering matrix method and Comsol environment, and the relative error of the resonance frequencies between the two methods is less than 6%. Besides, more than 10dB gain in sound insulation of the hybrid active acoustic structure can be obtained at resonance frequencies with active control, which have been validated in chapter 3.

In addition, these hybrid structures are not too large, just 66mm in edge length. Hence, for controlling the noise in a large-area domain, these structures become ineffective and useless because of its limited dimension. In this case, a multi-cell active acoustic structure concept will be realized by compositing these hybrid structures in chapter 6.

Chapter 5

Experiments of hybrid active acoustic structure based on two source-location method

In the preceding chapters, the numerical results in the acoustic performance of the hybrid active acoustic structure have been obtained by the scattering matrix method and the finite element method with Comsol software. The two methods agree each other very well in some frequency range, while some differences exhibit in the resonance or higher frequencies because of the poroelastic materials. Therefore, some experiments should be carried out to validate the numerical results of the hybrid active packages.

The most common approach for measuring the transmission loss of the acoustic structures is in the reverberation room and in the standing wave tube. In the reverberation room method, some types of equipment such as reverberation room and high quality microphone are required. Besides, the dimension of the tested structure should be large enough. In the standing wave tube, the transmission loss of the tested structure is determined by the incident power in decomposition theory and the transmitted power in the plane wave approximation assuming an anechoic termination [165-168]. If a two-microphone random-excitation technique is used, the sound pressure may be decomposed into its incident and reflected waves [159]. And the transmitted wave is obtained by the third microphone. The major drawback of this method is that an anechoic termination is required. In practice, an anechoic termination could be constructed using a long exhaust tube, high absorbing materials, horn shapes pipes or an active sound anechoic termination [159]. However, a fully anechoic termination is difficult to be built, particularly one that is effective at low frequencies.

Thus, two alternative measurement approaches are considered, which do not require an anechoic termination: the two-load method and the two source-location method. Both methods are realized by measuring acoustic pressures at four fixed locations, two upstream and two downstream of the tested structure, with a different load or a random source on both sides of the test tube respectively. Then the four-pole parameters of the tested structure are calculated by means of a dual-channel FFT analyzer. Due to the two-load method suffers from an additional disadvantage in that the two loads may not be sufficiently different at all frequencies of interest, the two source-location method is much more stable and entirely independent of the loading terminations.

This chapter aims to apply the two source-location method based on the scattering matrix to measuring the acoustic performance of the hybrid active acoustic structure, using a dSPACE-DS1103 controller implemented with Simulink for finding the optimal signal of the secondary sound source in active control. The measurement was carried out in a rectangular tube, and no anechoic termination is required. The reflection and transmission coefficients of each layer in the hybrid active acoustic structures are measured. Besides, the acoustic performance of some hybrid active acoustic structure are deduced and compared to the numerical data. Their transmission losses are improved by active control, which agrees well with the numerical results in the scattering matrix method and the finite element method with Comsol software.

5.1 The two source-location method based on the scattering matrix

The measurement characterization of the two source-location method based on the scattering matrix is shown in Fig.5-1. The definition of the scattering matrix can be rewritten in Eq. (5-1), which gives linear relationships between the incoming pressure wave vector $\left[P^{+}(z^{up}) \quad P^{-}(z^{dn})\right]^{T}$ and the outgoing pressure wave vector $\left[P^{-}(z^{up}) \quad P^{+}(z^{dn})\right]^{T}$.

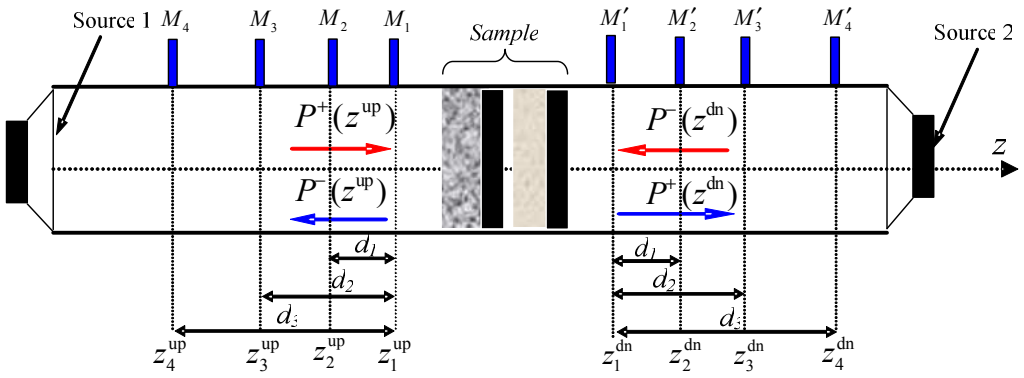

Fig.5-1 The two source-location measurement method based on the scattering matrix

$$\begin{bmatrix} P^{-}(z^{up}) \\ P^{+}(z^{dn}) \end{bmatrix} = \mathbf{D} \cdot \begin{bmatrix} P^{+}(z^{up}) \\ P^{-}(z^{dn}) \end{bmatrix}, \qquad \mathbf{D} = \begin{bmatrix} D_{11} & D_{12} \\ D_{21} & D_{22} \end{bmatrix} \tag{5-1}$$

Here, D_{11} and D_{21} represents respectively anechoic reflection and transmission coefficients associated with the left side incoming waves; D_{22} and D_{12} represents respectively anechoic reflection and transmission coefficients associated with the right side incoming waves.

Eq. (5-1) shows that the incoming and outgoing pressures on both sides of the samples are needed to calculate the scattering matrix, but in fact, the total sound pressure at $M_{1\sim4}$ is measured by microphones; hence, it requires at least two measuring points on each side to separate the incoming and outgoing pressures from the total pressure. However, due to the existence of standing waves in the tube, the spacing between the two measuring points can not be equal to an integer multiple of the half-wavelength of the maximum measuring frequency, and must satisfy the condition of $d < 2c_0 / 5f_{\max}$ [161], where c_0 is the sound speed and $f_{\max}$ is the maximum measuring frequency. In addition, if some measuring points are adjacent to the nodes of some singularity frequencies, the measurement error will be increased due to the low signal-to-noise ratio (SNR), hence, more measuring points can be set on both sides of the tested structure to eliminate this phenomenon. In this chapter, four measuring points in each side were used, and the scattering matrix can be written as follows when one of the sources switches on:

$$\begin{bmatrix} P^{-(1)}(z^{up}) \\ P^{+(1)}(z^{dn}) \end{bmatrix} = \mathbf{D} \cdot \begin{bmatrix} P^{+(1)}(z^{up}) \\ P^{-(1)}(z^{dn}) \end{bmatrix} \qquad \begin{bmatrix} P^{-(2)}(z^{up}) \\ P^{+(2)}(z^{dn}) \end{bmatrix} = \mathbf{D} \cdot \begin{bmatrix} P^{+(2)}(z^{up}) \\ P^{-(2)}(z^{dn}) \end{bmatrix} \tag{5-2}$$

Here, $P^{\pm(i)}(z^{up})$ and $P^{\pm(i)}(z^{dn})$ represent the incoming and outgoing waves in the *i* source switched on, $i = 1, 2$.

Eq. (5-2) can be transmitted into the form of a matrix:

$$\begin{bmatrix} P^{-(1)}(z^{up}) & P^{-(2)}(z^{up}) \\ P^{+(1)}(z^{dn}) & P^{+(2)}(z^{dn}) \end{bmatrix} = \mathbf{D} \cdot \begin{bmatrix} P^{+(1)}(z^{up}) & P^{+(2)}(z^{up}) \\ P^{-(1)}(z^{dn}) & P^{-(2)}(z^{dn}) \end{bmatrix} \tag{5-3}$$

Therefore, the scattering matrix $\mathbf{D}$ is calculated by the expression in follows:

$$\mathbf{D} = \left[P^{out} \right]_{2\times2} \cdot \left[P^{in} \right]_{2\times2}^{-1} \tag{5-4}$$

Here $\left[P^{out} \right]_{2\times2} = \begin{bmatrix} P^{-(1)}(z^{up}) & P^{-(2)}(z^{up}) \\ P^{+(1)}(z^{dn}) & P^{+(2)}(z^{dn}) \end{bmatrix}_{2\times2}$, $\left[P^{in} \right]_{2\times2} = \begin{bmatrix} P^{+(1)}(z^{up}) & P^{+(2)}(z^{up}) \\ P^{-(1)}(z^{dn}) & P^{-(2)}(z^{dn}) \end{bmatrix}_{2\times2}$.

In fact, the measured pressures at $M_{1,\cdots,4}$ and $M'_{1,\cdots,4}$ by microphones is the total sound pressure, hence, we need decompose the incident, reflected and transmitted waves according to the plane wave propagation principle:

$$\begin{bmatrix} P^{(i)}(z_1^{up}) \\ P^{(i)}(z_2^{up}) \\ P^{(i)}(z_3^{up}) \\ P^{(i)}(z_4^{up}) \end{bmatrix} = \begin{bmatrix} 1 & 1 \\ e^{jkd_1} & e^{-jkd_1} \\ e^{jkd_2} & e^{-jkd_2} \\ e^{jkd_3} & e^{-jkd_3} \end{bmatrix} \begin{bmatrix} P^{+(i)}(z^{up}) \\ P^{-(i)}(z^{up}) \end{bmatrix} \qquad \begin{bmatrix} P^{(i)}(z_1^{dn}) \\ P^{(i)}(z_2^{dn}) \\ P^{(i)}(z_3^{dn}) \\ P^{(i)}(z_4^{dn}) \end{bmatrix} = \begin{bmatrix} 1 & 1 \\ e^{-jkd_1} & e^{jkd_1} \\ e^{-jkd_2} & e^{jkd_2} \\ e^{-jkd_3} & e^{jkd_3} \end{bmatrix} \begin{bmatrix} P^{+(i)}(z^{dn}) \\ P^{-(i)}(z^{dn}) \end{bmatrix} \tag{5-5}$$

After some mathematic operations, the incoming and outgoing waves on both sides of the tested structure can be expressed as:

$$\begin{bmatrix} P^{+(i)}(z^{up}) \\ P^{-(i)}(z^{up}) \end{bmatrix} = \left[\left[Md^{up} \right]_{2\times4}^{H} . \left[Md^{up} \right]_{4\times2} \right]^{-1} . \left[Md^{up} \right]_{2\times4}^{H} . \left[P^{(i)}(z_k^{up}) \right]_{4\times1} \tag{5-6}$$

$$\begin{bmatrix} P^{-(i)}(z^{dn}) \\ P^{+(i)}(z^{dn}) \end{bmatrix} = \left[\left[Md^{dn} \right]_{2\times4}^{H} . \left[Md^{dn} \right]_{4\times2} \right]^{-1} . \left[Md^{dn} \right]_{2\times4}^{H} . \left[P^{(i)}(z_k^{dn}) \right]_{4\times1} \tag{5-7}$$

Here, the superscript 'H' denotes the conjugate transpose; $P^{(i)}(z_k^{up})$ and $P^{(i)}(z_k^{dn})$ represent the pressures given by microphones, $i = 1,2$, $k = 1,\cdots,4$. $d_1,\cdots,d_3$ are the spacing between the microphones.

$$\left[Md^{up} \right]_{4\times2} = \begin{bmatrix} 1 & e^{jkd_1} & e^{jkd_2} & e^{jkd_3} \\ 1 & e^{-jkd_1} & e^{-jkd_2} & e^{-jkd_3} \end{bmatrix}^{T} \qquad \left[Md^{dn} \right]_{4\times2} = \begin{bmatrix} 1 & e^{-jkd_1} & e^{-jkd_2} & e^{-jkd_3} \\ 1 & e^{jkd_1} & e^{jkd_2} & e^{jkd_3} \end{bmatrix}^{T} \tag{5-8}$$

Therefore, the transmission loss and absorption coefficient can be calculated by the scattering matrix, D_{21} and D_{11}, respectively:

$$TL = 10\lg\left(1/\left|D_{21}\right|^2\right) \qquad \alpha = 1-\left|D_{11}\right|^2 \tag{5-9}$$

5.2 Experimental disposition

The experiment was realized in **LFMA**, at **Ecole Centrale de Lyon**. All measurements were carried out in a rectangular tube. The cross-section of this rectangular tube (seeing in Fig.5-2) was 66×66mm^2, and its cut-off frequency was 2500Hz, which allowed a normal plane wave to be transmitted in the tube for the frequencies lower than 2500Hz.

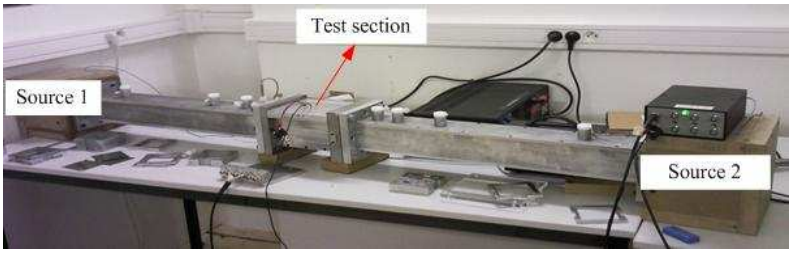

Fig.5-2 The rectangular tube used in measurements

The experimental disposition consisted of four parts: the source, the test section, the control system and the data processing. The two sources used in experiments generated white noise signals with the emission band from 50 to 2000 Hz, and one of the sources located on the upstream of the test section was the primary source. The piezoelectric ceramics were added onto the active plate behaving as a secondary source.

The tested structure was installed in the test section, and each layer of the structure was fixed on the frame which can slide freely in the tube. These frames can be applied to isolate air layers with different thickness, and quickly form different multilayer active acoustic structures. The radiating and active plates have an area slightly larger than the cross section of the tube, which makes the two plates adhered to the frame, whereas the porous material has the same cross section of the tube, just embedded in the frame, shown in Fig.5-3. The parameters of the plates and porous materials were given in Table.2-1.

(a) The plates adhered on the frame (b) The porous embedded in the frame

Fig.5-3 The layers with the frames

In the two source-location measurement, Siglab dynamic system analyzer generated the broadband noise signals and then transmitted them to the source 1 or source 2. In active control, the error sensor signal was amplified and filtered, and then was controlled by the classical FXLMS algorithm implemented on a dSPACE-DS1103 controller with Simulink to find out the control signal. Fig.5-4 showed the characterization of the control system and data processing. The microphones used for acoustic pressure measurements are B&K ¼ 4939-type. The pressure signals were then pre-amplified with a gain of 10dB.

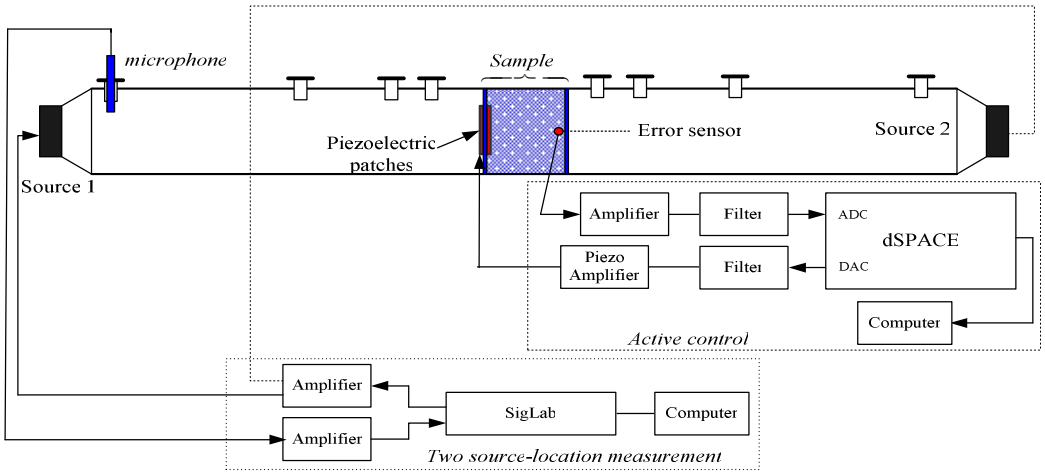

Fig.5-4 The characterization of the control system and data processing

5.3 Experimental results

5.3.1 Sound leakage analysis

The rectangular tube used in measurement is steel with a thickness 15mm, and the upstream, downstream and test sections are bonded by rivets, which maybe bring on the sound leakage in the tube. Therefore, the measurement is carried out to analyze the sound leakage in the condition that no tested structure is installed in the test section.

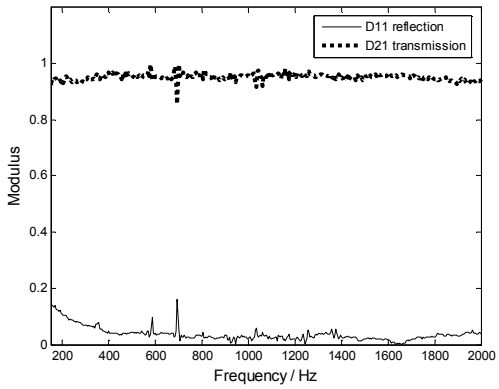

Fig.5-5 The reflection and transmission coefficients of the tube without tested structure

Fig.5-5 shows the modulus of the reflection and transmission coefficients (D_{11} and D_{21}) of the tube without tested structure. In this case, the ideal transmission coefficient should be equal to one and the reflection coefficient is to zero, because there was no tested structure in

the test section, thus no sound is reflected and all acoustic wave can be transmitted. However, the measurement result shows that transmission coefficient is equal to 0.95 and the reflection coefficient is adjacent to 0.02 in the all-range frequency. Hence, the crack between each section makes 5% of sound energy being leaked, and the remaining 95% of the sound wave can be transmitted through the tested structure. The sound leakage produces -0.45dB correction of the transmission loss, which is slight and can be ignored in the measurements.

5.3.2 The radiating and active plates

The radiating plate used in the hybrid active acoustic structure is an elastic thin plate in steel with a thickness of 0.2mm, and the active plate is the elastic thin steel plate bonded on piezoelectric patches with a thickness of 0.5mm on both sides. Their physical parameters are given in Table.2-1. Fig.5-6 gives the reflection and transmission coefficients of the radiating plate. The modal frequency of the radiating plate is adjacent to 230Hz. The curve shows that the reflection and transmission coefficients associated with the left side incoming waves respectively agree well with that of the right side incoming waves. It means that this radiating plate is symmetrical and the glue fixing this plate to the frame has very slight effect on the performance of the plate.

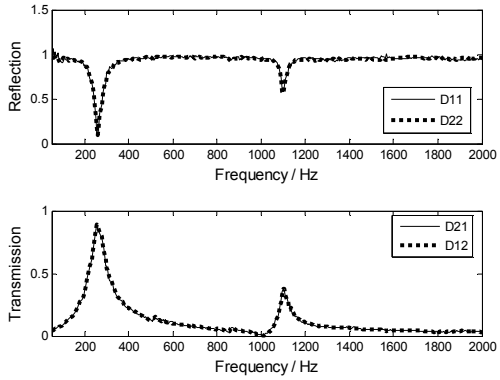

Fig.5-6 The reflection and transmission coefficients of the radiating plate

Fig.5-7 gives the reflection and transmission coefficients of the active plate. Compared to Fig.5-6, the modal frequency of the active plate shifts to 315Hz and its transmission coefficient decreases obviously, due to the piezoelectric ceramic attached to the plate increases the thickness of the active plate, which improves sound insulation.

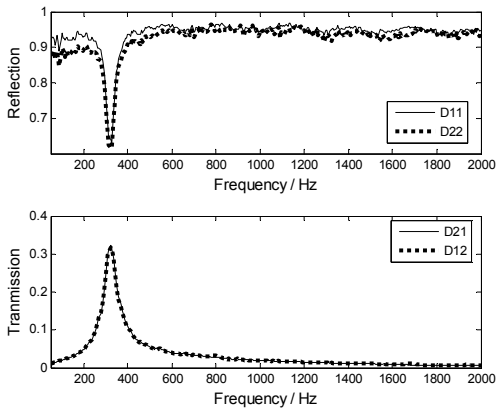

Fig.5-7 The reflection and transmission coefficients of the active plate

Fig.5-8 shows the transmission loss of the radiating and active plate in experiment result and simulation results: in the scattering matrix method and in the finite element method. The curves show that the measurement in the transmission loss of the radiating and active plates agrees well with the simulation results in whole frequency band, except that the second peak of transmission loss cannot be displayed in the scattering matrix method because only the first vibration mode is used to calculate the transfer matrix of this plate.

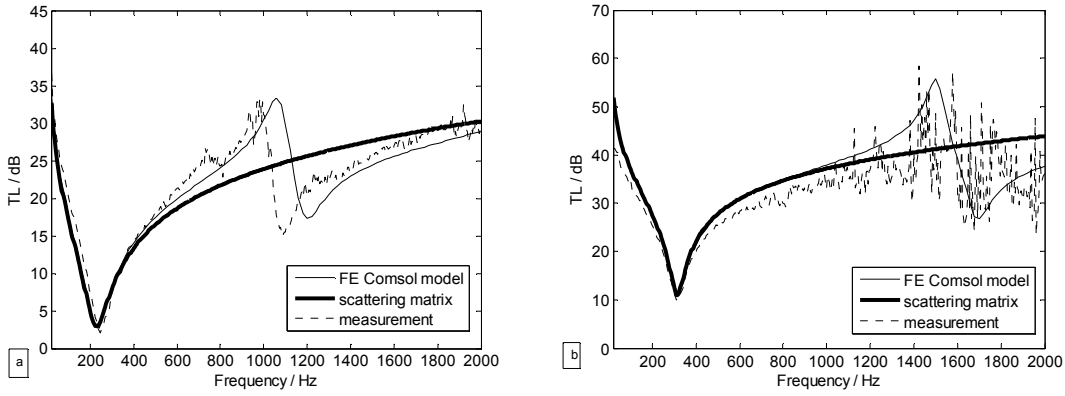

Fig.5-8 The transmission loss of the plates; a) the radiating plate; b) the active plate

5.3.3 The porous material

The properties of the porous material used in the hybrid active acoustic structure are shown in Table.2-1. Fig.5-9 gives the modulus of the reflection and transmission coefficients of the porous material. The curve shows that the reflection and transmission coefficients associated with the left side incoming waves respectively agree well with that of the right side incoming waves. It means that this porous material is symmetrical.

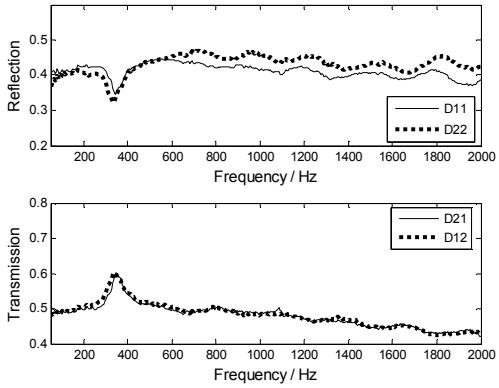

Fig.5-9 The reflection and transmission coefficients of the porous material

The absorption coefficient and transmission loss of this porous material is plotted in Fig.5-10 with measurement and simulation results: in the scattering matrix method and in the finite element method. In Comsol environment and measurement, the first resonance frequency of this material is about 360Hz, and its absorption coefficient is excellent, more than 0.8 over the range of frequencies of interest, whereas its transmission loss is less than 7dB. However, no resonance frequency can be obtained in the scattering matrix method, due to this porous material is elastic which makes an equivalent fluid with a rigid frame unsuitable to model this material.

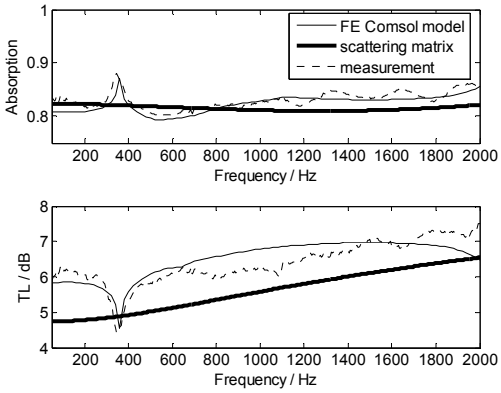

Fig.5-10 Comparison of numerical and experimental results of the porous material

5.3.4 Hybrid active acoustic structure

A. A double-wall structure with air gap

The transmission loss of the double-wall active acoustic structure with air gap shown in Fig.4-11 is curved in Fig.5-11 with measurement and simulation results: in the scattering

matrix method and in the finite element method. Without active control, the comparison shows that the transmission loss in measurement has a good agreement with that in the numerical result of the finite element method in all-range frequency. However, more differences in the transmission loss of the results between measurement and the scattering matrix method has been displayed over the resonance frequency, that is because only the first vibration mode is used to calculate the transfer matrix of the radiating plate and active plate.

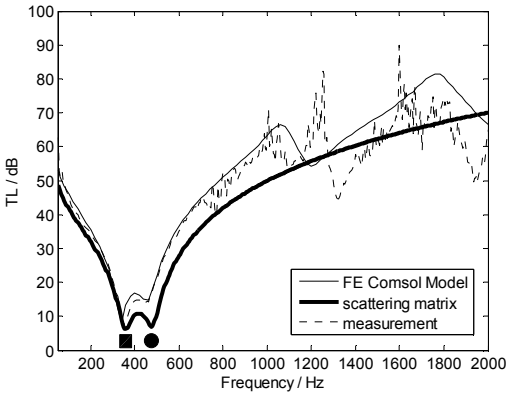

Fig.5-11 Comparison of numerical and experimental results of a double-wall structure with air gap without active control

■ : The first mode frequency of the active plate
● : The resonance frequency of the structure

In active control, one error sensor is located at the center of the radiating plate, and the minimum pressure is used as the control objective. The error signal is controlled by the classical FXLMS algorithm implemented on a dSPACE-DS1103 controller to find out the best signal exciting the piezoelectric ceramics. Besides, the sound wave radiated by the source 1 in Fig.5-4 is used as the reference signal. Fig.5-12 shows the configuration of the active control. The experimental signals of this error sensor are shown in Fig.5-13 with or without active control. Obvious reduction can be seen after active control is applied, and the convergence time is short.

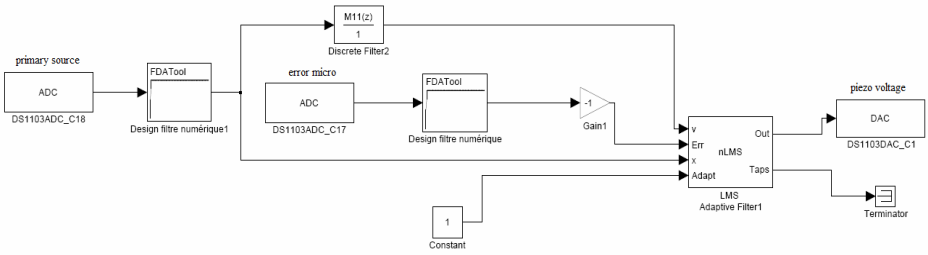

Fig.5-12 The configuration of the active control

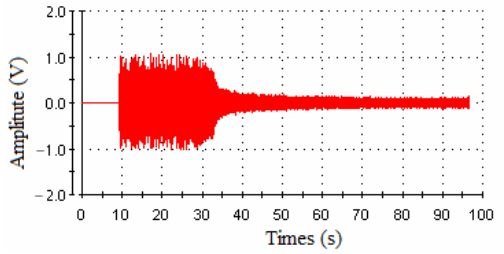

Fig.5-13 The error sensor signals before and after active control

Fig.5-14 shows the experimental results in the transmission loss of this double-wall structure with passive or active control. The resonance frequencies of the double-wall structure are 340Hz and 460Hz in numerical result (seeing in Fig.4-13), and 350Hz and 440Hz in measurement; the relative error between the two methods is less than 5%. The curves in Fig.5-14 shows that about 15dB gain is obtained near the resonance frequencies in measurement, and no improvements are realized at frequencies above 500Hz with active control; however, the results in Fig.4-13 in chapter 4 shows that the active control is valid until 1660Hz, and about 15dB of the transmission loss can be obtained at the resonance frequencies. The reason lies in the fact that the active control is operated only for frequencies less than 500Hz in the experiment. Note that no improvement is obtained under 100Hz in the experiment due to very low voltage imposed on the piezoelectric ceramic leading to an overly weak secondary source.

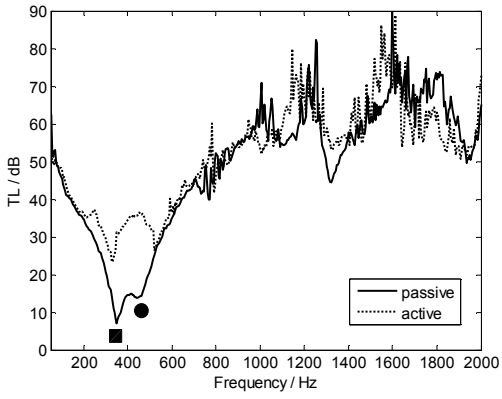

Fig.5-14 The transmission loss of the double-wall structure with air gap in measurement with or without active control;

■ : The first mode frequency of the active plate
● : The resonance frequency of the structure

B. A double-wall structure with porous material

The transmission loss of the double-wall active acoustic structure with porous material is presented in Fig.5-15 with measurement and simulation results: in the scattering matrix method and in the finite element method. Without active control, the comparison shows that the transmission loss in measurement is in good agreement with that in the numerical result of the finite element method in all-range frequency. However, more differences in the transmission loss of the results between measurement and the scattering matrix method has been displayed over 800Hz, that is because only the first vibration mode is used to calculate the transfer matrix of the radiating plate and active plate, besides, the porous material is coupled with the elastic plates and it cannot be considered as an equivalent fluid with a rigid frame.

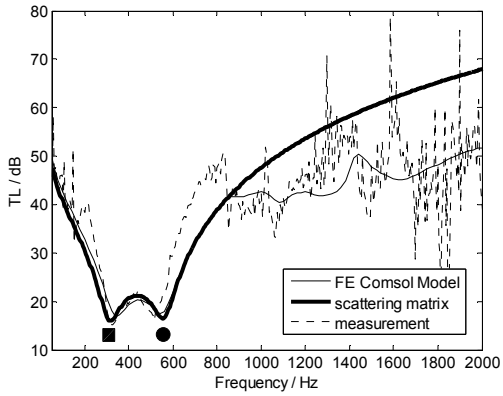

Fig.5-15 Comparison of numerical and experimental results of the double-wall structure with porous material without active control

■ : The first mode frequency of the active plate
● : The resonance frequency of the structure

Fig.5-16 shows the experimental results in the transmission loss of this double-wall structure with passive or active control. The resonance frequencies of the double-wall structure are 340Hz and 540Hz in the numerical results (seeing in Fig.4-16), and 320Hz and 515Hz in the experiment; the relative error between the two methods is less than 7%. The results in Fig.4-16 in chapter 4 shows that the active control is valid until 800Hz, and the transmission loss can be improved around resonance frequencies by about 10 dB; whereas, the curves in Fig.5-16 shows that about 10dB gain is obtained near the resonance frequencies under 500Hz, and no improvement is obtained under 120Hz in the experiment due to very low voltage imposed on the piezoelectric ceramic.

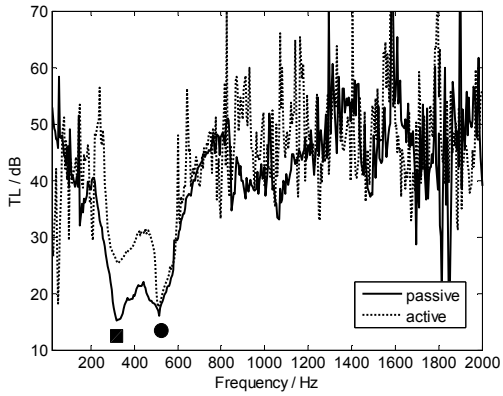

Fig.5-16 The transmission loss of a double-wall structure with porous material in measurement with passive and active control

■ : The first mode frequency of the active plate
● : The resonance frequency of the structure

C. A hybrid structure with several layers

The transmission loss and absorption coefficient of the hybrid active acoustic structure with several layers (Cell A) shown in Fig.4-18 have been plotted in Fig.5-17 with measurement and simulation results: in the scattering matrix method and in the finite element method. Without active control, the comparison shows that the transmission loss in measurement matches well with that in the numerical result of the finite element method in all-range frequency. However, more differences in the transmission loss of the results between measurement and the scattering matrix method can be observed over 600Hz, which is because the porous medium is poroelastic and cannot be considered as an equivalent fluid with a rigid frame. The absorption coefficient of this hybrid structure in the three methods matches each other very well, and the absolute error doesn't exceed 0.2 in the frequency of interest.

Fig.5-18 shows the experimental results in the transmission loss and absorption coefficient of Cell A with passive or active control. The resonance frequencies of Cell A are 320Hz and 420Hz in the numerical results (seeing in Fig.4-20), and 325Hz and 400Hz in the experiment; the relative error between the two methods is less than 5%. The results in Fig.4-20 and Fig.5-18 show that the transmission loss can be improved by a maximum of 15 dB in the range of 300~500Hz, while the absorption coefficient has a little offset in both results. Besides, the absorption coefficient in numerical and experimental results exceeds 0.6 for frequencies above 500Hz.

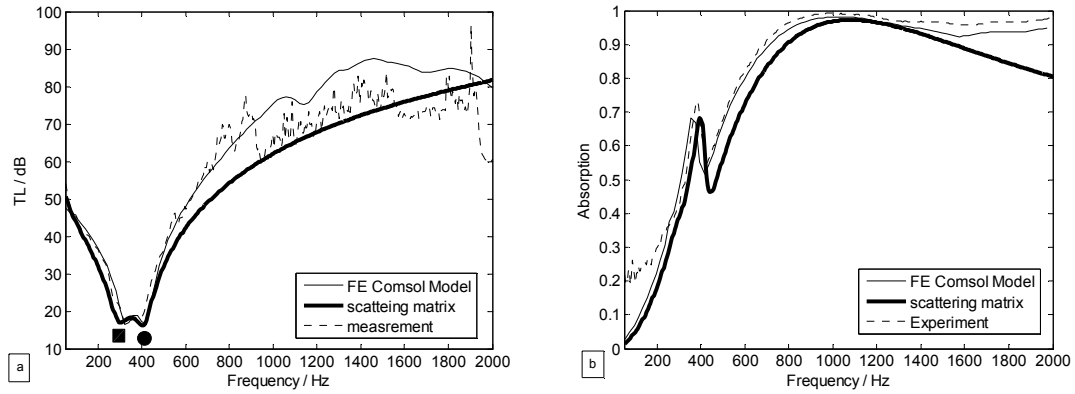

Fig.5-17 Comparison of numerical and experimental results of Cell A without active control; a) transmission loss; b) absorption coefficient

■ : The first mode frequency of the active plate
● : The resonance frequency of the structure

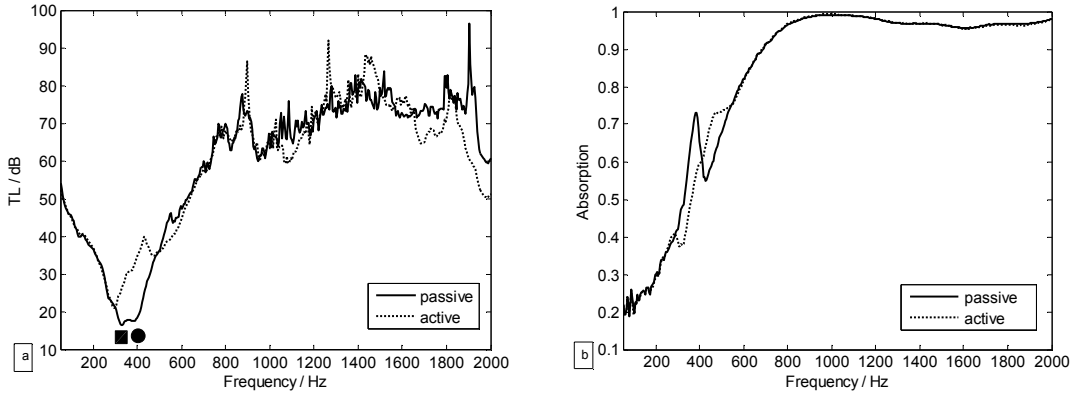

Fig.5-18 The acoustic performance of Cell A in measurement with passive and active control; a) transmission loss; b) absorption coefficient

■ : The first mode frequency of the active plate
● : The resonance frequency of the structure

5.4 Error analysis of the measurement

In this section, the measurement error of the two source-location method is analyzed in order to evaluate the accuracy of the transmission loss calculated by the measured pressures. Indeed, the transmission loss herein is obtained by measuring the pressures on both sides of the tested structure; hence, the error of TL_{dB} depends on the measured pressure's error. Eq. (5-6) and (5-7) show that the incoming and outgoing waves on both sides of the tested structure are related to the microphone's error and their position error; while the position error is weak and can be neglected, only the microphone's error should be considered. For convenience of

analysis, just considering the two measuring points on each side, the vectors $\left[Md^{up}\right]$ and $\left[Md^{dn}\right]$ can be rewritten as:

$$\left[Md^{up}\right]_{2\times 2}=\begin{bmatrix}1 & 1\\ e^{jkd_1} & e^{-jkd_1}\end{bmatrix}\quad \left[Md^{\mathrm{dn}}\right]_{2\times 2}=\begin{bmatrix}1 & 1\\ e^{-jkd_1} & e^{jkd_1}\end{bmatrix} \tag{5-10}$$

The incoming and outgoing waves on the left side of the tested structure can be formulated as (similar in the right side):

$$\begin{bmatrix}P^{+}(z^{up})\\ P^{-}(z^{up})\end{bmatrix}=\left[Md^{up}\right]_{2\times 2}^{-1}\cdot\left\{P(z_i^{up})\right\}_{2\times 1}=\frac{1}{2\sin kd_1}\begin{bmatrix}e^{-jkd_1} & 1\\ e^{jkd_1} & 1\end{bmatrix}\begin{bmatrix}P(z_1^{up})\\ P(z_2^{up})\end{bmatrix} \tag{5-11}$$

Eq. (5-11) shows that it is solvable under the condition that $\sin kd_1\neq 0$, that is, the spacing d_1 between the two microphones can not be an integer multiple of the half-wavelength. If not, Eq. (5-11) is insolvable, which leads to an invalid measurement. Suppose P is the true value of $\left[P(z_1^{up})\quad P(z_2^{up})\right]^T$ and its measurement error is ΔP, which induces a calculated error ΔR of $\left[P^{+}(z^{up})\quad P^{-}(z^{up})\right]^T$, whose true value is R. If the matrix $\left[Md^{up}\right]_{2\times 2}^{-1}$ is nonsingular, the relation between the relative errors of R and P can be expressed as [169]:

$$0\le\frac{\left\|\Delta R\right\|_1}{\left\|R\right\|_1}\le\frac{2}{\left|\sin kd_1\right|}\frac{\left\|\Delta P\right\|_1}{\left\|P\right\|_1} \tag{5-12}$$

Here $\|\ \|_1$ denotes the matrix norm, defined as the maximum absolute column sum of the matrix. Because of $\frac{\left\|\Delta R\right\|_1}{\left\|R\right\|_1}=\frac{\left|\Delta P^{+}(z^{up})\right|+\left|\Delta P^{-}(z^{up})\right|}{\left|P^{+}(z^{up})\right|+\left|P^{-}(z^{up})\right|}$ and $\frac{\left|P^{-}(z^{up})\right|}{\left|P^{+}(z^{up})\right|}\le 1$, we have:

$$0<\frac{\left|\Delta P^{+}(z^{up})\right|}{2\left|P^{+}(z^{up})\right|}\le\frac{\left|\Delta P^{+}(z^{up})\right|+\left|\Delta P^{-}(z^{up})\right|}{2\left|P^{+}(z^{up})\right|}\le\frac{\left|\Delta P^{+}(z^{up})\right|+\left|\Delta P^{-}(z^{up})\right|}{\left|P^{+}(z^{up})\right|+\left|P^{-}(z^{up})\right|}=\frac{\left\|\Delta R\right\|_1}{\left\|R\right\|_1}$$

Therefore, Eq. (5-13) is obtained with the inequality operation:

$$0<\frac{\left|\Delta P^{+}(z^{up})\right|}{\left|P^{+}(z^{up})\right|}\le\frac{4}{\left|\sin kd_1\right|}\frac{\left\|\Delta P\right\|_1}{\left\|P\right\|_1} \tag{5-13}$$

Similarly,

$$0<\frac{\left|\Delta P^{+}(z^{dn})\right|}{\left|P^{+}(z^{dn})\right|}\le\frac{4}{\left|\sin kd_1\right|}\frac{\left\|\Delta P\right\|_1}{\left\|P\right\|_1} \tag{5-14}$$

Suppose TL is the true value of TL_{dB} and its calculated value is TL^{*}, the error $\Delta TL=TL-TL^{*}$ can be written as:

$$\Delta TL = 20\lg\frac{\left|1-\Delta P^{+}(z^{dn})/P^{+}(z^{dn})\right|}{\left|1-\Delta P^{+}(z^{up})/P^{+}(z^{up})\right|} \tag{5-15}$$

Eq. (5-15) can be further simplified as [169]:

$$\left|\Delta TL\right| \le 20\lg\frac{1+\left|\Delta P^{+}(z^{dn})/P^{+}(z^{dn})\right|}{1-\left|\Delta P^{+}(z^{up})/P^{+}(z^{up})\right|} \tag{5-16}$$

Suppose $\pm\delta$ dB is the microphone's error, the corresponding maximum relative error of the sound pressure can be written as $\eta = |\Delta P|/|P| = 10^{\delta/20} - 1$, and the range of ΔTL can be deduced from Eq. (5-13), (5-14) and (5-16):

$$\left|\Delta TL\right| \le 20\lg\frac{1+4\eta/\left|\sin kd_1\right|}{1-4\eta/\left|\sin kd_1\right|} \tag{5-17}$$

Equation (5-17) shows that ΔTL depends on kd_1 and δ, hence, the function of their relationships can be drawn in the $(0,\pi)$ interval, shown in Fig.5-19. To ensure that ΔTL not exceed 5dB, the condition of $(0.3+n)\pi \le kd_1 \le (0.7+n)\pi$ should be satisfied and the microphone' error must be within ±0.5dB. When the microphone' error is certain, ΔTL is minimum for $kd_1 = (0.5+n)\pi$, $n = 0,1,\cdots$, therefore, the spacing between the microphones should be equal to the 1/4 wavelength integer of frequency of interest.

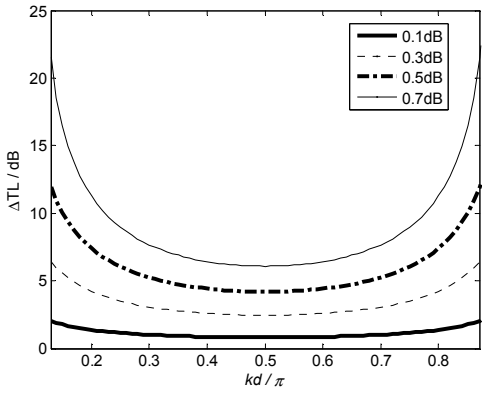

Fig.5-19 The relationship between ΔTL, the microphone's error and spacing

5.5 Conclusions

In this chapter, the two source-location method based on the scattering matrix is applied to measuring the acoustic performance of the hybrid active acoustic structure, using a dSPACE-DS1103 controller implemented with Simulink for finding the optimal signal. It proves that the results in measurement are in good agreement with that in simulation, and the

transmission loss of these hybrid structures can be improved obviously with active control in the resonance frequency.

Besides, more attention should be paid in experimental measurement:

① The spacing between the two measuring points can not be equal to an integer multiple of the half-wavelength in the measuring frequency, and must satisfy the condition of $d < 2c_0 / 5f_{\max}$.

② Locating the microphones adjacent to the surface of the testes structure must be avoided, because the surface acoustic field of the test element is inhomogeneous and it can yield to errors.

③ More measuring points can be set on both sides of the tested structure to avoid that some measuring points are adjacent to the nodes of some singularity frequencies, which increases the measurement error due to the low signal-to-noise ratio.

④ The maximum measurement error ΔTL depends on kd_1 and the microphone's error δ. To ensure that ΔTL not exceed 5dB, the condition of $(0.3+n)\pi \le kd_1 \le (0.7+n)\pi$ should be satisfied and the microphone' error δ must be within ±0.5dB. When the microphone' error δ is certain, ΔTL is minimum for $kd_1 = (0.5+n)\pi$, $n = 0,1,\cdots$, therefore, the spacing between the microphones should be equal to the 1/4 wavelength integer of frequency of interest.

⑤ The measuring precision also depends on the installation of the tested structure. The crack between each section of the tube should be eliminated to prevent the sound leakage.

Chapter 6

Multi-cell hybrid active acoustic structure concept for noise control over a large surface

In the preceding chapters, some hybrid active acoustic structure, combining passive method and active control technique, have been validated and their acoustic absorption or/and transmission performance can be improved over a certain extent. The numerical results of the scattering matrix method and the finite element method are validated by the experimental data based on the two source-location method. All the results show that the acoustic performance of these hybrid active acoustic structure have been improved obviously by active control, more than 10dB gain in sound insulation can be obtained at resonance frequencies, and excellent absorption coefficient can be achieved with several poroelastic materials in appropriate parameters and disposition.

In fact, the hybrid active acoustic structures mentioned in the preceding chapters are small, just 66mm in length and width, and lower than 10cm in thickness. However, these hybrid active acoustic structure are planned to be applied to automobiles, aircrafts, buildings and other engineering applications, in which large-area domain need to be improved in sound absorption or/and insulation. One way for controlling the noise in a large-area domain is to augment the dimension of the hybrid active acoustic structure. In this case, the hybrid structures become more complicate, because these structures may be manufactured in the form of curves or other complex shape. Besides, the complex response even in the low frequency range requires that more error sensors and secondary sources should be used for active control, which results in complicated algorithm. Another way for controlling the noise in a large-area domain is to juxtapose several cells of the hybrid structure and then to form a

multi-cell hybrid structure. In this multi-cell hybrid structure, each cell has its error sensor and secondary source for active control; the coupling interface between each hybrid cell can be rigid or elastic. This multi-cell hybrid structure can be disposed in different forms to satisfy the noise control in a large-area domain.

Based on the second method above, this chapter aims at proposing a multi-cell hybrid active acoustic structure concept, juxtaposing several single hybrid cells. For example, the acoustic performance of some two-cell hybrid active acoustic structures is calculated with an incident plane wave by the finite element method, and the effect on the acoustic properties of the structures has been discussed with a rigid or elastic coupling interface. Beside, the interaction between the secondary sources and the error sensors in each cell has also been considered.

6.1 The multi-cell hybrid active acoustic structure concept

The configuration of the multi-cell hybrid active acoustic structure is drawn in Fig.6-1 by juxtaposing several single hybrid cells which are disposed in the form of an $m\times n$ array ($m,n=1,2,3,\cdots$). The single hybrid cell (seeing in Fig.6-1(a)) consists of an elastic plate, an active plate with piezoelectric ceramics vibrating as secondary source, and several dissipative layers such as air, porous materials… Each hybrid cell has an error sensor located near to the center of the elastic plate for minimizing the sound pressure of the sensor. The multi-cell hybrid structure is composed by an $m\times n$ array of single hybrid cell coupled together by a rigid or elastic plate (named 'a separate plate').

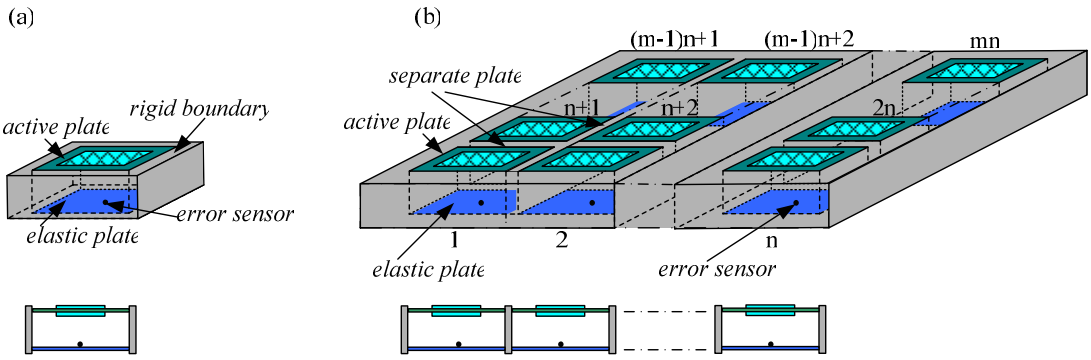

Fig.6-1 The configuration of the hybrid active structure; a) single cell; b) multi-cell hybrid structure

When the separate plate is thick enough and can be considered as a rigid wall, the coupling between each cell is weak, and then the acoustic performance of the multi-cell hybrid structure is similar to that of the single hybrid cell. However, when the separate plate is too thin, the vibration of the elastic and active plates in the single cells will make the sound wave transmitted by the separate plate. In this case, each error sensor receives not only the

direct sound signal from the secondary source in the same single hybrid cell, but also the indirect sound signal from the secondary source in the other single hybrid cells. Therefore, active control is complex to carry out.

6.2 Analysis of active control

Suppose that P_i is the pressure of the incident plane wave in the i th single hybrid cell, V_i is the voltage imposed on the piezoelectric patches of the i th cell, the active behavior of the multi-cell hybrid active acoustic structure is obtained in three steps under the condition that this whole process is linear. Herein considering an $m\times n$ array of the multi-cell hybrid active acoustic structure, the direct and interaction transfer function of the multi-cell hybrid structure is shown in Fig.6-2.

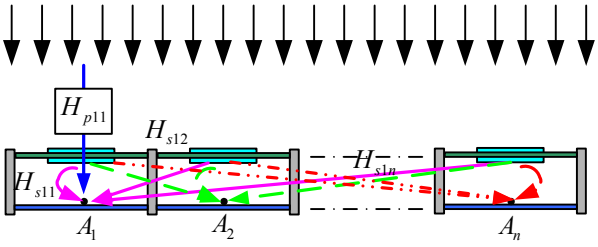

Fig.6-2 The transfer function schematic of multi-cell hybrid structure

6.2.1 The primary pathway matrix

The primary pathway matrix is defined as the transfer function between the primary sources and the error sensors in the multi-cell hybrid structure. Under a plane wave excitation, the pressure P_i of the incident acoustic wave in each single hybrid cell is equal to P_0, and the voltage V_i imposed on the piezoelectric ceramics of each cell is zero, that is, the active control is turned off. The sound pressure at point A_i where the error sensors are located can be expressed as $w_{pk}(\omega)$, $k=1,2,\cdots,mn$. Then the element of the primary pathway matrix can be written as:

$$H_{pk}(\omega)=\frac{w_{pk}(\omega)}{P_0},k=1,2,\cdots,mn \tag{6-1}$$

Therefore, the primary pathway matrix can be written as:

$$\mathbf{H_p}=\begin{bmatrix} H_{p1} & 0 & \cdots & 0 \\ 0 & H_{p2} & & \vdots \\ \vdots & & \ddots & 0 \\ 0 & \cdots & 0 & H_{p(mn)} \end{bmatrix}_{mn\times mn} \tag{6-2}$$

6.2.2 The secondary pathway matrix

The secondary pathway matrix is defined as the transfer function between the secondary sources and the error sensors in the multi-cell hybrid structures. In this step, no more incident wave is transmitted in each hybrid cell ($P_i = 0$), and the active plate in the i th cell is imposed by an electric potential V_0 applied to the piezoelectric ceramics. Once again, the sound pressures at point A_i can be expressed as $w_{sij}(\omega)$, $i, j = 1, 2, \cdots, mn$. Then the elements of the secondary pathway matrix can be respectively written as:

$$H_{sij}(\omega) = \frac{w_{sij}(\omega)}{V_0} \tag{6-3}$$

Therefore, the secondary pathway matrix can be written as:

$$\mathbf{H_s} = \begin{bmatrix} H_{s11} & H_{s12} & \cdots & H_{s1(mn)} \\ H_{s21} & H_{s22} & \cdots & H_{s2(mn)} \\ \vdots & \vdots & \ddots & \vdots \\ H_{s(mn)1} & H_{s(mn)2} & \cdots & H_{s(mn)(mn)} \end{bmatrix}_{mn \times mn} \tag{6-4}$$

6.2.3 The optimal vector for the secondary sources

The voltage vector is defined as the electric signal V_s applied to the piezoelectric patches. The total sound pressure vector of the acoustic wave at point A_i can be written as:

$$\mathbf{P} = \mathbf{H_p P_i} + \mathbf{H_s V_s} \tag{6-5}$$

where $\mathbf{P} = \begin{bmatrix} P_{A1} & P_{A2} & \cdots & P_{A(mn)} \end{bmatrix}^T$ represent the sound pressures at point A_i; $\mathbf{P_i} = \begin{bmatrix} P_{i1} & P_{i2} & \cdots & P_{i(mn)} \end{bmatrix}^T$ represent the pressures of the primary sound wave transmitted in each hybrid cell; $\mathbf{V_s} = \begin{bmatrix} V_{s1} & V_{s2} & \cdots & V_{s(mn)} \end{bmatrix}^T$ represent the voltages imposed on the piezoelectric ceramics of each hybrid cell.

For minimizing the sound pressure at each error sensors, the optimal signal for the secondary sources should be equal to:

$$\mathbf{V_s} = \text{-}\mathbf{H_s}^{-1}\mathbf{H_p P_i} \tag{6-6}$$

6.3 Numerical results

In this section, the acoustic characteristics of some two-cell hybrid structures are calculated by the finite element method with Comsol software under the condition that the separate plate between the cells is either rigid or elastic. Because the correctness of Comsol

software has been verified by the calculation in the foregoing chapters, the following numerical results are credible.

6.3.1 The two-cell structure with air gap

A two-cell structure is filled with an air gap of 20mm as shown in Fig.6-3. In each cell, the active and elastic plates are simply support, and two error sensors are positioned at point A and B. In Comsol environment, the 5×10×1, 5×10×2, 4×8×1 3D mesh are applied respectively to a half of the plate, the air gap and the piezoelectric patches, and the interface between the cells is a rigid wall or elastic plate.

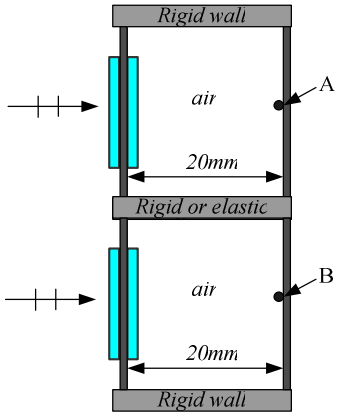

Fig.6-3 The two-cell structure with air gap

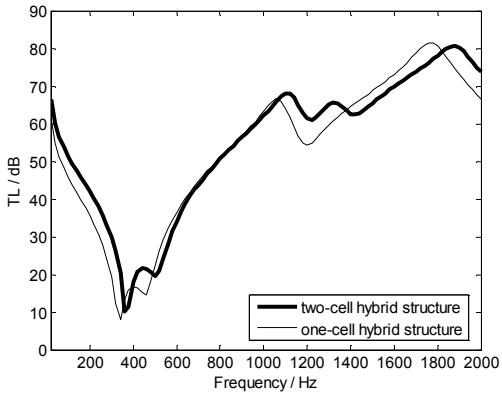

Fig.6-4 Comparison of the transmission loss in the one-cell and two-cell structures having a rigid interface without active control

Fig.6-4 shows the comparison of the transmission loss between the one-cell and two-cell structures without active control. The separate plate between the two cells is steel, and has a thickness of 5mm. The first resonance frequency of this separate plate is adjacent to 6000Hz, and its transmission loss is more than 70dB below 2000Hz, therefore, it can be approximated

as a rigid interface. Compared to the one-cell structure, the resonance frequency of the two-cell structure has a slight shift due to the existence of the separate plate, and its transmission loss has a few changes in whole analysis frequency. It means that the rigid interface between the cells has little effect on the acoustic performance of the two-cell structure.

Fig.6-5 shows that the transmission loss of the two-cell structure having a rigid interface before and after active control. With active control, the transmission loss of the two-cell structure is improved obviously for frequencies lower than 1700Hz. At the resonance frequencies, about 10dB gain can be obtained at 360Hz and 500Hz respectively.

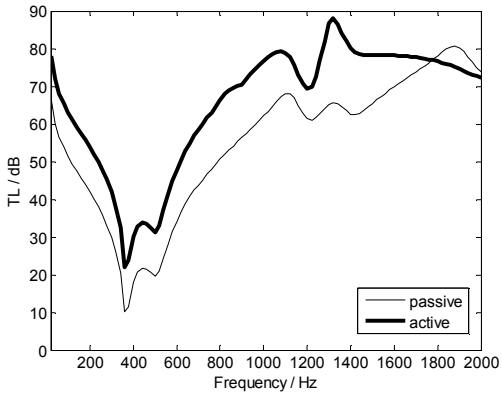

Fig.6-5 The transmission loss of the two-cell structure having a rigid interface

When the interface between the cells is elastic and could transmit sound waves, the results of the transmission loss will be interested in passive and active control. Fig.6-6a describes the comparison of the transmission loss between the two-cell structure having a rigid interface of 5mm thickness and that having an elastic one of 1mm thickness without active control. The first resonance frequency of this elastic separate plate is adjacent to 1200Hz, and its transmission loss is about 20dB at the resonance frequencies, therefore, it can be approximated as an elastic interface. The curves show that the transmission loss has been decreased in the latter because the elastic separate plate vibrates and increases the radiating noises. Meanwhile, the resonance frequency of the latter has been changed because of the elastic separate plate.

Fig.6-6b describes the transmission loss of this two-cell structure with elastic interface before and after active control. The curves show that the transmission loss can be improved obviously below 900Hz with active control. It can be concluded that the property of the two-cell structure can be changed and its acoustic performance will be reduced when the interface between the cells is elastic.

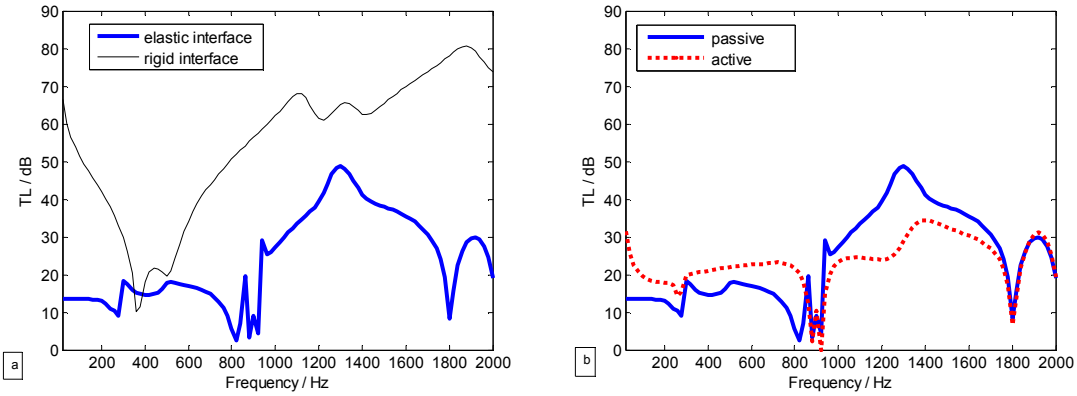

Fig.6-6 The transmission loss of the two-cell structure; a) TL of the structures having rigid or elastic interface without active control; b) TL of the structure having elastic interface before and after active control

Fig.6-8a describes the secondary pathway matrix $\mathbf{H}_s$ of the rigid coupled two-cell structure. The curves show that $H_{s12} = H_{s21} = 0$, which proves the interaction between the error sensor and the secondary source in nearby cell is weak. Fig.6-8b describes t the secondary pathway matrix $\mathbf{H}_s$ of the elastic coupled two-cell structure. The curves show that $H_{s11} \approx H_{s21}$ and $H_{s12} \approx H_{s22}$, which indicates that the interaction between the error sensor and the secondary source in nearby cell is strong.

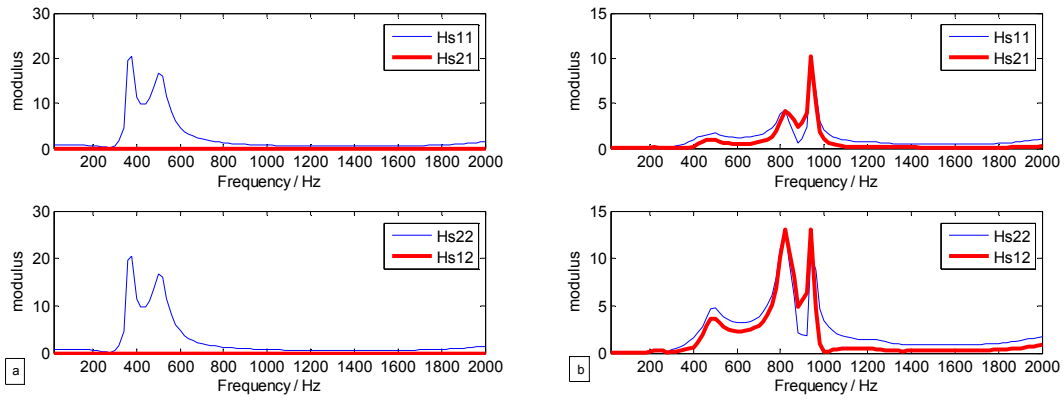

Fig.6-7 The secondary pathway matrix of the two-cell structure; a) rigid interface; b) elastic interface

Fig.6-8 gives the comparison of the velocity at point A between the two-cell structure having a rigid interface and that having an elastic one without active control. It shows that the velocity amplitude of the structure with elastic interface is much greater than that of the structure with a rigid one, which can also validate that the elastic interface augments the lateral radiating noises and changes the resonance frequency of the structure.

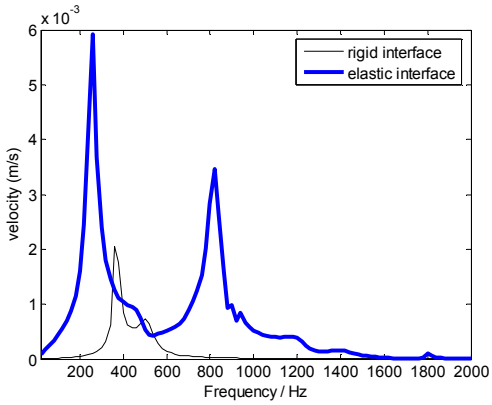

Fig.6-8 The velocity at point A of the two-cell structure without active control

6.3.2 The two-cell structure with porous material

The two-cell structure with porous material of 20mm is shown in Fig.6-9. Similarly, the active and elastic plates are simply support in each cell, and two error sensors are positioned at point A and B. In Comsol environment, the 5×10×1, 5×10×2, 4×8×1 3D mesh are applied respectively to a half of the plate, the porous material and the piezoelectric patches, and the interface between the cells is either rigid or elastic.

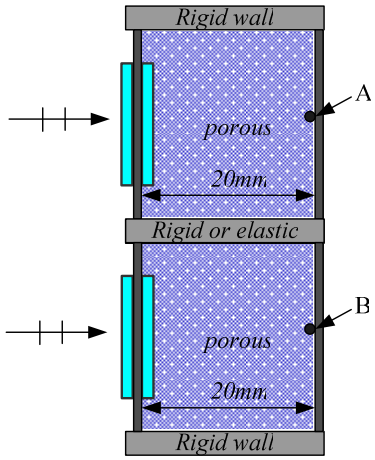

Fig.6-9 The two-cell structure with porous material

Fig.6-10 shows the comparison of the transmission loss between the one-cell and two-cell structures without active control. The separate plate between the two cells is steel, and has a thickness of 5mm, which can be approximated as a rigid interface. Compared to the one-cell structure, the resonance frequency of the two-cell structure has a slight shift due to the existence of the separate plate, meanwhile its transmission loss has a few changes in whole analysis frequency. It means that the rigid interface has little effect on the acoustic performance of the two-cell structure.

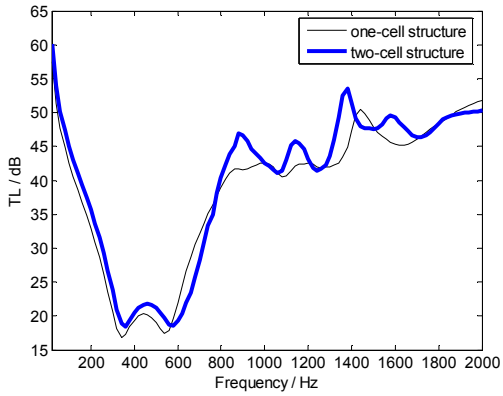

Fig.6-10 Comparison of the transmission loss in the one-cell and two-cell structures having a rigid interface without active control

Fig.6-11 shows that the transmission loss of the two-cell structure having a rigid interface before and after active control. With active control, the transmission loss of the two-cell structure is improved obviously for frequencies lower than 900Hz. At the resonance frequencies, about 8dB gain can be obtained at 360Hz and 570Hz respectively.

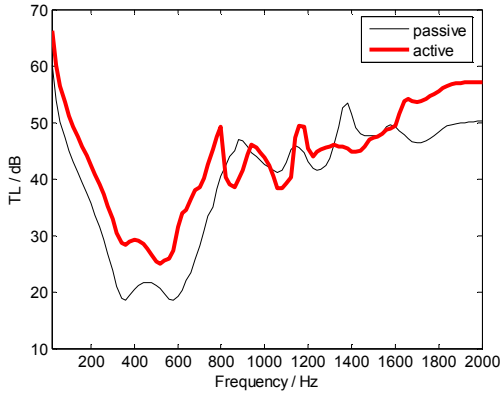

Fig.6-11 The transmission loss of the two-cell hybrid structure having a rigid interface

Fig.6-12a describes the comparison of the transmission loss between the two-cell structure having a rigid interface and that having an elastic interface without active control. The curves show that the transmission loss has been decreased in the latter for frequencies higher than 800Hz, whereas it has obvious improvement in the latter for frequencies lower than 600Hz. The reason may be that the elastic separate plate vibrates and increases the radiating noises, but the presence of the poroelastic material eliminates the noise at low frequency. Meanwhile, the resonance frequency of the latter has been changed because of the elastic separate plate. Fig.6-12b describes the transmission loss of this two-cell structure having an elastic interface before and after active control. The curves show that the transmission loss can be improved obviously below 600Hz with active control. It can also be

concluded that the property of the two-cell structure can be changed and its acoustic performance will be reduced when the separate plate between each cell is elastic.

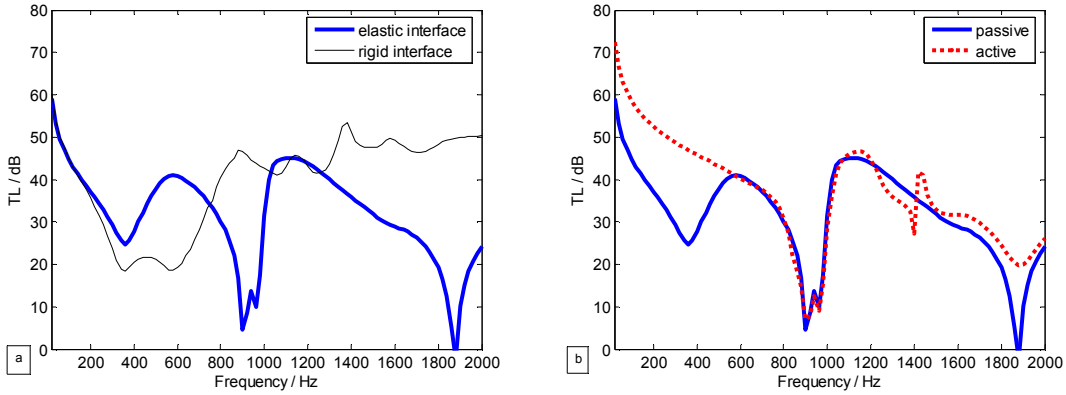

Fig.6-12 The transmission loss of the two-cell structure; a) TL of the structures having rigid or elastic interface without active control; b) TL of the structure having elastic interface before and after active control

Fig.6-13 gives the comparison of the velocity at point A between the two-cell structure having a rigid interface and that having an elastic interface without active control. It shows the velocity amplitude of the structure having an elastic interface is much greater than that having a rigid interface at frequencies higher than 800Hz, but much lower at frequencies lower than 800Hz, which can also validate that the elastic separate plate augments the lateral radiating noises after 800Hz and changes the resonance frequency of the structure.

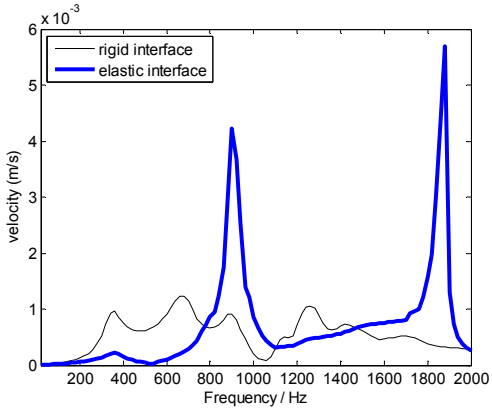

Fig.6-13 The velocity at point A of the two-cell structure without active control

6.3.3 The two-cell structure with several layers

The two-cell structure with several layers is shown in Fig.6-14. Similarly, the active and elastic plates are simply support in each cell, and two error sensors are positioned at point A and B. In Comsol environment, the same 3D meshes are applied respectively to the plate, the

porous material and the piezoelectric patches, and the interface between the cells is either rigid or elastic.

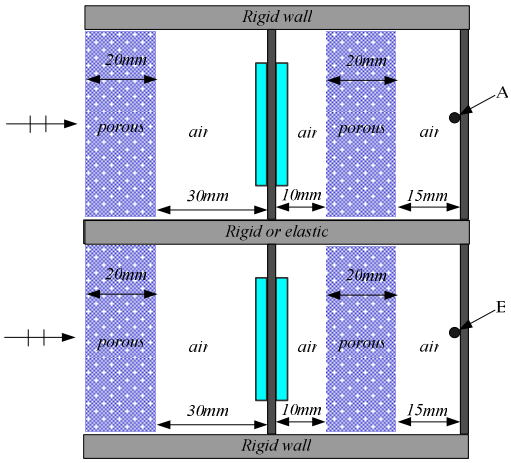

Fig.6-14 The two-cell structure with several layers

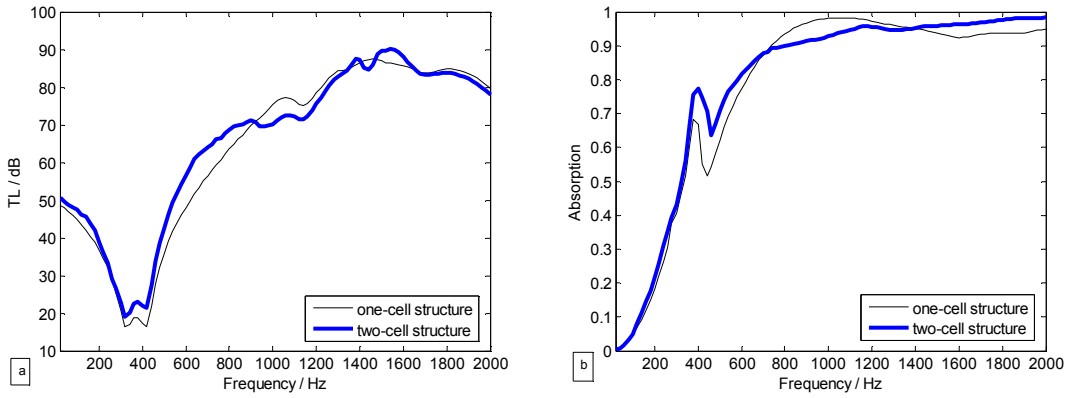

Fig.6-15 The acoustic performance of the one-cell structure and the two-cell structure having a rigid interface; a) transmission loss; b) absorption coefficient

Fig.6-15 shows the comparison of the acoustic performance between the one-cell structure and the two-cell structure having a rigid interface without active control. The separate plate between the two cells can still be approximated as a rigid interface. Comparing to the results of the one-cell structure, the resonance frequency of the two-cell structure has a slight shift due to the existence of the separate plate, meanwhile the transmission loss and absorption coefficient of this two-cell structure has a few improvements at the band of the analysis frequencies. It can also be concluded that the rigid separate plate has little effect on the acoustic performance of the two-cell structure.

Fig.6-16 shows that the acoustic performance of the two-cell structure having a rigid interface before and after active control. With active control, the transmission loss of this two-cell structure is improved obviously at the band of the resonance frequency, and a maximum 15dB gain can be obtained at frequencies of 300~500Hz. Besides, its absorption coefficient with or without active control exceeds 0.6 for frequencies over 500Hz. In means this two-cell structure having a rigid interface still has good sound insulation and absorption performance.

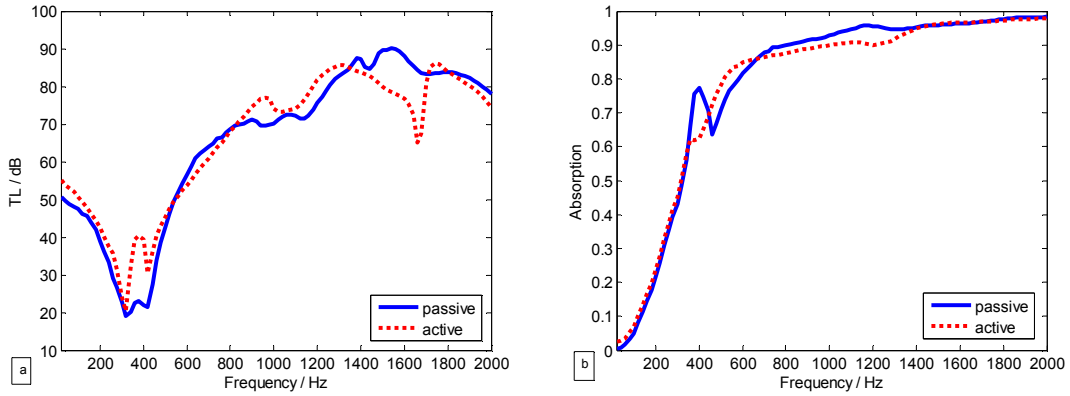

Fig.6-16 The acoustic performance of the two-cell structure having a rigid interface before and after active control; a) transmission loss; b) absorption coefficient

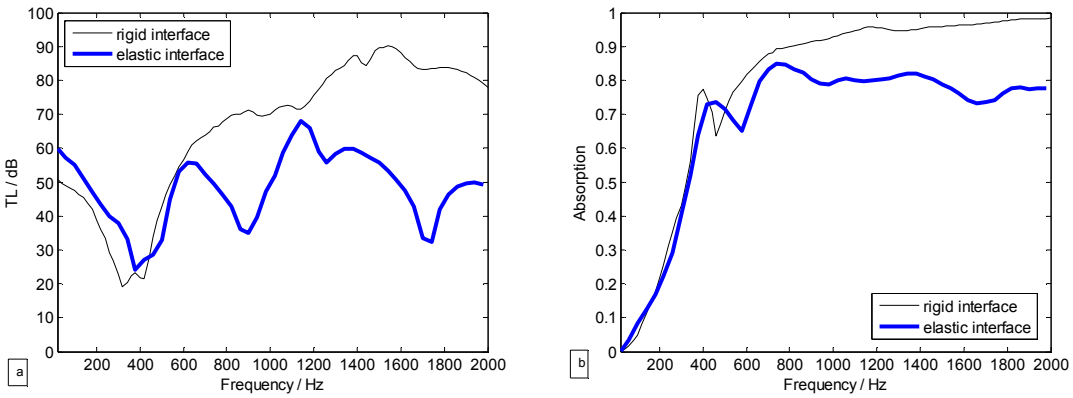

Fig.6-17 The acoustic performance of the two-cell structure a) transmission loss; b) absorption coefficient

Fig.6-17 describes the comparison of the transmission loss and absorption coefficient between the two-cell structure having a rigid interface and that having an elastic interface without active control. The curves in Fig.6-17 show that the transmission loss has been decreased in the latter at frequencies higher than 600Hz, and the absorption coefficient is reduced obviously over 600Hz compared to that of the two-cell structure having a rigid interface. The reason may be that the noise radiated by the elastic separate plate enhances the lateral transmitted wave of the structure. Meanwhile, the resonance frequency of the latter has

been changed because of the elastic separate plate. It can also be concluded that the property of the two-cell structure can be changed and its acoustic performance will be reduced when the separate plate between the cells is elastic.

Fig.6-18 describes the transmission loss and absorption coefficient of this two-cell structure having an elastic interface before and after active control. The curves show that the transmission loss of this two-cell structure can be improved obviously at frequencies of 300~500Hz with active control. But its absorption coefficient with or without active control is similar, and exceeds 0.6 for frequencies over 500Hz.

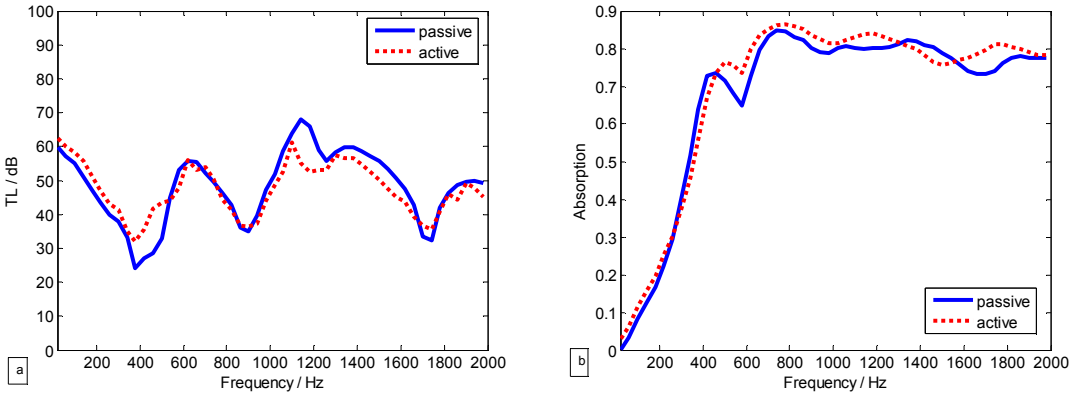

Fig.6-18 The acoustic performance of the two-cell structure having an elastic interface before and after active control; a) transmission loss; b) absorption coefficient

Fig.6-19 gives the comparison of the velocity at point A between the two-cell structure having a rigid interface and that having an elastic interface without active control. It shows the velocity amplitude of the structure having elastic interface is similar to that of the structure having rigid one lower than 600Hz, but much higher over 600Hz, which can also validate that the lateral transmitted wave is increased by the elastic separate plate.

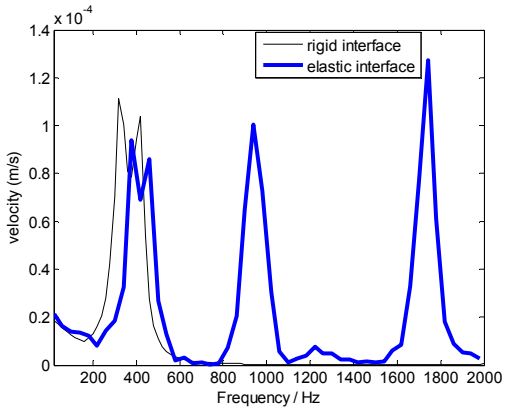

Fig.6-19 The velocity at point A of the two-cell structure without active control

Based on the above analysis, it can be concluded that: (1) the multi-cell hybrid active acoustic structure concept is available for noise control over a large surface by juxtaposing several single hybrid cells; (2) when the separate plate between the cells is rigid, the resonance frequency of the multi-cell structure has a slight shift, and its acoustic performance is similar to that of the one-cell structure; (3) when the separate plate between the cells is elastic, the resonance frequency of the multi-cell structure changes obviously, and its acoustic performance is reduced because of the vibration of the elastic separate plate. Therefore, the interface between the cells in the multi-cell structure should be rigid for holding good sound insulation or absorption performance.

6.4 Conclusions

In this chapter, the multi-cell hybrid active acoustic structure concept is proposed by juxtaposing several single hybrid cells. In the multi-cell hybrid structure, the interface between the cells is rigid or elastic, and each cell has an error sensor for active control with the objective function of a minimum sound pressure. The direct and indirect interaction between the primary/secondary sources and the error sensors are given in the form of the primary and secondary pathway matrices.

For the convenience of analysis, the acoustic properties of the two-cell structures filled with air gap, porous material or their combinations have been calculated in a plane wave excitation by the finite element method. The numerical results show that the existence of the elastic separate plate would change the resonance frequency of the structures and reduce their acoustic performance.

Chapter 7

Conclusions

A new type of hybrid active acoustic structure combining the passive absorption properties and active noise control is designed in this thesis. It can be use to reduce the unwanted room noise in building application or cabin noise in transport application. It has good acoustic absorption and insulation in wide frequency band. This hybrid active acoustic structure consists of an elastic plate, an active plate and several layers such as air gaps or porous material.

7.1 The finished works

The following works have been completed:

1. A hybrid structure allowing good acoustic insulation and absorption for a wide frequency range have been developed based on passive and active means by using passive layers and active plate. It is a combination of a sound absorbent system as 'an equivalent of the λ/4 resonance absorber', and a sound insulation system for improving the transmission loss. The secondary source is realized by an active plate consisting of two piezoelectric patches bonded to an elastic thin plate in order to improve acoustic insulation at low and resonances frequencies.
2. The acoustic properties of the developed structure are modeled by the scattering matrix method. The active plate has been completely described in form of a scattering matrix and a source strength vector which represents respectively the passive and active proprieties of this plate. In active control mode, the source strength vector of the active plate is calculated in order to minimize the sound pressure at the location of the error

sensor. The absorption coefficient and transmission loss of the hybrid structure, are then deduced from the secondary source vector and the scattering matrix coefficients of all layers or elements composing this system. Results show that a significant gain on transmission loss (higher than 15 dB) has been obtained by active control around the resonance frequency, and the absorption coefficient of this hybrid system exceeds 0.6 over 500Hz.

3. The influence factors which affect the acoustic properties of the developed hybrid active acoustic structure have been investigated. It can be concluded that more attention should be paid to the layers located at the front of the active plate when designing a hybrid structure. The appropriate thickness, porosity and resistivity of the porous material and the air gap's thickness should be chosen for getting better acoustic performance of the hybrid system.

4. The poroelastic material is modeled by the finite element method with the (*u, p*) formulation. This model has considered the elasticity of the skeleton of the poroelastic material and the strong coupling between the solid and fluid phases. The boundary conditions on the coupling surface of the elastic, poroelastic and air layers were formulated in Comsol modes. The surface impedance of the poroelastic material was validated by Biot's theory for different boundary conditions.

5. Experiments are implemented to evaluate the acoustic properties of the hybrid active acoustic structure. An experimental device to measure the performance of acoustic treatments has been developed at the **Centre Acoustique** of the **Ecole Centrale de Lyon**. The hybrid structure is thus directly characterized in the test section. The two source-location method based on the scattering matrix is applied to measure the acoustic performance of the hybrid active acoustic structure. A dSPACE-DS1103 controller is implemented with Simulink for feeding the secondary sound source in active control mode.

6. A multi-cell hybrid active acoustic structure concept is proposed by juxtaposing several single hybrid cells for reducing the noise in a large-area domain. The acoustic properties of the multi-cell hybrid active acoustic structure are calculated for a plane wave excitation with the finite element method in Comsol environment. It is concluded that the interface between the cells should be rigid for obtaining good sound insulation or absorption performance.

7.2 Perspectives

This thesis has developed a hybrid active acoustic structure, which has been validated by theoretical and experimental means. In order to apply widely this structure to reduce an unwanted room noise and cabin noise, some further researches should be investigated:

1. Noise control on curved and stiffened plates. The elastic plate used in the developed hybrid active acoustic structure is rectangular and planar; however, the practical structures in airplane and automobile cabins are curved, stiffened or more complex. Therefore, the research on the curved and stiffened plate should be carried out in the hybrid active acoustic structure in future work.
2. Optimization of the hybrid structure based on a loudspeaker as secondary source. The secondary source in the developed hybrid structure is realized by piezoelectric ceramics, and then active control is limited by the voltage on the ceramics. For broadening the working frequency in active control, a loudspeaker could be used as a secondary source. Therefore, the number and location of the loudspeakers should be optimized in the hybrid active acoustic structure. Besides, the near field effect and interaction between loudspeakers have to be investigated.
3. Environmental effects on the acoustic performance of the hybrid structure. In this thesis, the acoustic properties of the hybrid structure are calculated under incident plane wave. However, in engineering application, this hybrid structure would be located on an environment with much more complicated sound field. The effects of the environment on the hybrid active acoustic structure also need to be taken into account.
4. Interaction between the secondary sources and error sensors. In this thesis, all the interactions between the secondary sources and error sensors are considered when expressing the secondary pathway matrix. However, it could be interesting to reduce the complexity of the control algorithm, to be able to design configuration allowing neglect some distant secondary sources. Therefore, in order to obtain the least storage space and computing time, the effect of the relative location between the secondary sources and error sensors should be investigated.
5. Experimental research on the multi-cell hybrid structure. The numerical results conclude that the coupling interface between the cells should be rigid for obtaining good performance of the multi-cell hybrid structure. For validating this conclusion, the experiments should be carried out in future.

Notations

ϕ	Porosity
σ	Resistivity (rayls/m)
α_∞	Tortuosity
Λ	Viscous characteristic length (m)
Λ'	Thermal characteristic length (m)
s	Viscous shape factor
s'	Thermal shape factor
η	Dynamic viscosity of air
γ	Specific heat ratio
e	Thickness of porous sample (m)
ΔP	Gradient of acoustic pressure transmitting a porous sample
ρ_0	Acoustic density (kg/m^3)
c_0	Acoustic velocity (m/s)
Pr	Prandtl number
ρ_e	Effective density of porous sample (kg/m^3)
K	Bulk modulus of porous sample
$\boldsymbol{\sigma}^{\mathbf{s}}$	Frame stress tensor
$\boldsymbol{\sigma}^{\mathbf{f}}$	Fluid stress tensor
ρ_{11}	Relative density of frame (kg/m^3)
ρ_{22}	Relative density of fluid (kg/m^3)
ρ_{12}	Strong inertial coupling between the frame and fluid
K_b	Bulk modulus of solid phase in vacuum
K_f	Bulk modulus of fluid phase with the solid phase in motionless
Z_0	Impedance of air (rayls)
Z_c	Impedance of porous sample (rayls)
Z_s	Surface impedance of porous sample at normal incident (rayls)

k_0	Wave number of air
k_c	Wave number of porous sample
$\mathbf{u}^s$	Frame displacement
$\mathbf{U}^f$	Fluid displacement
μ	Poisson ratio
N	Shear modulus of poroelastic medium (N/m^2)
$\mathbf{T}$	Transfer matrix
$\mathbf{D}$	Scattering matrix
α	Absorption coefficient
TL	Transmission loss (dB)

List of tables

List of figures

Appendix

Scattering matrix method modeling the hybrid active structures

This section presents to model the hybrid active structures by the scattering matrix method. The intensity of the secondary source and the transmission coefficient are given in different structures.

A.1 Sound insulation system

According to the chapter 3, the hybrid active structure on the noise insulation is shown in Fig.A-1. Suppose an anechoic acoustic condition at the back of the active plate, $P_4^-(z_4)=0$, the scattering matrices equations can be rewritten as:

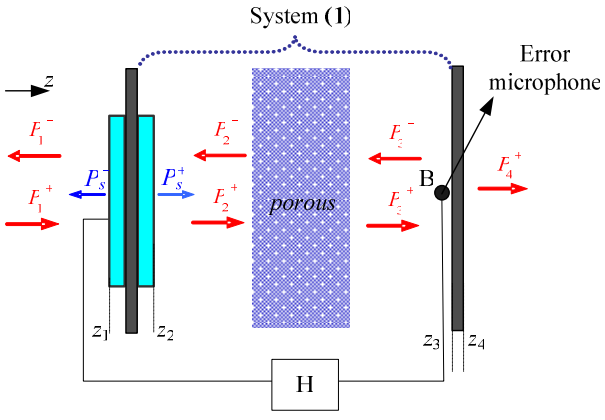

Fig.A-1 The double-wall active insulation system

$$\begin{bmatrix} P_1^-(z_1) \\ P_2^+(z_2) \end{bmatrix} = \mathbf{D^S} \cdot \begin{bmatrix} P_1^+(z_1) \\ P_2^-(z_2) \end{bmatrix} + \begin{bmatrix} P_S^-(z_1) \\ P_S^+(z_2) \end{bmatrix} \tag{A-1}$$

$$\begin{bmatrix} P_2^-(z_2) \\ P_3^+(z_3) \end{bmatrix} = \mathbf{D^1} \cdot \begin{bmatrix} P_2^+(z_2) \\ P_3^-(z_3) \end{bmatrix} \tag{A-2}$$

$$\begin{bmatrix} P_3^-(z_3) \\ P_4^+(z_4) \end{bmatrix} = \mathbf{D^P} \cdot \begin{bmatrix} P_3^+(z_3) \\ 0 \end{bmatrix} \tag{A-3}$$

Here, $\mathbf{D^1}$ is the scattering matrix of the system (1) located between axial coordinates z_1 and z_2; $\mathbf{D^P}$ is the scattering matrix of the elastic thin plate located between axial coordinates z_3 and z_4; $\mathbf{D^S}$ is the scattering matrix of the active plate; The vector $\begin{bmatrix} P_S^-(z_1) & P_S^+(z_2) \end{bmatrix}^T$ is the radiating pressure of the active plate; The other pressure vectors in each equation respectively are the incoming and outgoing waves of each systems.

From Eq. (A-1) ~ (A-3), we can calculate $P_3(z_3)$ as well as the reflected and transmitted pressures $P_1^-(z_1)$ and $P_4^+(z_4)$ at the emission and the transmission side based on the symmetry of the active plate, respectively:

$$P_3(z_3) = b_1 P_1^+(z_1) + b_2 P_S^+(z_2) \tag{A-4}$$

$$P_1^-(z_1) = b_3 P_1^+(z_1) + b_4 P_S^+(z_2) \tag{A-5}$$

$$P_4^+(z_4) = b_5 P_1^+(z_1) + b_6 P_S^+(z_2) \tag{A-6}$$

Here,

$$C_1 = \frac{D_{21}^1}{1 - D_{22}^1 D_{11}^P} \qquad E_1 = D_{11}^1 + D_{12}^1 D_{11}^P C_1 \qquad C_2 = \frac{D_{21}^S}{1 - D_{22}^S E_1} \qquad E_2 = \frac{1}{1 - D_{22}^S E_1}$$

$$b_1 = C_1 C_2 (D_{11}^P + 1) \qquad b_2 = C_1 E_2 (D_{11}^P + 1) \qquad b_3 = D_{11}^S + D_{12}^S E_1 C_2$$

$$b_4 = D_{12}^S E_1 E_2 + 1 \qquad b_5 = D_{21}^P C_1 C_2 \qquad b_6 = D_{21}^P C_1 E_2$$

D_{ij}^1, D_{ij}^P, D_{ij}^S, $i, j = 1, 2$, are the elements of the scattering matrices $\mathbf{D^1}$, $\mathbf{D^P}$, $\mathbf{D^S}$. These scattering matrices are deduced from analytical transfer matrices associated respectively to the system (1), the elastic thin plate and the active plate (Chapter 2).

In active control, the pressure P_3 vanishes, thus

$$P_3(z_3) = 0 \quad \Rightarrow P_S^+(z_2) = -\frac{b_1}{b_2} P_1^+(z_1) \tag{A-7}$$

With the factor χ for describing the active control degree, its expression as follows:

$$P_S^+(z_2) = -\chi \cdot \frac{b_1}{b_2} P_1^+(z_1) \tag{A-8}$$

The reflection and transmission coefficients at z_1 and z_4, respectively, are determined from Eq. (A-5) ~ (A-8):

$$R(\chi) = P_1^-(z_1)/P_1^+(z_1) = \left(b_3 - \chi \cdot \frac{b_1 b_4}{b_2}\right) \tag{A-9}$$

$$\tau(\chi) = P_4^+(z_4)/P_1^+(z_1) = \left(b_5 - \chi \cdot \frac{b_1 b_6}{b_2}\right) \tag{A-10}$$

A.2 Hybrid systems

A.2.1 Active control with one error sensor based on sound insulation

According to the chapter 3, the hybrid active structure on the noise insulation with one error sensor is shown in Fig.A-2. Suppose an anechoic acoustic condition at the back of the active plate, the scattering matrices equations can be rewritten as:

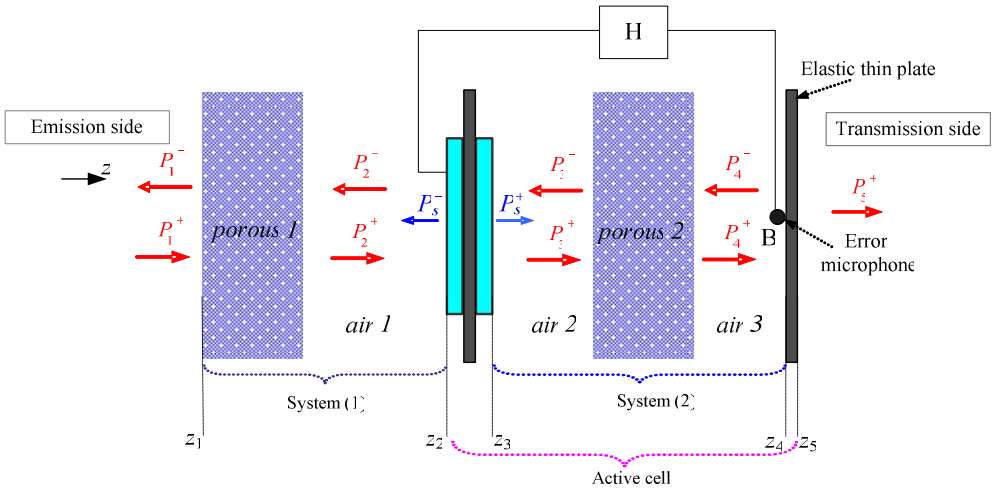

Fig.A-2 General configuration of the multilayer hybrid active acoustic structures

$$\begin{bmatrix} P_1^-(z_1) \\ P_2^+(z_2) \end{bmatrix} = \mathbf{D^1} \cdot \begin{bmatrix} P_1^+(z_1) \\ P_2^-(z_2) \end{bmatrix} \tag{A-11}$$

$$\begin{bmatrix} P_2^-(z_2) \\ P_3^+(z_3) \end{bmatrix} = \mathbf{D^S} \cdot \begin{bmatrix} P_2^+(z_2) \\ P_3^-(z_3) \end{bmatrix} + \begin{bmatrix} P_S^-(z_2) \\ P_S^+(z_3) \end{bmatrix} \tag{A-12}$$

$$\begin{bmatrix} P_3^-(z_3) \\ P_4^+(z_4) \end{bmatrix} = \mathbf{D^2} \cdot \begin{bmatrix} P_3^+(z_3) \\ P_4^-(z_4) \end{bmatrix} \tag{A-13}$$

$$\begin{bmatrix} P_4^-(z_4) \\ P_5^+(z_5) \end{bmatrix} = \mathbf{D^P} \cdot \begin{bmatrix} P_4^+(z_4) \\ 0 \end{bmatrix} \tag{A-14}$$

Here, $\mathbf{D^1}$ is the scattering matrix of the system (1) located between axial coordinates z_1 and z_2; $\mathbf{D^2}$ is the scattering matrix of the system (2) located between axial coordinates z_2 and z_3; $\mathbf{D^S}$ is the scattering matrix of the active plate; $\mathbf{D^P}$ is the scattering matrix of the elastic thin plate;

From Eq. (A-11) ~ (A-14), we can calculate $P_4(z_4)$ as well as the reflected and transmitted pressures $P_1^-(z_1)$ and $P_5^+(z_5)$ at the emission and the transmission side based on the symmetry of the active plate, respectively:

$$P_4(z_4) = g_1 P_1^+(z_1) + g_2 P_S^+(z_3) \tag{A-15}$$

$$P_1^-(z_1) = g_3 P_1^+(z_1) + g_4 P_S^+(z_3) \tag{A-16}$$

$$P_5^+(z_5) = g_5 P_1^+(z_1) + g_6 P_S^+(z_3) \tag{A-17}$$

Here,

$$F_1 = \frac{D_{21}^2}{1 - D_{22}^2 D_{11}^P} \qquad G_1 = D_{11}^2 + D_{12}^2 D_{11}^P F_1 \qquad F_2 = \frac{D_{21}^S}{1 - D_{22}^S G_1} \qquad G_2 = \frac{1}{1 - D_{22}^S G_1}$$

$$F_3 = D_{11}^S + D_{12}^S G_1 F_2 \qquad G_3 = D_{12}^S G_1 G_2 \qquad d_1 = \frac{D_{21}^1}{1 - D_{22}^1 F_3} \qquad d_2 = \frac{D_{22}^1 G_3}{1 - D_{22}^1 F_3} \qquad d_3 = \frac{D_{22}^1}{1 - D_{22}^1 F_3}$$

$$g_1 = F_1 F_2 d_1 (D_{11}^P + 1) \qquad g_2 = (F_1 F_2 d_2 + F_1 G_2 + F_1 F_2 d_3)(D_{11}^P + 1)$$

$$g_3 = D_{11}^1 + D_{12}^1 F_3 d_1 \qquad g_4 = D_{12}^1 (F_3 d_2 + G_3 + F_3 d_3 + 1)$$

$$g_5 = D_{21}^P F_1 F_2 d_1 \qquad g_6 = D_{21}^P (F_1 F_2 d_2 + F_1 G_2 + F_1 F_2 d_3)$$

D_{ij}^1, D_{ij}^2, D_{ij}^P, D_{ij}^S, $i, j = 1, 2$, are the elements of the scattering matrices $\mathbf{D^1}$, $\mathbf{D^2}$, $\mathbf{D^P}$, $\mathbf{D^S}$. These scattering matrices are deduced from analytical transfer matrices associated respectively to the system (1), the system (2), the elastic thin plate and the active plate (Chapter 2).

In active control, $P_S^+(z_3)$ which cancel the pressure at z_4 is:

$$P_4(z_4) = 0 \quad \Rightarrow P_S^+(z_3) = -\frac{g_1}{g_2} P_1^+(z_1) \tag{A-18}$$

Considering the factor χ for describing the active control degree, its expression can be rewritten as follows:

$$P_S^+(z_3) = -\chi \cdot \frac{g_1}{g_2} P_1^+(z_1) \tag{A-19}$$

Reflection and transmission coefficients at z_1 and z_5 are determined respectively:

$$R(\chi) = P_1^-(z_1)/P_1^+(z_1) = \left(g_3 - \chi \cdot \frac{g_1 g_4}{g_2} \right) \tag{A-20}$$

$$\tau(\chi) = P_5^+(z_5)/P_1^+(z_1) = \left(g_5 - \chi \cdot \frac{g_1 g_6}{g_2} \right) \tag{A-21}$$

A.2.2 Active control with one error sensors based on sound absorption

Another hybrid active acoustic structure with one error senor in active control is shown in Fig.A-3, in which the error sensor (point A) makes the system (1) as an equivalent of the $\lambda/4$ resonance absorber. In this case, the system (1) is divided into two parts: the scattering matrix written by $\mathbf{D}^{1a}$ in the range of $z_1 < z < z_1'$ and $\mathbf{D}^{1b}$ in the range of $z_1' < z < z_2$.

$$\begin{bmatrix} P_1^-(z_1) \\ P_2^+(z_1') \end{bmatrix} = \mathbf{D}^{1a} \cdot \begin{bmatrix} P_1^+(z_1) \\ P_2^-(z_1') \end{bmatrix}, \quad \begin{bmatrix} P_2^-(z_1') \\ P_2^+(z_2) \end{bmatrix} = \mathbf{D}^{1b} \cdot \begin{bmatrix} P_2^+(z_1') \\ P_2^-(z_2) \end{bmatrix} \tag{A-22}$$

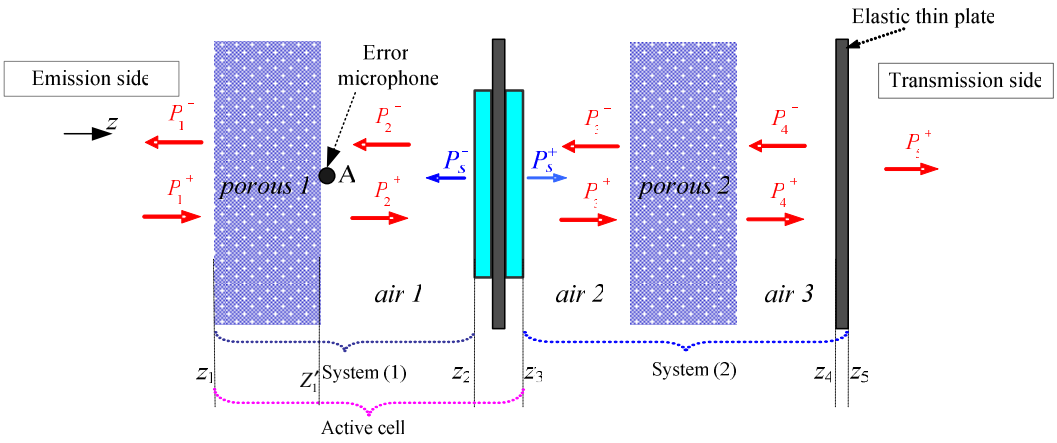

Fig.A-3 The hybrid system in active control with two error sensor

The scattering matrices of the active plate, the system (2) and the elastic thin plate are expressed by Eq. (A-12) ~ (A-14), in the case of anechoic upstream acoustic conditions $\left(P_5^-(z_5) = 0\right)$.

Because of the symmetrical geometry and material proprieties of the used active plate, we calculate the pressure $P_2(z_1')$, $P_4(z_4)$ as well as the reflected and transmitted pressures $P_1^-(z_1)$ and $P_5^+(z_5)$ at the emission and the transmission side, respectively:

$$P_2(z_1') = e_1 P_1^+(z_1) + e_2 P_S^+(z_3) \tag{A-23}$$

$$P_4(z_4) = e_3 P_1^+(z_1) + e_4 P_S^+(z_3) \tag{A-24}$$

$$P_1^-(z_1) = e_5 P_1^+(z_1) + e_6 P_S^+(z_3) \tag{A-25}$$

$$P_5^+(z_5) = e_7 P_1^+(z_1) + e_8 P_S^+(z_3) \tag{A-26}$$

Here,

$$m_1 = \frac{D_{21}^{1b}}{1 - D_{22}^{1b} F_3} \qquad m_2 = \frac{D_{22}^{1b} G_3}{1 - D_{22}^{1b} F_3} \qquad m_3 = \frac{D_{22}^{1b}}{1 - D_{22}^{1b} F_3}$$

$$n_1 = D_{11}^{1b} + D_{12}^{1b} F_3 m_1 \qquad n_2 = D_{12}^{1b}(F_3 m_2 + G_3) \qquad n_3 = D_{12}^{1b}(F_3 m_3 + 1)$$

$$q_1 = \frac{D_{21}^{1a}}{1 - D_{22}^{1a} n_1} \qquad q_2 = \frac{D_{22}^{1a} n_2}{1 - D_{22}^{1a} n_1} \qquad q_2 = \frac{D_{22}^{1a} n_3}{1 - D_{22}^{1a} n_1}$$

$$e_1 = n_1 q_1 + q_1 \qquad e_2 = (n_1 + 1)(q_2 + q_3) + n_2 + n_3 \qquad e_3 = (D_{11}^{P} + 1) F_1 F_2 m_1 q_1$$

$$e_4 = F_1(F_2 m_1 q_2 + F_2 m_2 + G_2 + F_2 m_1 q_3 + F_2 m_3)(D_{11}^{P} + 1) \qquad e_5 = D_{11}^{1a} + D_{12}^{1a} n_1 q_1$$

$$e_6 = D_{12}^{1a}(n_1 q_2 + n_2 + n_1 q_3 + n_3) \qquad e_7 = D_{21}^{P} F_1 F_2 m_1 q_1$$

$$e_8 = D_{21}^{P} F_1 (F_2 m_1 q_2 + F_2 m_2 + G_2 + F_2 m_1 q_3 + F_2 m_3)$$

The parameters F_i, G_i, $i, j = 1,2,3$ are defined in the section C.1. D_{ij}^{1a}, D_{ij}^{1b}, D_{ij}^{2}, D_{ij}^{P}, D_{ij}^{S}, $i, j = 1,2$, are the elements of the scattering matrices $\mathbf{D^{1a}}$, $\mathbf{D^{1b}}$, $\mathbf{D^{2}}$, $\mathbf{D^{P}}$, $\mathbf{D^{S}}$.

In active control, $P_S^+(z_3)$ which cancel the pressure at z' is:

$$P_2(z_1') = 0 \quad \Rightarrow P_S^+(z_3) = -\frac{e_1}{e_2} P_1^+(z_1) \tag{A-27}$$

Considering the factor χ for describing the active control degree, its expression can be rewritten as follows:

$$P_S^+(z_3) = -\chi \cdot \frac{e_1}{e_2} P_1^+(z_1) \tag{A-28}$$

Reflection and transmission coefficients at z_1 and z_5, respectively, are determined from Eq. (3-28), (3-25) and (3-26):

$$R(\chi) = P_1^-(z_1) / P_1^+(z_1) = \left(e_5 - \chi \cdot \frac{e_1 e_6}{e_2} \right) \tag{A-29}$$

$$\tau(\chi) = P_5^+(z_5) / P_1^+(z_1) = \left(e_7 - \chi \cdot \frac{e_1 e_8}{e_2} \right) \tag{A-30}$$

A.2.3 Active control with two error sensors

A hybrid active acoustic structure with two error senor in active control is shown in Fig.A-4, in which the combination of the active cells in the section A.2.1 and A.2.2 makes the system (1) as an equivalent of the $\lambda/4$ resonance absorber and the system (2) as a sound insulation system.

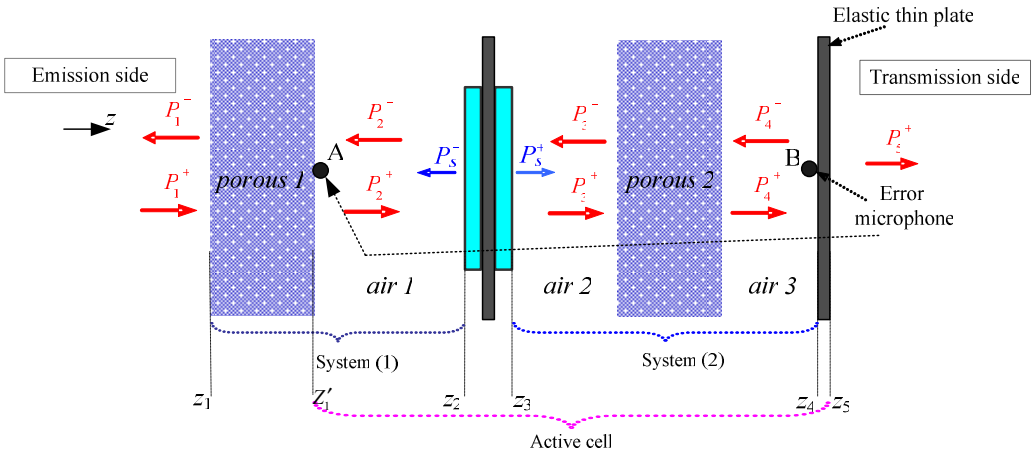

Fig.A-4 The hybrid system in active control with two error sensors

To simulate the active control of the error sensors located at z_1', z_4 (point A and B), the pressure radiated by the active plate in the both sides must be introduced in computations in order to minimize the acoustic power. Therefore, the control objective is written as:

$$J = \left|P_2(z_1')\right|^2 + \left|P_4(z_4)\right|^2 = P_2(z_1')P_2^*(z_1') + P_4(z_4)P_4^*(z_4) \tag{A-31}$$

Suppose $P_1^+(z_1) = \left|P_1^+\right| e^{j\varphi_1}$, $P_S^+(z_3) = \left|P_S^+\right| e^{j\varphi_s}$, the control objective is rewritten as:

$$J = (e_1\left|P_1^+\right| e^{j\varphi_1} + e_2\left|P_S^+\right| e^{j\varphi_s})(e_1^*\left|P_1^+\right| e^{-j\varphi_1} + e_2^*\left|P_S^+\right| e^{-j\varphi_s}) + (e_3\left|P_1^+\right| e^{j\varphi_1} + e_4\left|P_S^+\right| e^{j\varphi_s})(e_3^*\left|P_1^+\right| e^{-j\varphi_1} + e_4^*\left|P_S^+\right| e^{-j\varphi_s})$$

$$= a\left|P_S^+\right|^2 + b\left|P_S^+\right| + c \tag{A-32}$$

Here, $a = \left|e_2\right|^2 + \left|e_4\right|^2$, $b = (e_1e_2^* + e_3e_4^*)\left|P_1^+\right| e^{j\Delta\varphi} + (e_2e_1^* + e_4e_3^*)\left|P_1^+\right| e^{-j\Delta\varphi}$, $c = \left(\left|e_1\right|^2 + \left|e_3\right|^2\right)\left|P_1^+\right|^2$, $\Delta\varphi = \varphi_1 - \varphi_s$.

To make the control objective equal to minimum P_S^+ should satisfy the condition with the phase φ_s fixed:

$$P_S^+(z_3) = -\frac{b}{2a}e^{j\varphi_s} \tag{A-33}$$

Considering the factor χ of the active control degree, Eq. (A-33) submits to:

$$P_S^+(z_3) = -\chi \cdot \frac{b}{2a} e^{j\varphi_s} \tag{A-34}$$

Reflection and transmission coefficients at z_1 and z_5, respectively, are determined from Eqs. (A-34), (A-25) and (A-26):

$$R(\chi) = P_1^-(z_1) / P_1^+(z_1) = \left(e_5 - \chi \cdot \frac{be_6}{2a\left|P_1^+\right|} e^{-j\Delta\varphi} \right) \tag{A-35}$$

$$\tau(\chi) = P_5^+(z_5) / P_1^+(z_1) = \left(e_7 - \chi \cdot \frac{be_8}{2a\left|P_1^+\right|} e^{-j\Delta\varphi} \right) \tag{A-36}$$

Bibliography

1. Kean Chen. Active Noise Control, chap. 1 in Traditional noise control approaches and its characteristics, National Defense Industry Press, Beijing, China, (2003).
2. P.A. Nelson, S.J. Elliott, Active control of sound, Academic Press, London, (1992).
3. C.R. Fuller, S.J. Elliott, P.A. Nelson, Active control of vibration, Academic Press, San Diego, (1996).
4. X.F. Yin, Kean Chen. Active acoustic structure: concept, realization and application, J. Vib. Eng., 16(3), 261-268, (2003).
5. P. Leug. Process of silencing sound oscillations, German patent DRP No. 655508, (1933).
6. P. Leug. Process of silencing sound oscillations, US patent No.2043416, (1936).
7. H.F. Olson, E.G. May. Electronic sound absorber, J. Acoust. Soc. Am., 25, 1130-1136, (1953).
8. L.J. Eriksson. A brief social history of active sound control, Sound and Vibration, 33(7), 14-17, (1999).
9. Kean Chen, Y.L. Ma. Adaptive active noise control- theory, arithmetic and realization, Northwestern Polytechnique Univsrsity Press, Xi'an, (1993).
10. C.H. Hansen. Active noise control: from laboratory to industrial implementation, Proceedings of NOISE-CON 97, State College, Pennsylvania, 3-39,(1997).
11. L.J. Eriksson, M.C. Allie. A practical system for active attenuation in ducts, Sound and Vibration, 22, 30-34, (1988).

12. H.S. Kim, J.S. Hong, D.G. Sohn, et al. Development of an active muffler system for reducing exhaust noise and flow restriction in a heavy vehicles, Noise Control Engineering Journal, 47(2), 57-63, (1999).

13. J.G. Casali, G.S. Robinson. Narrow band digital active noise reduction in a siren-canceling headset: real-ear and acoustical manikin insertion loss, Noise Control Engineering Journal, 42(3), 101-115, (1994).

14. J. Zeta, A.J. Brammer, G.J. Pan. Comparison between subjective and objective measures of active hearing protector and communication headset attenuation, J Acoust Soc Am., 101 (6): 3486-3497, (1997).

15. E.G. Goodfellow. A prototype active noise reduction in-ear heating protector, Applied Acoustics, 42, 299-312, (1994).

16. J.G. Bonito, S.J. Elliont, C.C. Boucher. Generation of zones of quiet using a virtual microphone arrangement, J Acoust Soc Am., 101, 3498-3516, (1997).

17. H.V. Auweraer, D. Otte, G. Venet., et al. Aircraft interior sound field analysis in view of active control: Results from the ASANCA project, Proceedings of Noise-Con'93, 219-224, (1993)

18. C.M. Dorling. A demonstration of active noise reduction in an aircraft cabin, J Sound Vib., 128, 358-360, (1989).

19. S.J. Elliott, P.A. Nelson, I.M. Stothers, et al. Preliminary results of in-flight experiments on the active control of propeller-induced cabin noise, J Sound Vib., 128, 355-357, (1989).

20. S.J. Elliott, P.A. Nelson, I.M. Stothers, et al. In-flight experiments on the active control of propeller-induced cabin noise, J Sound Vib., 140, 219-238, (1990).

21. S.J. Elliott, I.M. Stothers, P.A. Nelson, et al. The active control of engine noise inside cars, Proceedings of Inter-Noise' 88, 987- 990, (1988).

22. T.J. Sutton, S.J. Elliott, A.M. McDonald, et al. Active control of road noise inside vehicles, Noise Control Engineering Journal, 42(4), 137- 147, (1994).

23. R.J. Benhard. Active control of road noise inside automobiles, Proceedings of Active'95, 21-32, (1995).

24. C. Deffayet, P.A. Nelson. Active control of low-frequency harmonic sound radiated by a finite panel, J Acoust Soc Am., 84(6), 2192-2199, (1988)

25. C.R. Fuller. Experiments on reduction of aircraft interior noise using of active control of fuselage vibration, J Acoust Soc Am., 78(S1), S79, (1985).

26. H.C. Lester, C.R. Fuller. Active control of propeller-induced noise fields inside a flexible cylinder, AIAA Journal, 28, 1374-1380, (1990).

27. M.A. Simpson, T.M. Luong, C.R. Fuller, et al. Full scale demonstration tests of cabin noise reduction using vibration, AIAA Journal of Aircraft, 28, 208-215, (1991).

28. C.R. Fuller, C.H. Hansen, S D Snyder. Active control of sound radiation from a vibration rectangular panel by sound sources and vibration inputs: an experimental comparison, J Sound Vib., 145, 195-215, (1991).

29. C.R. Fuller. Active control of sound transmission/radiation from elastic plates by vibration inputs, I: Analysis, J Sound Vib., 136(1), 1-15, (1990).

30. J. Pan, S. DSynder, C.H. Hansen, et al. Active control of far-field sound radiated by a rectangular panel a general analysis, J Acoust Soc Am., 91, 2056-2066, (1992).

31. C.R. Fuller, C.H. Hansen, S.D. Snyder. Experiments on active control of sound radiated from a panel using piezoelectric actuators, J Sound Vib., 150, 179-190, (1991).

32. B. Wang, C.R. Fuller, E.K. Dimitriadis. Active control of noise transmission through rectangular plates using multiple piezoelectric or point force actuators, J Acoust Soc Am., 90(5), 2820-2830, (1991).

33. C. Bao, J. Pan. Experimental study of different approach for active control of sound transmission through double walls, J Acoust Soc Am., 102, 1662-1670, (1997).

34. B. Wang. Optimal placement of microphone and piezoelectric transducer actuators for far-field sound radiation control, J Acoust Soc Am., 99(5), 2975-2984, (1996).

35. M. Salikuddin, H.K. Tanna, R.H. Burrin, et al. Application of active noise control to model propeller noise, J Sound Vib., 137, 9-41, (1990).

36. S.M. Hirsch, J.Q. Sun. An analytical study of interior noise control using segmented panels, J Sound Vib., 231: 1007-1021, (2000)

37. S.M. Hirsch, N.E. Meyer, M.A. Westervelt, et al. Experimental study of smart segmented trim panels for aircraft interior noise control, J Sound Vib., 231, 1023-1037, (2000).

38. Kean Chen, G.H. Koopmann, Theoretical study on active control of sound radiation based on planar sound sources, Chinese Journal of Acoustics, 22(4), 360-368, (2003).

39. C.R. Fuller, C.A. Rogers, H.H. Robertshaw. Control of sound radiation with active/adaptive structure, J Sound Vib., 157, 19-39, (1992).

40. Kean Chen, H. Nykanen, G.H. Koopmann. Application of EMFi acoustic actuators into active control of sound radiation, Proceedings of the 4-th European Con. On Noise Control, Patras, Greece, (2001).

41. R.L. Pierre, G.H. Koopmann, W. Chen. Volume velocity control of sound transmission through composite panels, J Sound Vib., 210(4), 441-460, (1998).

42. G.P. Gibbs, R.L. Clark, D.E. Cox, et al. Radiation modal expansion: Application to active structural acoustic control, J Acoust Soc Am., 107(1), 332-339, (2000).

43. C. Guigou, Z. Li, C.R. Fuller. The relationship between volume velocity and far field radiated pressure of a planar structure, J Sound Vib., 197(2), 252-254, (1996).

44. B. Wang. the PVDF-based wave number domain sensing techniques for active sound radiation control from a simply supported beam, J Acoust Soc Am., 103(4), 1904-1915, (1998).

45. G.V. Borgiotti. The determination of the acoustic far field of a radiating body in an acoustic fluid from boundary measurements, J Acoust Soc Am., 93, 2788-2797, (1993).

46. A. Berry, X. Qiu, C.H. Hansen. Near-field sensing strategies for the active control of the sound radiated from a plate, J Acoust Soc Am., 106(6), 3394-3406, (1999).

47. A.P. Berkhoff. Sensor scheme design for active structural acoustic control, J Acoust Soc Am., 108(3), 1037-1045, (2000).

48. E.F. Crawley. Intelligent structures for aerospace: a technology overview and assessment. AIAA Journal, 32, 1689-1699, (1994).

49. M. Paajanen, H. Valimaki, J. Lekkala. Modelling the electromechanical film (EMFi), Journal of Electrostatics, 48, 193-204, (2000).

50. R. Heydt, R. Pelrine, J. Joseph, et al. Acoustic performance of an electrostrictive polymer film, J Acoust Soc Am., 107, 833-839, (2000).

51. T. Samejima. Development of panel loudspeaker system: design, evaluation and enhancement, J Acoust Soc Am., 109(6), 2751-2761, (2001).

52. I. Berger. Deep thoughts on shallow speaker, Audio Magazine, April 1999

53. H. Nykanen, M. Antila, J. Kataja, et al. Active control of sound based on utilizing EMFi technology, ACTIVE'99, Fort Lauderdale, Florida, (1999).

54. H. Nykanen, R. Aimasso, D. Bondoux, et al. EMFi based ANC systems in transporation system, FACTS Report PR.7.1, (2000).

55. DAFNOR. Distributed Active Foils for Noise Reduction, Final Technical Report, Brite-EuRam Ⅲ project No. BE97-4970.

56. FACTS. Film Actuators and Active Control of Sound for Comfort in Tranportation System, Brite-EuRam Ⅲ project No.BE95-1578.

57. SMARTCUS. Smart Acoustics House, Brite-EuRam Ⅲ project No. BE97-4970.

58. Kean Chen, G.H. Koopmann. Active control of low-frequency sound radiation from vibrating panel using planar sound sources, ASME, J Sound Vib., 124(1), 2-9, (2002).

59. Kean Chen, G.H. Koopmann. Active enhancement of low frequency sound transmission loss using planar sound sources, Proceedings of the ASME International Mechanical Engineering Congress & Exposition, Orlando, Florida, Dec., (2000).

60. Kean Chen. Generalized Engineering Analysis of Active Surface of Sound Absorption, Journal of Northwestern Polytechnique University, 17(2), 181-186, (1999).

61. Kean Chen. The mechanism of active sound absorption unit, J Vib Eng., 11(4), 402-409, (1998).

62. Kean Chen. Design strategy and Algorithm for adaptive control of active sound absorption, Journal of Northwestern Polytechnique University, 17(3), 382-386, (1999).

63. Kean Chen, G.H. Koopmann. Theoretical study on active control of sound radiation based on planar sound sources, Chinese Journal of Acoustics, 2003, 28 (4), 279-293

64. Kean Chen, W.B.Zhong, X.Y. Zeng. the acoustic characteristics of panel loudspeakers, Audio Engineering, 9, 21-23, (2003).

65. Kean Chen, X.F. Yin. Active control of radiated sound using near field pressure sensing, Chinese Journal of Acoustics, 23(3), 193-202, (2004).

66. Kean Chen. Error Sensing Strategies for Adaptive Acoustic Structures, J Vib Eng., 17(3), 301-305, (2004).

67. W.B. Zhong, Kean Chen, H.W. Li. Experimental study of flat panel loudspeakers applied to active noise control, Appl Acoust, 25(4), 246-251, (2006).

68. H.R. Pan. Optimum configuration design for active acoustic structure, thesis of Master, Northwestern Polytechnique University, (2006).

69. X.F. Yin. An adaptive combined inverse algorithm applied to multi-channel active control system, Ph.D thesis, Northwestern Polytechnique University, (2005).

70. C.A. Gentry, C. Guigou, C.R. Fuller. Smart foam for applications in passive/active noise radiation control, J Acoust Soc Am., 101(4):1771-1778, (1997).

71. D.J. Rossetti, M.A. Norris. A comparison of actuation and sensing techniques for aircraft cabin noise control, Noise Control Engineering Journal, 44(1):53-58, (1996).

72. C.K. Lee. Theory of laminated piezoelectric plates for the design of distributes sensors/actuators, part I: governing equations and reciprocal relationships. J Acoust Soc Am., 87, 1144-1158, (1990).

73. E.F. Crawley, J.D. Luis. Use of piezoelectric actuators as elements of intelligent structures. AIAA Journal, 25, 1373-1385, (1987).

74. N.N. Rogacheva. The Theory of Piezoelectric Shells and Plates. Boca Raton: CRC Press, (1994).

75. H.S. Tzou. Piezoelectric Shells Distributed Sensing and Control of Continua. Dordrecht: Kluwer Academic Publishers, (1993).

76. E.H. ANDERSON, N.W. HAGOOD. Simultaneous piezoelectric sensing/actuation: analysis and application to controlled structures. J Sound Vib., 174, 617-639, (1994).

77. F.P. Mechel, Hybrider Schalldamplfer, Patent No. DE4027511.

78. D. Guicking, E. Lorenz. An active sound absorber with porous plate, J. Vib. Acoust., Stress Reliab. Design, 106, 393-396, (1984).

79. D. Thenail, M. Galland, M. Sunyach, M. Sunhack. Active enhancement of the absorbent properties of a porous material, Smart Mater. Struct, 3, 18-25, (1994).

80. S. Beyene, R.A. Burdisso. A new hybrid passive/active noise absorption system. J Acoust Soc Am., 101(3), 1512-1515, (1997).

81. M. Furstoss, D. Thenail, M.A. Galland. Surface impedance control for sound absorption: direct and hybrid passive/active strategies. J Sound Vib., 203(2), 219-236, (1997).

82. O. Lacour, M.A. Galland, D. Thenail. Preliminary experiments on noise reduction in cavities using active impedance changes. J Sound Vib., 230(1), 69–99, (2000).

83. M.A. Galland, P. Souchotte, P. Ladner, T. Mazoyer. Experimental investigation of noise reduction in a flow duct through hybrid passive/active liner. In: 7th AIAA/CEAS aeroacoustics conference, Maastricht, The Netherlands; 28–30 May 2001, 2001–221, (2001).

84. N. Sellen, M. Cuesta, M.A. Galland. Passive layer optimization for active absorbers in flow duct applications. In: 9th AIAA/CEAS aeroacoustics conference, Hilton Head, South Carolina. AIAA; 12–14 May 2003, 2003–3186, (2003).

85. M.A Galland, N. Sellen, O. Hilbrunner. Noise reduction in a flow duct by active control of wall impedance. In: 8th AIAA/CEAS aeroacoustics conference, Breckenridge, Colorado. AIAA; 17–19 June 2002, 2002–498, (2002).

86. O. Hilbrunner, B. Mazeaud, M.A. Galland. Multi-cell digital feedback control for noise reduction through hybrid absorbers. In: 9th AIAA/CEAS aeroacoustics conference, Hilton Head, South Carolina. AIAA; 12–14 May 2003, 2003–3187, (2003).

87. M. A. Galland, B. Mazeaud, N. Sellen. Hybrid passive/active absorbers for flow ducts, Applied Acoustics, 66, 691-708, (2005).

88. M. Melon, P. Herzog, A. Sitel, M.A. Galland. Etude unidimensionnelle d'une cellule hybride pour absorption et isolation simultanée, Acoustique Techniques, 60, 46-50,2010.

89. P. Leroy. Les mousses adaptatives pour l'amélioration de l'absorption acoustique : modélisation, mise en œuvre, mécanismes de contrôle, Thèse de l'Université Aix-Marseille I, 2008.

90. C. Guigou, C. R. Fuller. Control of aircraft interior broadband noise with foam-pvdf smart skin, J. Sound Vib., 220, 541-557, (1999).

91. B.D. Johnson, C.R. Fuller. Broadband control of plate radiation using a piezoelectric, double-amplifier active-skin and structural acoustic sensing, J. Acoust. Soc. Am., 107, 876-884, (2000).

92. J. Pan, C. Bao. Analytical study of different approaches for active control of sound transmission through double walls. J. Acoust. Soc. Am.,103, 1916-1922, (1998).

93. P.D. Fonseca, P. Sas, H.V. Brussel. Experimental study of the active sound transmission reduction through a double panel test section. Acustica, 85, 538-46, (1999).

94. P. Sas, C. Bao, F. Augusztinovisz, W. Desmet. Active control of sound transmission through a double-panel partition. J Sound Vib., 180, 609-25, (1995).

95. F.W. Grosveld, K.P. Shepherd. Active sound-attenuation across a double-wall structure, J Aircraft 31, 223-227, (1994).

96. J.P. Carneal, C.R. Fuller. Active structural acoustic control of noise transmission through double panel systems, AIAA, 33, 618-623, (1995).

97. C. Bao, J. Pan. Experimental study of different approaches for active control of sound transmission through double walls, J Acoust Soc Am., 102, 1664-1670, (1997).

98. C.Y. Wang, R. Vaicaitis. Active control of vibrations and noise of double wall cylindrical shells, J Sound Vib., 216, 865-888, (1998).

99. X. Pan, T.J. Sutton, Elliott SJ. Active control of sound transmission through a double-leaf partition by volume velocity cancellation, J Acoust Soc Am., 104, 2828-2835, (1998).

100. P. Gardonio, S.J. Elliott. Active control of structure-borne and airborne sound transmission through double panel, J Aircraft, 36, 1023-1032, (1998).

101. R. Paurobally, J. Pan, C. Bao. Feedback control of noise transmission through a double-panel partition, in Proceedings of Active 99, Fort Lauderdale, Florida, USA, 375-386, (1999).

102. O.E. Kaiser, S.J. Pietrzko, M. Morari. Feedback control of sound transmission through a double glazed window, J Sound Vib., 263, 775-795, (2003)..

103. A. Jakob, M. Moser. Active control of double-glazed windows Part I: Feedforward control, Appl Acoust, 64, 163-182, (2003).

104. A. Jakob, M. Moser. Active control of double-glazed windows. Part II: Feedback control, Appl Acoust, 64, 183-196, (2003).

105. J.P. Carneal, C.R. Fuller. An analytical and experimental investigation of active structural acoustic control of noise transmission through double panel system, J. Sound Vib., 272, 749-771, (2004).

106. J. K. Lee, J. Kim, C.J. Rhee, C.H. Jo, and S. B. Choi. Noise reduction of passive and active hybrid panels, Smart materials and structures, 11, 940-946, (2002).

107. Q. Mao, S. Pietrzko. Control of sound transmission through double wall partitions using optimally tuned Helmholtz resonators, ACTA Acustica United with Acustica, 91, 723-731, (2005).

108. S. Pietrzko, Q. Mao. New results in active and passive control of sound transmission through double wall structures, Aerospace Science and Technology, 12(1), 42-53, (2008).

109. Q. Mao, S. Pietrzko. Experimental study for control of sound transmission through double glazed window using optimally tuned Helmholtz resonators, Applied Acoustics, 71(1), 32-38, (2010).

110. B. Brouard, D. Lafarge, J.F. Allard, A general method of modeling sound propagation in layered media, J. Sound Vib., 183(1), 129-142, (1995).

111. M. Fringuellino, C. Guglielmone. Progressive impedance method for the classical analysis of acoustic transmission loss in multilayered walls, Applied Acoustics, 59, 275-285, (2000).

112. A. Pellicier, N. Trompette. A review of analytical methods based on the wave approach to compute partitions transmission loss, Applied Acoustics 68, 1192-1212, (2007).

113. J.S. Lowe. Matrix techniques for modeling ultrasonic waves in multilayered media, IEEE Transactions on Ultrasonics, Ferroelectrics, and Frequency control, 42(4), 525-542, (1995).

114. J.S. Sastry, M.L. Munjal. A transfer matrix approach for evaluation of the response of a multi-layer infinite plate to a two-dimensional pressure excitation, J. Sound Vib., 182(1), 109-128, (1995).

115. M.L. Munjal. Response of a multi-layered infinite plate on an oblique plane wave by means of transfer matrices, J. Sound Vib., 162, 333-343, (1993).

116. Y.Y. Li, L. Cheng. Mechanisms of active control of sound transmission through a linkes double-wall system into an acoustic cavity, Applied Acoustics, 69, 614-623, (2008).

117. U. Lee. Vibration analysis of one-dimensional structures using the spectral transfer matrix method, Engineering Structures, 22, 681-690, (2000).

118. L. Wang, S.I. Rokhlin. Stable reformulation of transfer matrix method for wave propogation in layered anisotropic media, Ultrasonics, 39, 413-42, (2001).

119. Q.S. Li, K. Yang, L. Zhang, N. Zhang. Frequency domain analysis of fluid-structure interaction in liquid-filled pipe systems by transfer matrix method, Mechanical Sciences, 44, 2067-2087, (2002).

120. D.H. Lee, Y.P. Kwon. Estimation of the absorption performance of multiple layer perforated panel systems by transfer matrix method, J. Sound Vib., 278, 847-860, (2004).

121. H. Liu, J.J. Lee, Z.M. Cai. Analysis of nonlinear acoustoelastic effect of surface acoustic wave in laminated structures by transfer matrix method, Mechanics Research Communications, 31, 667-675, (2004).

122. R. Daneshfaraz, B. Kaya. Solution of the propagation of the waves in open channels by the transfer matrix method, Ocean Engineering, 35, 1075-1079, (2008).

123. C.M. Lee, Y. Xu. A modified transfer matrix method for prediction of transmission loss of multilayer acoustic materials, J. Sound Vib., 326, 290-301, (2009).

124. T.E. Vigran. Sound transmission in multilayered structures - Introducing finite structural connections in the transfer matrix method, Applied Acoustics, 71, 39-44, (2010).

125. D.H. Lee, S.C. Hur, Y.P. Kwon. Estimation of the sound absorption performance for multiple layer perforated plate systems by transfer matrix method, Transactions of the Korean Society for Noise and Vibration Engineering, 12 (9), 709-716, (2002).

126. M. Aböm. Measurement of a scattering-matrix of acoustical two ports, Mechanical Systems and Signal Processing, 5(2), 89-104, (1991).

127. J. Lavrenjev, H. Bodèn, M. Aböm. A measurement method for determination the source data of acoustic two-port sources, J. Sound Vib., 197(1), 1-16, (1996).

128. R.Glav, M. Aböm. A general formalism for analyzing acoustic 2-port networks, J. Sound Vib., 202(5), 739-747, (1997).

129. N. Sellen, O. Hilbrunner, M.A. Galland. Identification of the characteristic parameters of porous media using active control, 8th AIAA/CEAS Aero acoustics Conference, AIAA Paper, 2002-2504, (2002).

130. J.F. Allard. Propagation of Sound in Porous Media: Modeling Sound Absorbing materials, Elsevier, New York, (1993).

131. M.A. Biot, The theory of propagation of elastic waves in a fluid-saturated porous solid, J Acoust Soc Am., 28, 168-191, (1956).

132. T.W. Geerits, O. Kelder. Acoustic wave propagation through porous media: Theory and experiments, J Acoust Soc Am., 102(5), 2495-2510, (1997).

133. M. Swift, K. Horoshenkov, P. Leclaire, D. Hotherall, K. Fujiwara, H. Torihama. On the effect of the bending vibration on the acoustic propertied of thin poroelastic plates, J Acoust Soc Am., 107, 1786-1789, (2000).

134. N. Dauchez, S. Sahraoui, N. Atalla. Convergence of poroelastic finite elements based on Biot displacement formulation, J Acoust Soc Am., 109(1), 33-40, (2001).

135. N. Dauchez, S. Sahraoui, N. Atalla. Investigation and moeling of damping in a plate with a bonded porous layer, J. Sound Vib., 265, 437-449, (2003).

136. J.P. Coyrtte, H. Wynendaele, A finite element model for predicting the acoustical transmission characteristics of layered structures, In: Proceedings of Inter-noise 95, 1279-1282, (1995).

137. Y.J. Kang, J.S. Bolton, Finite element modeling of isotropic elastic porous materials coupled with acoustical finite elements, J Acoust Soc Am., 98 (1), 635-643, (1995).

138. L. Taber. A theory for transverse deflection of poroelastic plates, J Appl. Mech., 59, 628-634, (1992).

139. D. Theodorakopoulos, D. Beskos. Flexural vibrations of poroelastic plates, Acta <echanica, 103, 191-203, (1994).

140. P. Leclaire, K. Horoshenkov, A. Cummings. Transverse vibrations of a thin rectangular porous plate saturated by a fluid, J. Sound Vib., 247, 1-18, (2001).

141. P. Leclaire, K. Horoshenkov, M. Swift, D. Hotherall. The vibrational response of a clamped rectangular porous plate, J. Sound Vib., 247, 19-31, (2001).

142. R. Panneton, N. Atalla, An efficient finite element scheme for solving the three-dimensional poroelasticity problem in acoustics, J Acoust Soc Am., 101, 3287-3298, (1997).

143. N. Atalla, R. Panneton, P. Debergue, A mixed displacement-pressure formulation for poroelastic materials, J Acoust Soc Am., 104(3), 1444-1452, (1998).

144. P. Debergue, R. Panneton, N. Atalla, Boundary conditions for the weak formulation of the mixed (u, p) poroelasticity problem, J Acoust Soc Am., 106(5), 2383-2390, (1999).

145. O. Dazel, F. Sgard, An extension of complex modes for the resolution of finite-element poroelastic problems, J. Sound Vib., 253(2), 421-445, (2002).

146. A. Bermudez, J. L. Ferrin, A. Prieto, Finite element solution of new displacement/pressure poroelastic models in acoustics, Comput Methods Appl Mech Engrg. 195, 1914-1932, (2006).

147. C. Batifol, T.G. Zielinski, M.N. Ichchou, M.A. Galland, A finite element study of a piezoelectric/poroelastic sound package concept, Smart Materials and Structures, 16, 168-177, (2007).

148. C. Batifol, M.N. Ichchou, M.A. Galland. Hybrid modal reduction for poroelastic materials, Comptes Rendus Mécanique, 336(10), 757-765, (2008).

149. M. Etchessahar, S. Sahraoui, B. Brouard. Bending vibrations of a rectangular poroelastic plate, C. R. Acad.Sci. Paris, Series II b, 329, 615-620, (2001).

150. M. Etchessahar, S. Sahraoui, B. Brouard. Vibrations of poroelastic plates: Mixed displacement-pressure modelisation and experiments, Acta Acoustica, 95, 857-865, (2009).

151. ASTM C423-08, Standard test method for sound absorption and sound absorption coefficients by the reverberation room method.

152. ISO 10534, Determination of sound absorption coefficient and impedance in impedance tubes.

153. D. Apfel, T. Guenther, J.S. Bolton, J. Pope. Development of a New Sound Transmission Test for Automotive Sealant Materials, SAE Trans, 106, 2651-2658, (1997).

154. ASTM Standard E 1050-90，Impedance and absorption of acoustical materials using a tube, two micro-phones, and a digital frequency analysis system.

155. B.H. Song, J.S. Bolton. A transfer-matrix approach for estimating the characteristic impedance and wave numbers of limp and rigid porous materials, J Acoust Soc Am., 107(3), 1131-1152, (2000).

156. B.L. Zhu, X.H. Luo. The measurement method of insulation in standing wave tube, Noise and Vibration Control, 6, 41-43, (2000).

157. Q. Bo, B.L. Zhu. Four-microphone method of sound transmission in the standing wave tube, Noise and Vibration Control, 6, 44-46, (2002).

158. D.L. Peng, P. Hu, B.L. Zhu. The Modified Computation of the Complex Transmission Coefficient of Acoustical Panel-in Standing Wave Tube, Journal of Shanghai Jiaotong University, 41(4), 649-653, (2007).

159. Z. Tao, A.F. Seybert. A review of current techniques for measuring muffler transmission loss. SAE Paper 03NVC-38, Warrendale, USA: SAE Int, (2001).

160. M.L. Munjal. Acoustics of ducts and mufflers. New York: Wiley-interscience, (1987).

161. M.L. Munjal, A.G. Doige. Theory of a two source-location method for direct experimental evaluation of the four-pole parameters of an aeroacoustic element. J. Sound. Vib., 142(2), 323-333, (1990).

162. N. Sellen. Modification de l'impédance de surface d'un matériau par contrôle actif (in French). Ph.D. dissertation, Ecole Centrale de Lyon, France, (2003).

163. D.J. Johnson, Theory of dynamic permeability and tortuosity in fluid-saturated porous media, J. Fluid. Mech., 176, 379-402, (1987).

164. Y. Champoux, J. F. Allard. Dynamic tortuosity and bulk modulus in air-saturated porous media, J. Appl. Phy., 70(4), 1975-1979, (1991).

165. A.F. Seybert, D.F. Ross. Experimental determination of acoustic properties using a two-microphone randam excitation technique, J. Acoust. Soc. Am., 61, 1362-1370, (1977).

166. J.Y. Chung, D.A. Blaser. Transfer function method of measuring in-duct acoustic properties, I: theory, J. Acoust. Soc. Am., 68, 907-913, (1980).

167. J.Y. Chung, D.A. Blaser. Transfer function method of measuring in-duct acoustic properties, II: experiment, J. Acoust. Soc. Am., 68, 914-921, (1980).

168. A.F. Seybert. Two-sensor method for the measurement of sound intensity and acoustic propertied in ducts, J. Acoust. Soc. Am., 83, 2233-2239, (1988).

169. H.J. Wu, W.K. Jiang, L.J. Li. Analysis of the tolerance of sound transmission loss measured by four-microphone in standing wave tube (in Chinese), Journal of Shanghai Jiaotong University, 42(8), 1265-1268, (2008).

Publications

Ying Hu, A. Sitel, M.A. Galland, Kean Chen. A plane wave study for improving acoustic performance of double wall systems using an active-passive method. *Noise Control Eng. J.*, 2009; 57(3): 193-202. (SCI: 000277302100004; EI: 201009 12735247)

Ying Hu, Kean Chen, M.A. Galland. Experimental study on acoustic performance of double-wall active sound packages based on two source-location method, Journal of Vibration Engineering, 32(4): 462-468, 2010.

Ying Hu, Kean Chen, M.A. Galland. Sound transmission of double-wall active sound package with porous materials based on (*u, p*) formulation, accepted by Chinese ACTA ACUSTICA, 2010.

Ying Hu, M.A Galland. Multi-cell hybrid sound packages concepts for improving sound absorption and insulation. 10eme Congres Français d'Acoustique, 12-26 Avril 2010, Lyon, France.

Ying Hu, A. Sitel, M.A Galland, Kean Chen. Hybrid sandwiches panels for reducing the sound reflection and transmission. *Inter-noise 2008*, 26-29 October, Shanghai, China.

A.Sitel, **Ying Hu**, M.A.Galland. Active multilayered panels based on porous materials for improving acoustic performance. *Symposium on the Acoustics of Poro-Elastic Materials*, 17-19 December, Bradford, UK, 2008.

A. Sitel, **Ying Hu**, M.A.Galland. Active-passive multilayered panels for reduction of both acoustic reflection and transmission. *J. Acoust. Soc. Amer.*, 2008; 123(5): 3874.

A.Sitel, **Ying Hu**, M.A.Galland. Active-passive multilayered panels for reduction of both acoustic reflection and transmission. *Proceedings of the* Acoustics 2008 *International Conference*, 29 June - 4 July, Paris, France.

Ying Hu, Kean Chen. A FE-SEA hybrid method for vibration analysis of complex structures, *Journals of Vibration and Shock*, 2008; 27(7): 88-94.

Ying Hu, Kean Chen, Kai Pan. Optimization design about plane cabin noise based on statistical energy analysis, *Noise and vibration Control*, 2007; 27(2): 65-68.

S. Li, Kean Chen, S.L. Zhao, **Ying Hu**. Experimental study on active control of sound

radiation based on planar sound sources. *Applied Acoustic of China*, 2008; 27(5): 363-373.